Optical microscopy

http://micro.magnet.fsu.edu/primer/anatomy/anatomy.html

Lecture notes on optical microscopy and related topics:
http://www.cyto.purdue.edu/flowcyt/educate/pptslide.htm

PH 673

Nanoscience and nanotechnology

November 24, 2025

ONLINE SOURCES

http://www.olympusconfocal.com/gfp/primer/index.html

http://www.microscopyu.com/

http://micro.magnet.fsu.edu/primer/index.html

Resolution

Basic requirement: ability to resolve details in the image.

Resolution defines the smallest separation of two points in the object that can be distinctly reproduced in the image.

Contrast is the difference between the brightness of various details in the object, and the difference as compared with the background

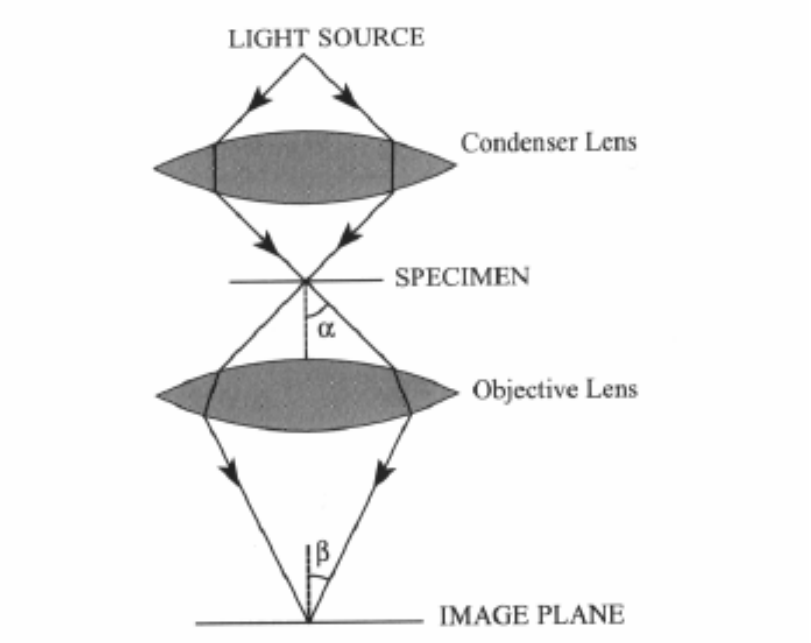

Diffraction – limited resolving power:

$$\delta = \frac{C\lambda}{\eta \sin\alpha} = \frac{C\lambda}{NA}$$

C – constant, usually 0.61 (coherence)
λ – wavelength of light
η – refractive index of medium between object and lens
α– semi-angle
NA – numerical aperture

Limitation in Optical Microscopy

Resolution limited by wavelength of light (diffraction)

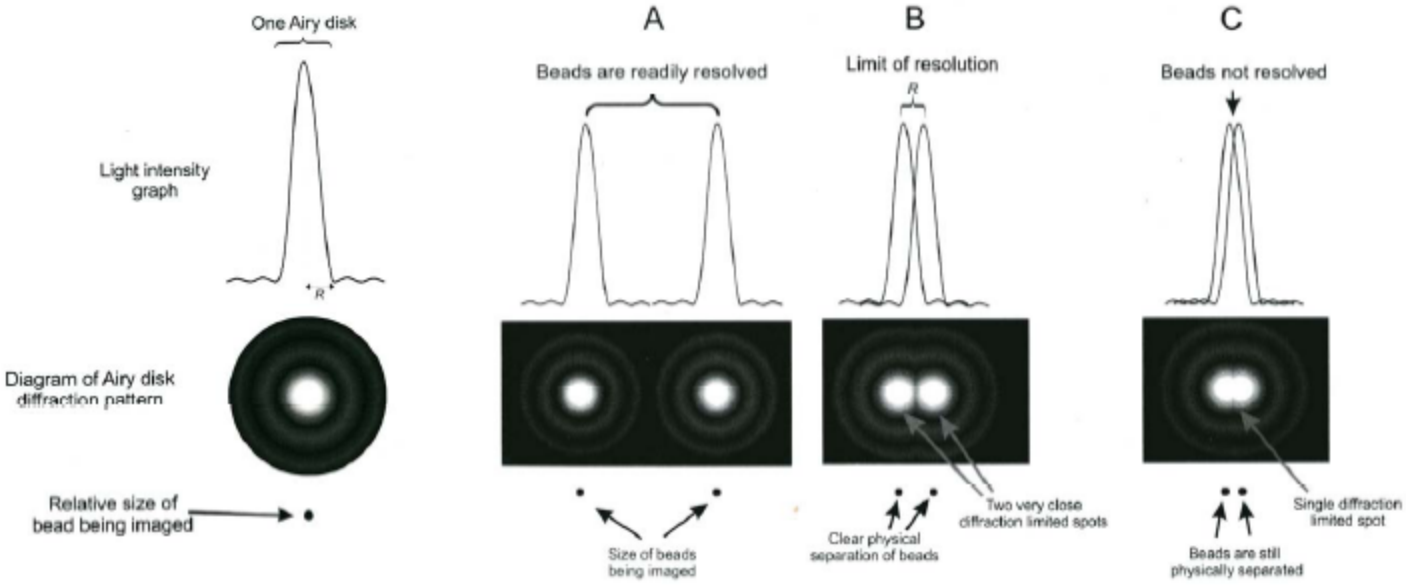

$$R = \frac{1.22\lambda}{NA_{objective} + NA_{condenser}} = \frac{1.22\lambda}{2NA_{objective}}$$

NA: numerical aperture

Resolution

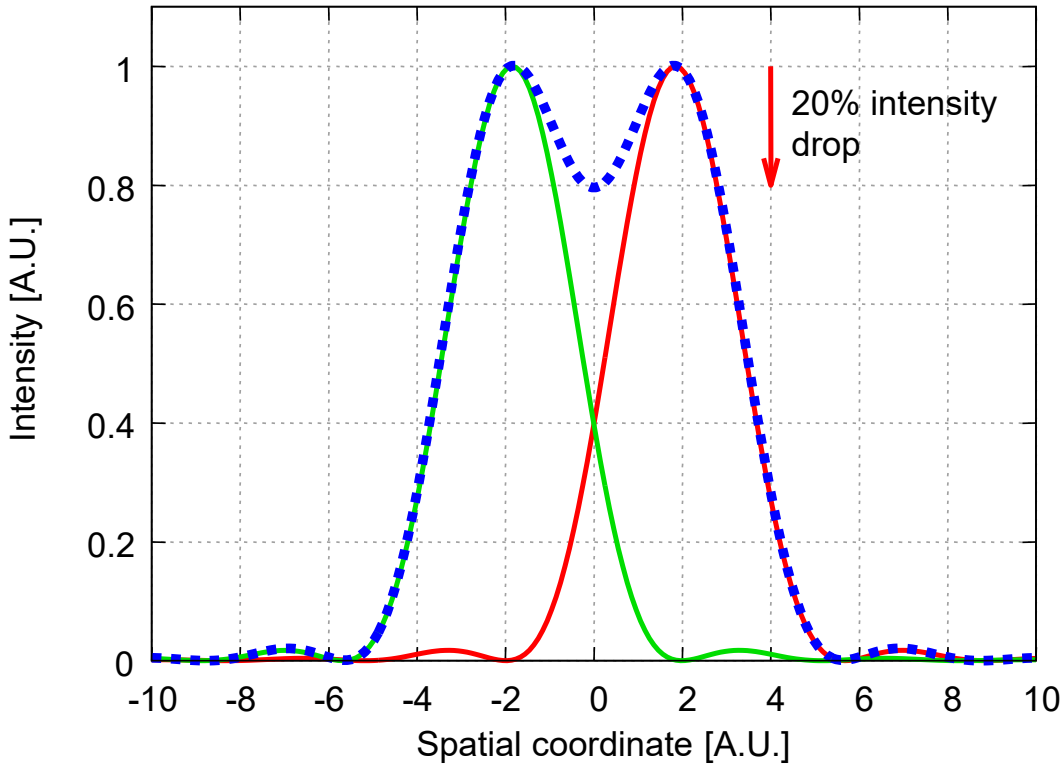

The **Rayleigh criterion** is the generally accepted, although arbitrary, criterion for the minimum resolvable detail – the imaging process is said to be diffraction-limited when the first diffraction minimum of the image of one source point coincides with the maximum of another.

Numerical aperture and resolution

Rayleigh criterion:

resolution ~ 0.61λ /NA

For dry samples, NA < 1.0

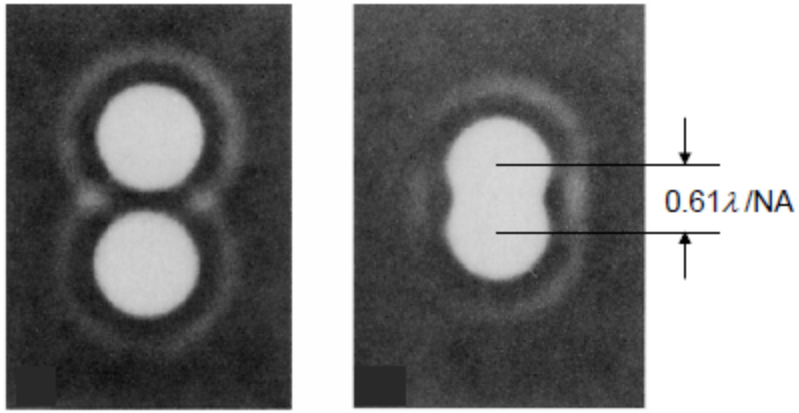

clearly resolved resolution limit

Ref: M. Born and E.Wolf, *Principles of Optics*, 6th ed. (Pergamon, Oxford, 1980), Chap. 8.

Numerical Aperture

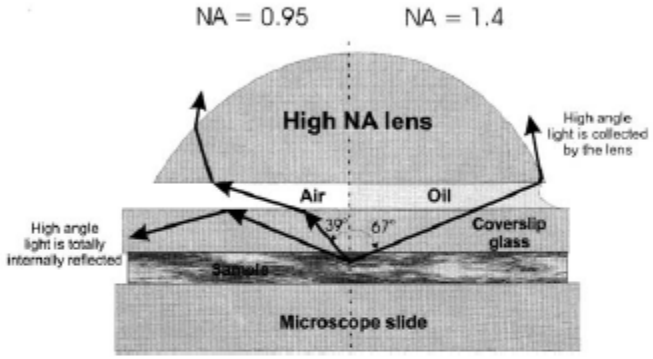

$NA = n\sin\theta$ n: refractive index

Lens in air:

n of air: 1

$\sin\theta \leqslant 1$

$\Big\}$ $NA \leqslant 1$

Lens in oil:

n of oil >1, similar to coverslip glass (~1.5)

$\sin\theta$ increase (total internal reflection occur at high θ)

Overall NA will increase, >1

$$R = \frac{1.22\lambda}{2NA_{objective}}$$

$$= \frac{1.22\ (400nm)}{2(1.4)}$$

$$= \sim 175nm$$

Numerical Aperture

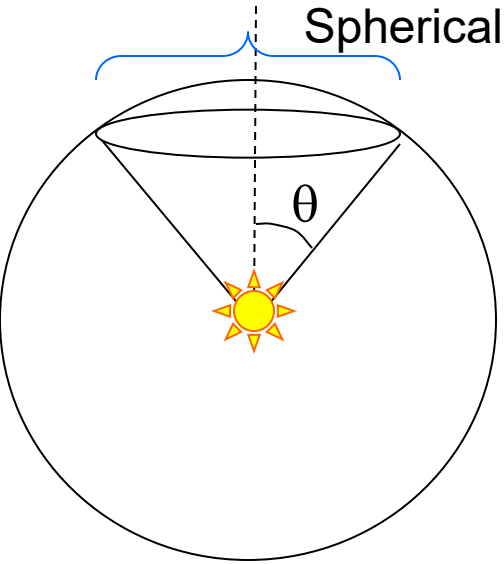

Light collection efficiency

S/4π

NA/n = 1 , 50%

NA/n = 0.6, 10%

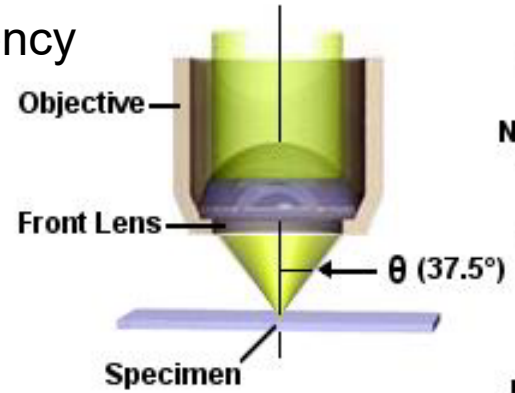

NA = n sin(θ)
0.60 = 1.0 sin 37.5°

NA = Numerical Aperture
n = Refractive Index
= 1.00 (Air)
θ = Angular Aperture

Approximate Magnification 40x

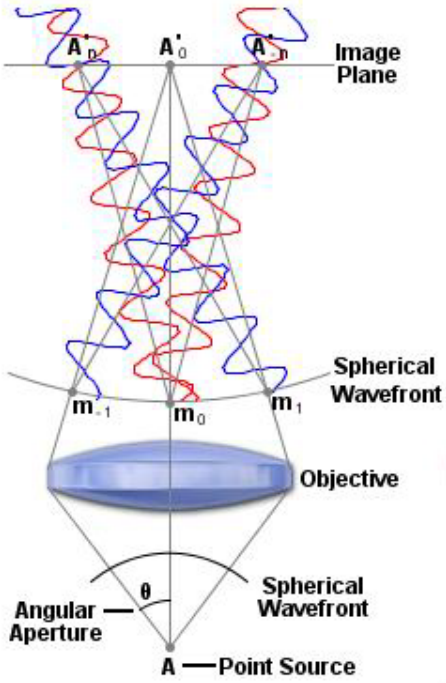

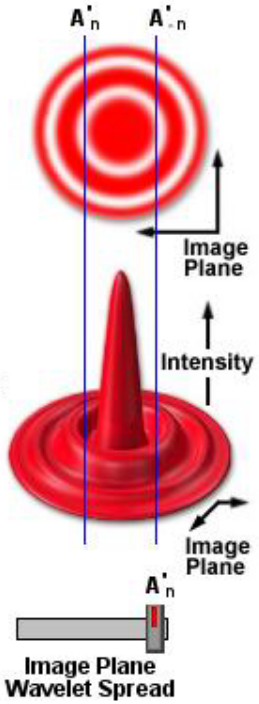

$$D = \frac{1.22 \cdot \lambda}{NA}$$

Fluorescence Microscope

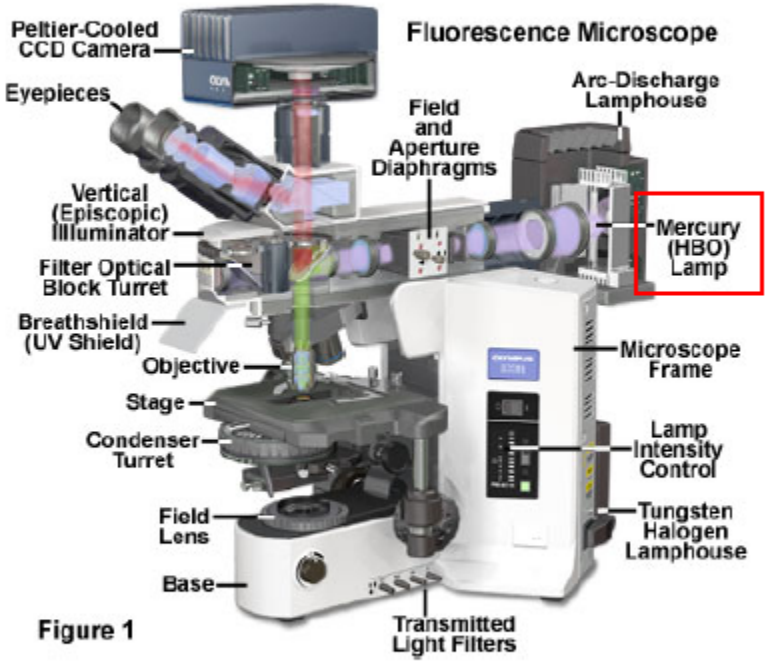

Figure 1

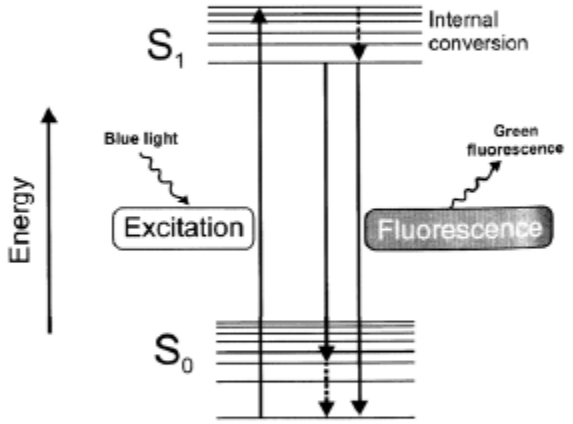

Fluorescence is the property of some atoms and molecules to absorb light at a particular wavelength and to subsequently emit light of longer wavelength

Fluorescence Microscope

Especially useful in the examination of biological samples:

- *Identify* the particular molecules in complex structure (e.g. cells)
- *Locate* the spatial distribution of particular molecules in the structure
- Biochemical dynamics
- High signal to noise ratio
- Both reflected and fluorescence light

Drawback:

- Chemical labeling

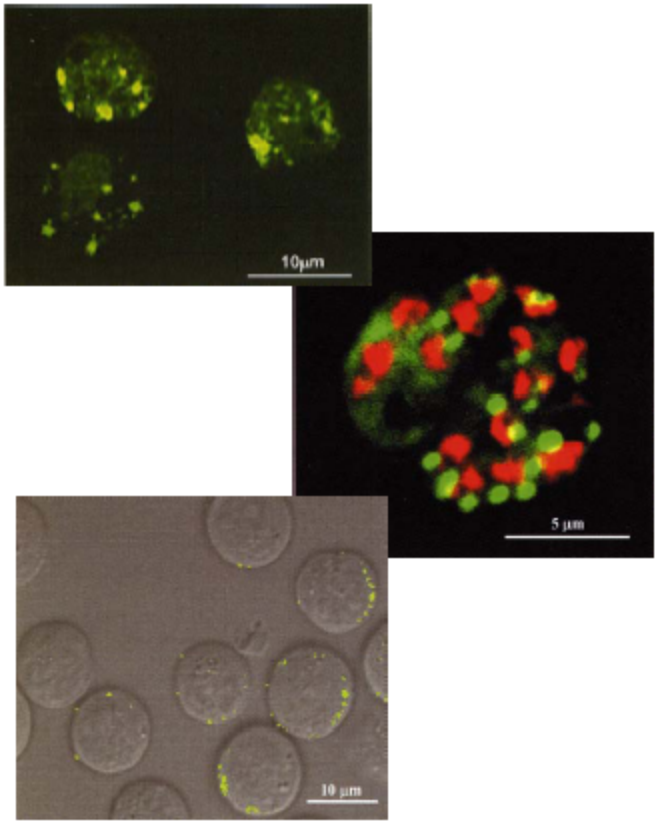

Multiphoton Microscopy

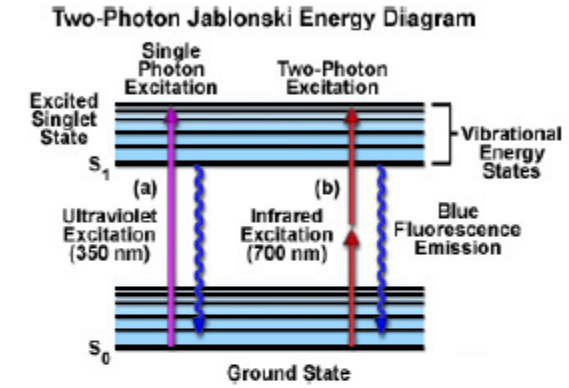

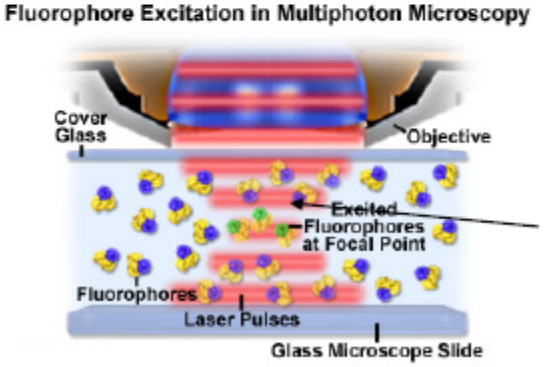

IR light can penetrate deeper into the tissues.

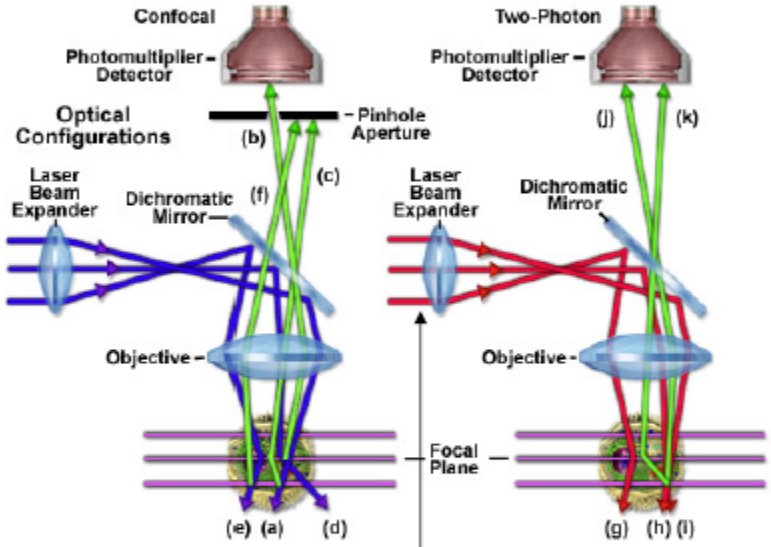

Femtosecond laser pulses are required to perform two-photon excitation.

Images are from http://micro.magnet.fsu.edu/

One-photon excitation

Two-photon excitation

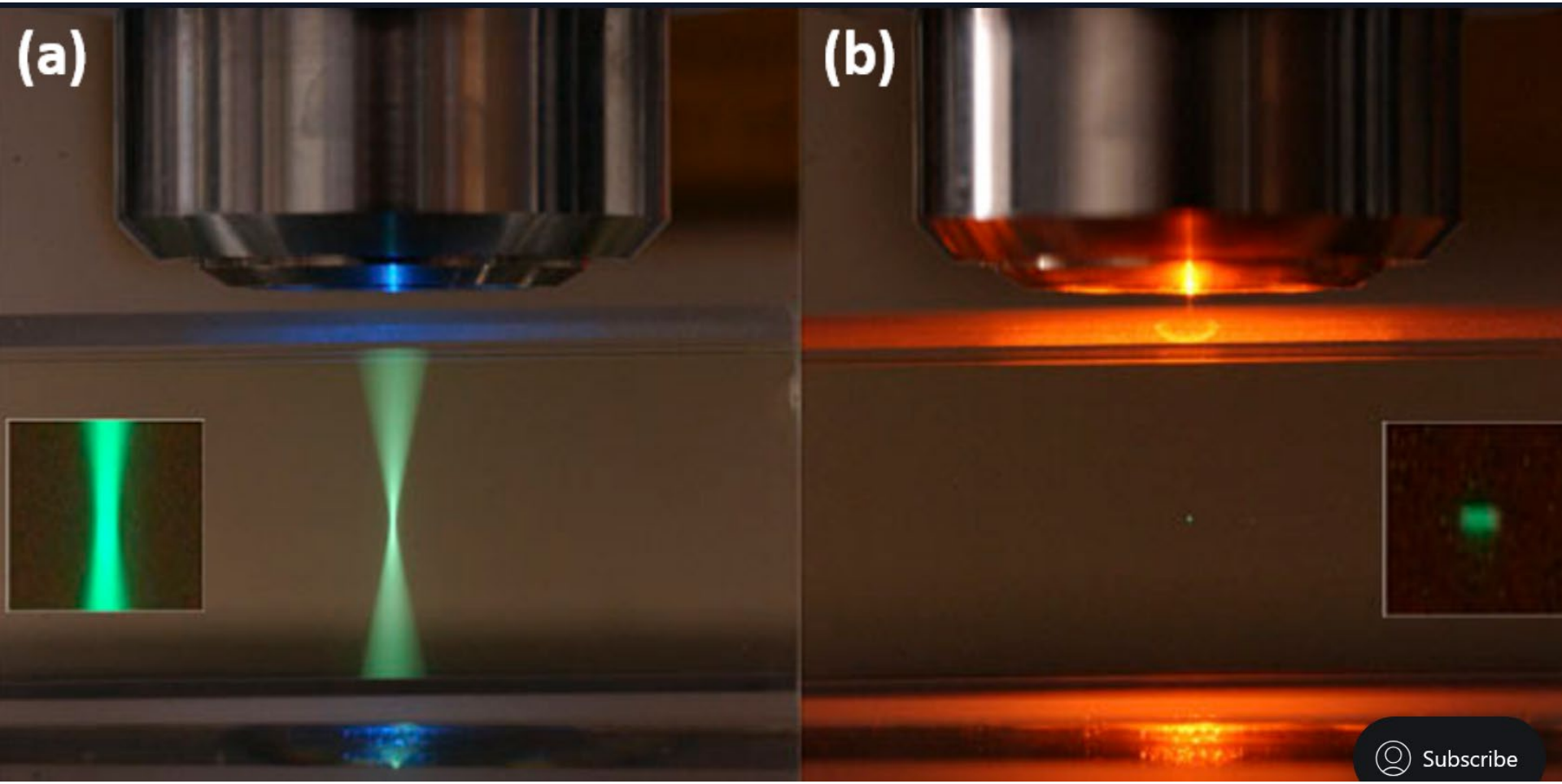

Imaging modes: wide-field vs confocal

CONVENTIONAL WIDEFIELD IMAGING

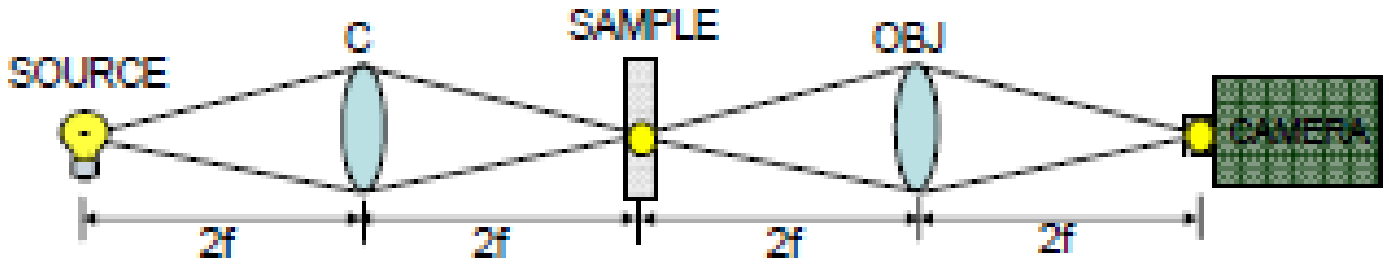

- Extended source
- Entire volume is illuminated
- Fast
- No axial sectioning (z-imaging)
- Relatively Inexpensive

Wide-field fluorescence microscope (SM4)

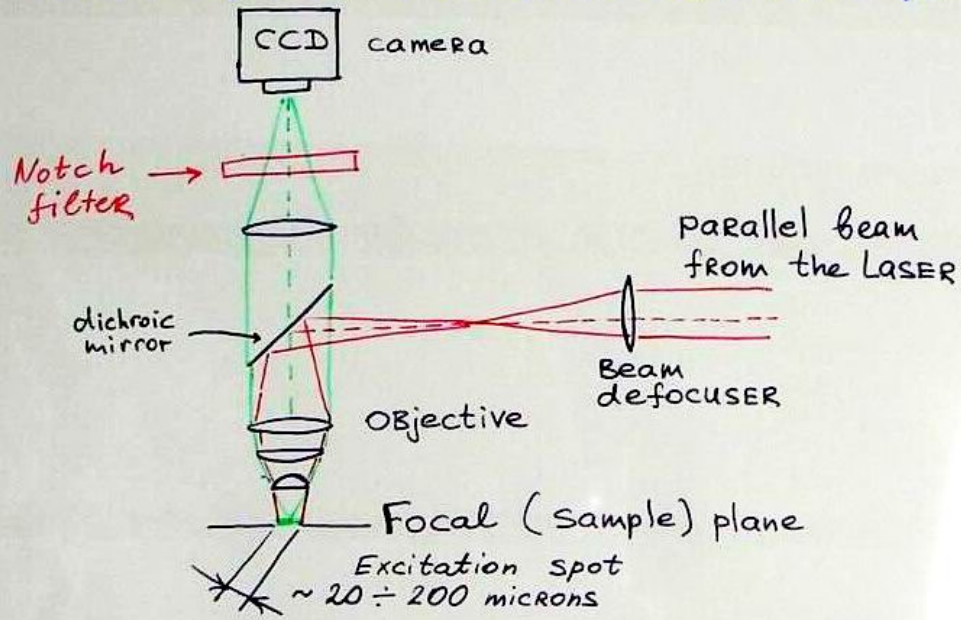

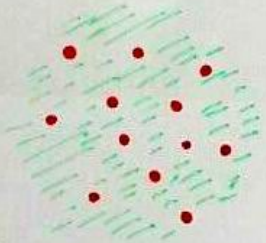

Advantage: many molecules are observed at a time

disadvantage: High background signal

CONFOCAL IMAGING

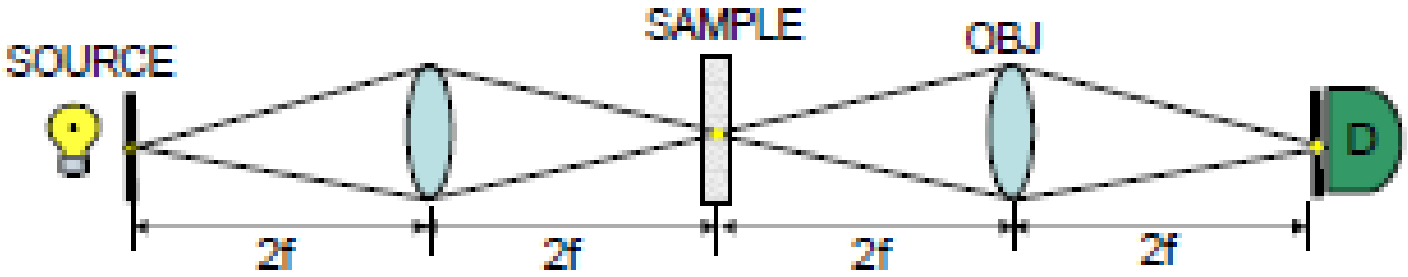

- Point source
- Minsky (1957) wanted images of neural networks from brains
- Rejects "out-of-focus" light
- Axial sectioning (z-imaging); 3D imaging possible
- Requires scanning
- Loose some "valuable" photons; Laser-based is expensive

$$d_{lateral} = \frac{0.4}{NA}\lambda \qquad d_{axial} = \frac{1.4n}{(NA)^2}\lambda$$

ex: λ=500 nm, NA =1.4, n =1.51
$d_{lateral}$ ~140 nm; d_{axial} ~ 540 nm

Confocal microscope

SMS

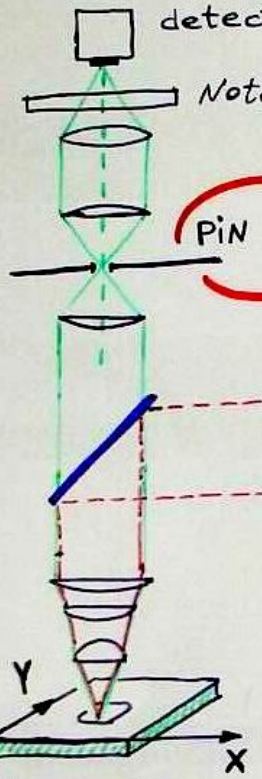

XY - piezo stage

Excitation light is focussed into a confocal spot (diffraction limited)

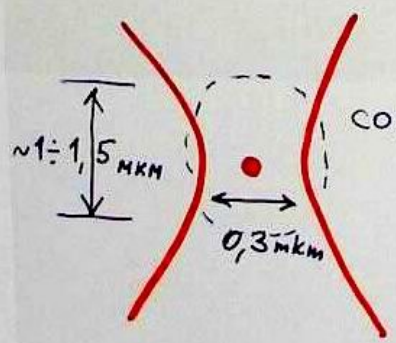

How the Pin Hole works

(SM6)

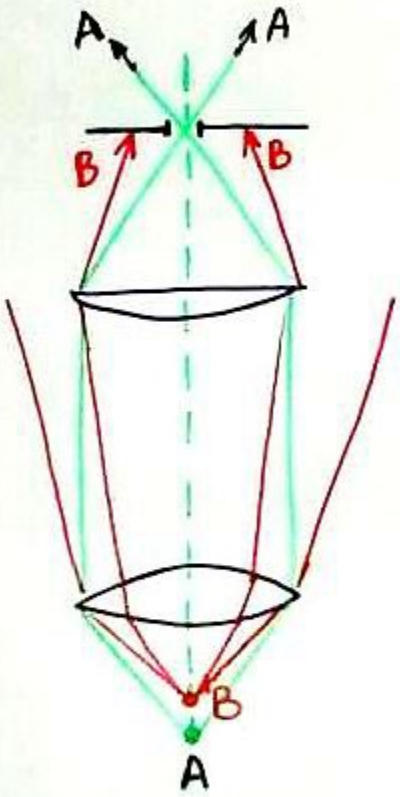

Fluorescence from the confocal volume is passing

All other light is blocked!

B is out of focuse.
A is in focuse

3D-imaging

A little bit of theory: PSF

The point spread function (PSF) describes 3-D light distribution in an image of a point source (for a given lens). An x-y slice through the center of the wide-field point spread function reveals a set of concentric rings: the so-called Airy disk that is commonly referenced in texts on classical optical microscopy.

Optical units:

$$\upsilon = d \cdot \frac{2\pi}{\lambda} \sin\theta \qquad u = z \cdot \frac{2\pi}{\lambda} \sin^2\theta$$

$$I(0,\upsilon) \propto \left| \frac{2J_1(\upsilon)}{\upsilon} \right|^2 \qquad I(u,0) \propto \left(\frac{\sin(u/4)}{u/4} \right)^2$$

Lateral and axial intensity distributions

THE (1st) FOCUSING PROBLEM

- Focusing of light results in asymmetric focal spot
- Axial spot is longer than lateral
- For aberration-free lens

$$d_{lateral} = \frac{0.61}{NA}\lambda$$

$$d_{axial} = \frac{2n}{(NA)^2}\lambda$$

ex: λ=500 nm, NA =1.4, n =1.51
$d_{lateral}$ = 200 nm; d_{axial} = 770 nm

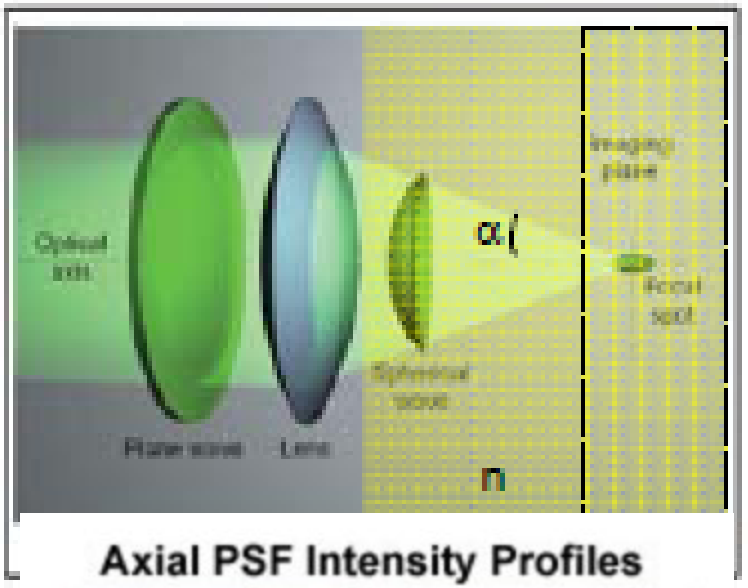

Axial PSF Intensity Profiles

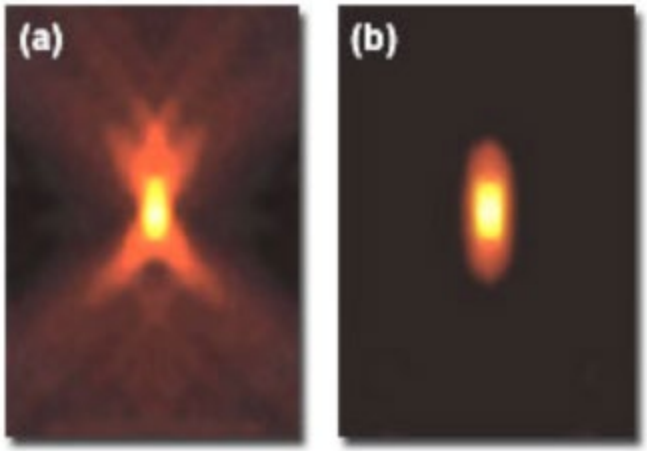

Wide field Confocal

Three-dimensional point-spread function

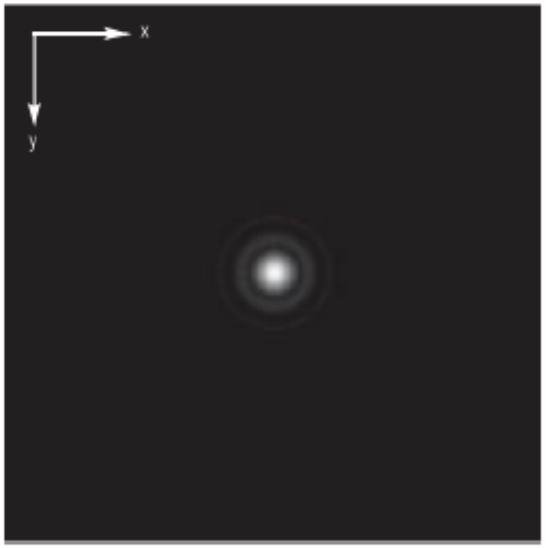

Lateral:

$$FWHM_{ill,lateral} = 0.51 \frac{\lambda_{exc}}{NA}$$

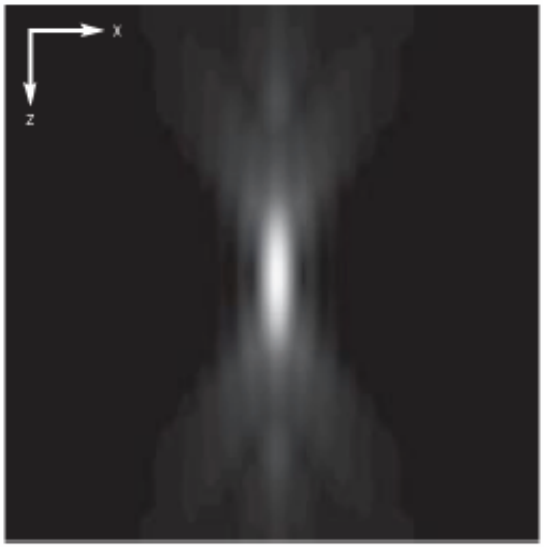

Axial:

$$FWHM_{ill,axial} = \frac{0.88 \cdot \lambda_{exc}}{(n-\sqrt{n^2-NA^2})}$$

n = *refractive index of immersion liquid,*
NA = *numerical aperture of the microscope objective,*
λ_{exc} = *wavelength of the excitation light*

Ref: Carl Zeiss, *Confocal Laser Scanning Microscopy*

Laser Scanning Confocal Microscope

Important technique for live cell and tissue imaging, the studies of biochemical dynamics!

Advantages:

- Optical sectioning ability
- 3D reconstruction
- Excellent resolution (0.1-0.2 μm)
- Specific wavelengths of light used
- Very high sensitivity

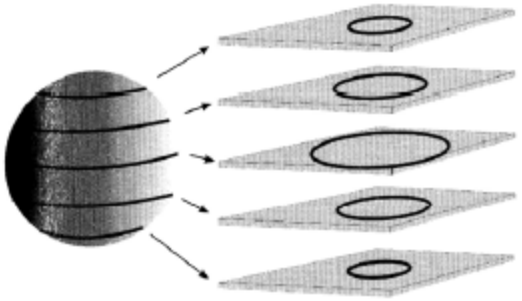

Optical sectioning

Drawbacks:

- Expensive
- Complex to operate
- Chemical labeling
- High intensity laser light

Confocal microscopy

Improved depth resolution

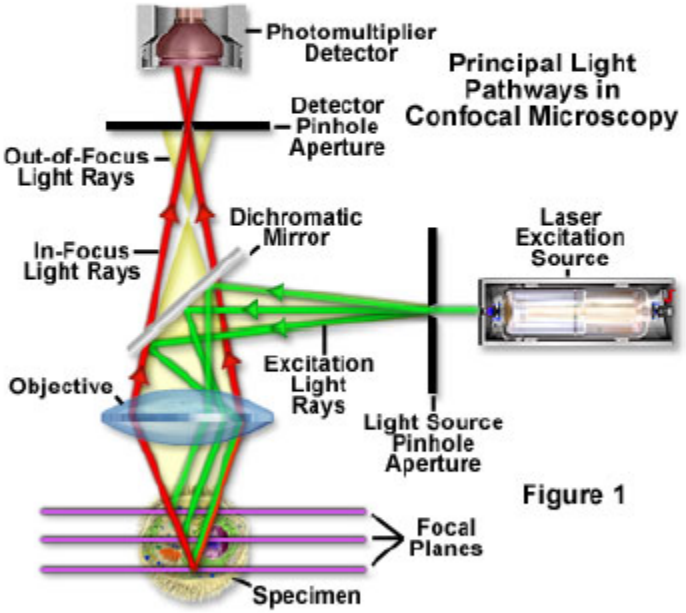

Figure 1

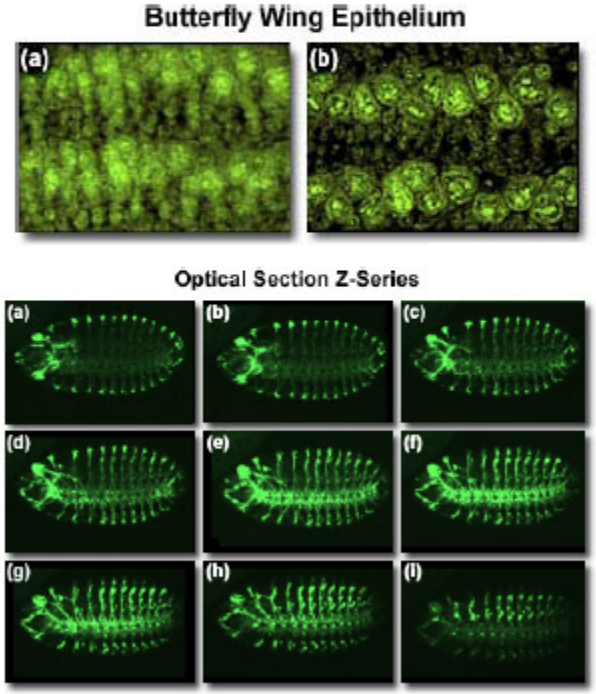

Images are from http://micro.magnet.fsu.edu/

Confocal fluorescence microscope Wide-field fluorescence microscope

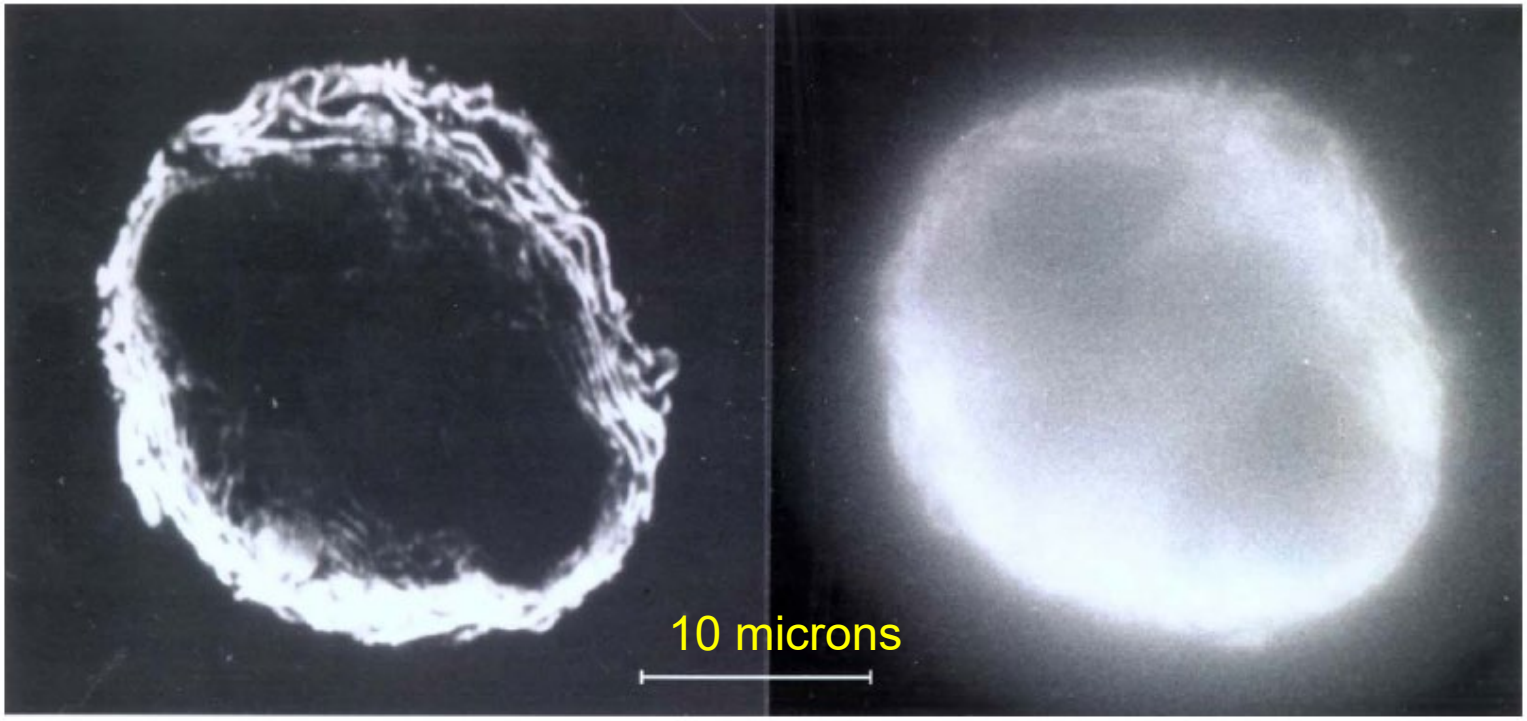

Fig. 3. An early comparison of a conventional epi-fluorescence image with a confocal one obtained with the polygon scanner. The specimen is a plasmacytoma cell labelled with anti-endoplasmin, which binds chiefly to cisternae of the endoplasmic reticulum. In the conventional image it is not possible to establish whether the central nucleus lacks endoplasmin and the individual cisternae are unclear. Scale bar = 10 um. (Specimen prepared by Gordon Koch. Image previously published in the Journal of Cell Biology, 105, p44 (1987)).

Confocal and Widefield Fluorescence Microscopy

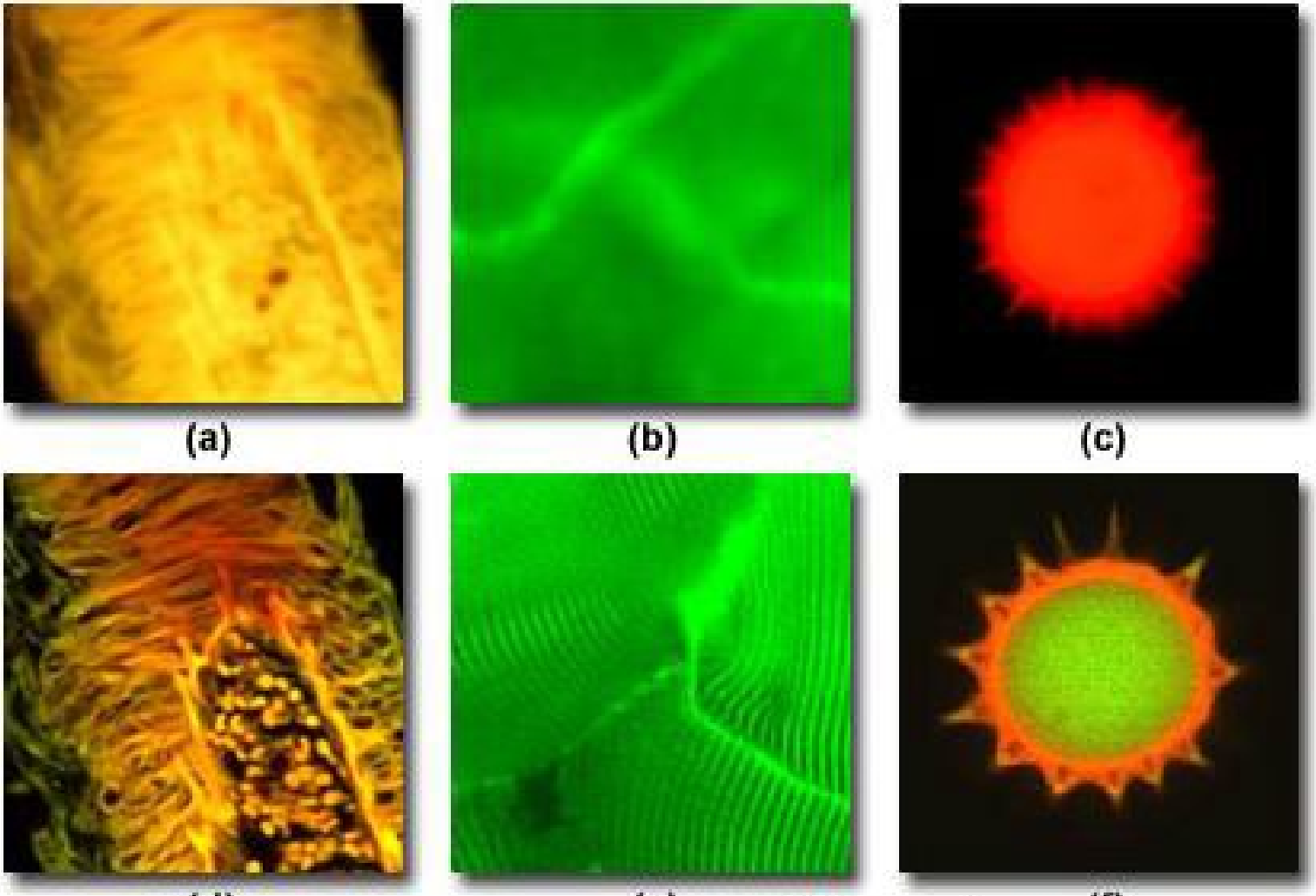

Figure 1

INTENSITY POINT SPREAD FUNCTION

- Useful to look at intensity PSF, $|h(\rho,z)|^2$
- We can break this down into $|h_{ill}(\rho,z)|^2$ and $|h_{det}(\rho,z)|^2$ for illumination and detection, respectively
- In general, $|h_{ill}(\rho,z)|^2$ and $|h_{det}(\rho,z)|^2$ are not the same b/c of optics
- Also, for fluorescence microscopy λ_{ill} and λ_{det} are not the same

Confocal Microscopy

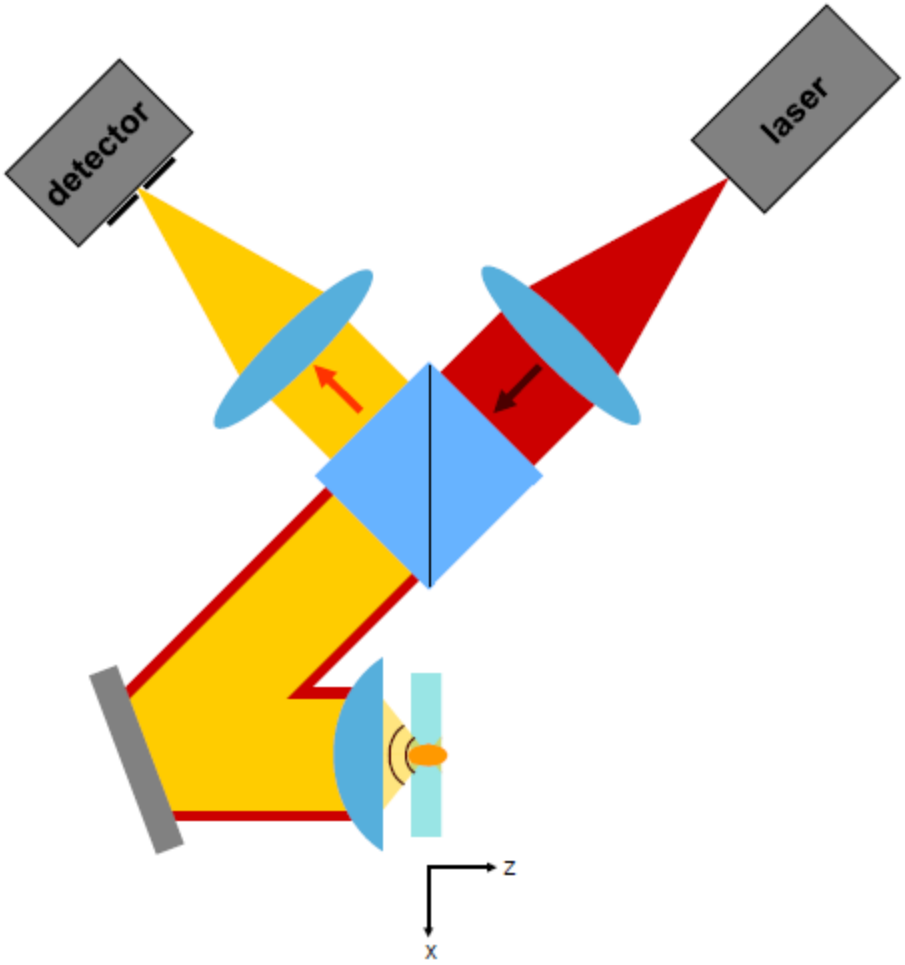

diffraction limit:

$$d_{\min} \approx 0.61 \frac{\lambda}{n \sin \alpha}$$

wavelength

numerical aperture

aperture angle

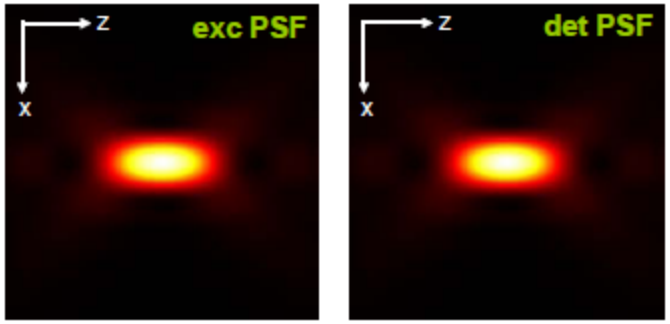

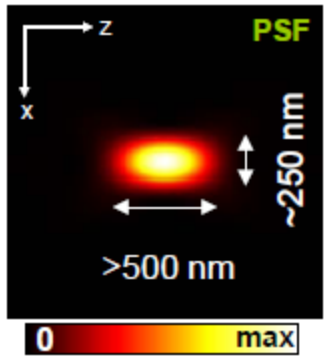

Confocal PSF

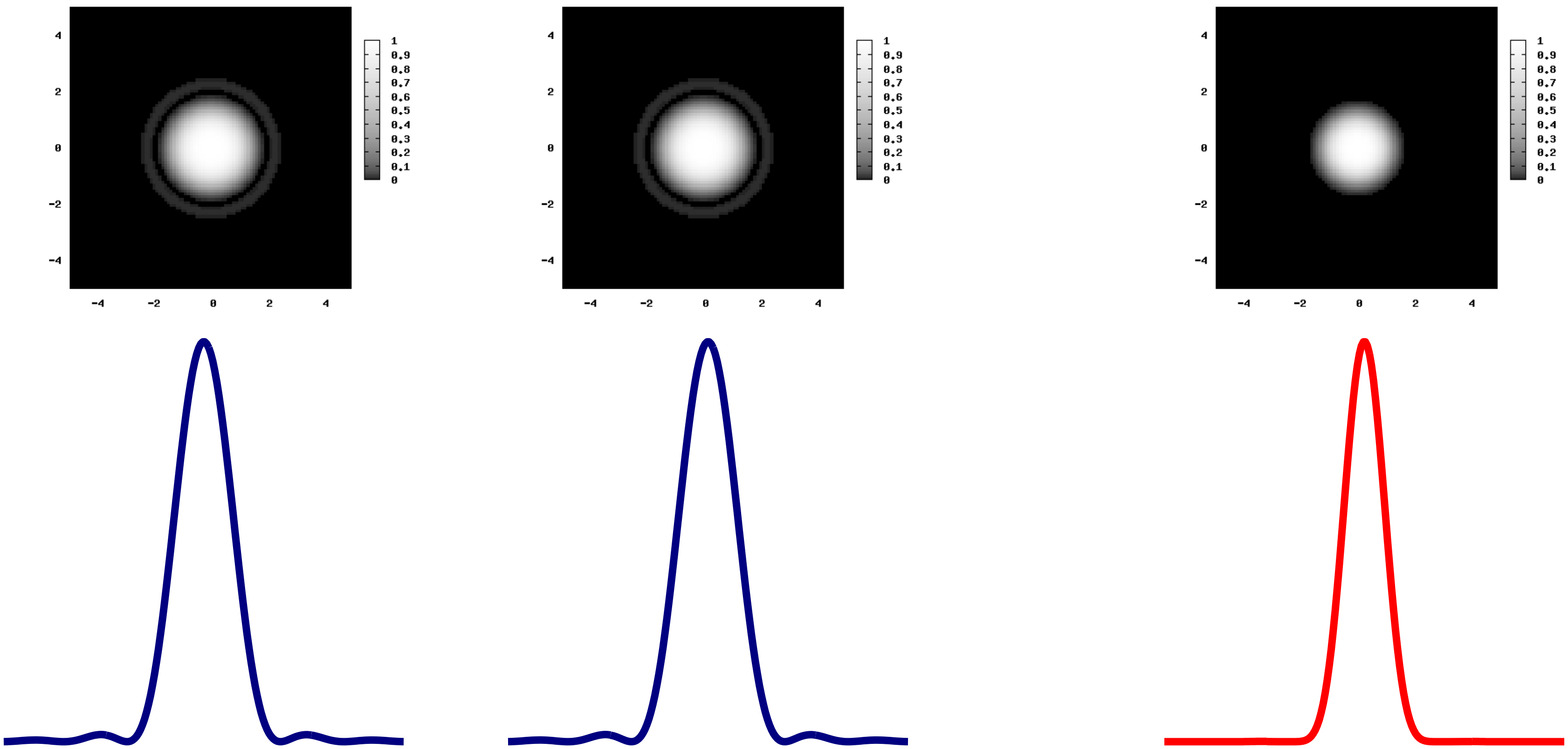

$$PSF_{exc} \bullet PSF_{det} = PSF_{conf}$$

n = 1
NA = 0.6

Confocal PSF – example

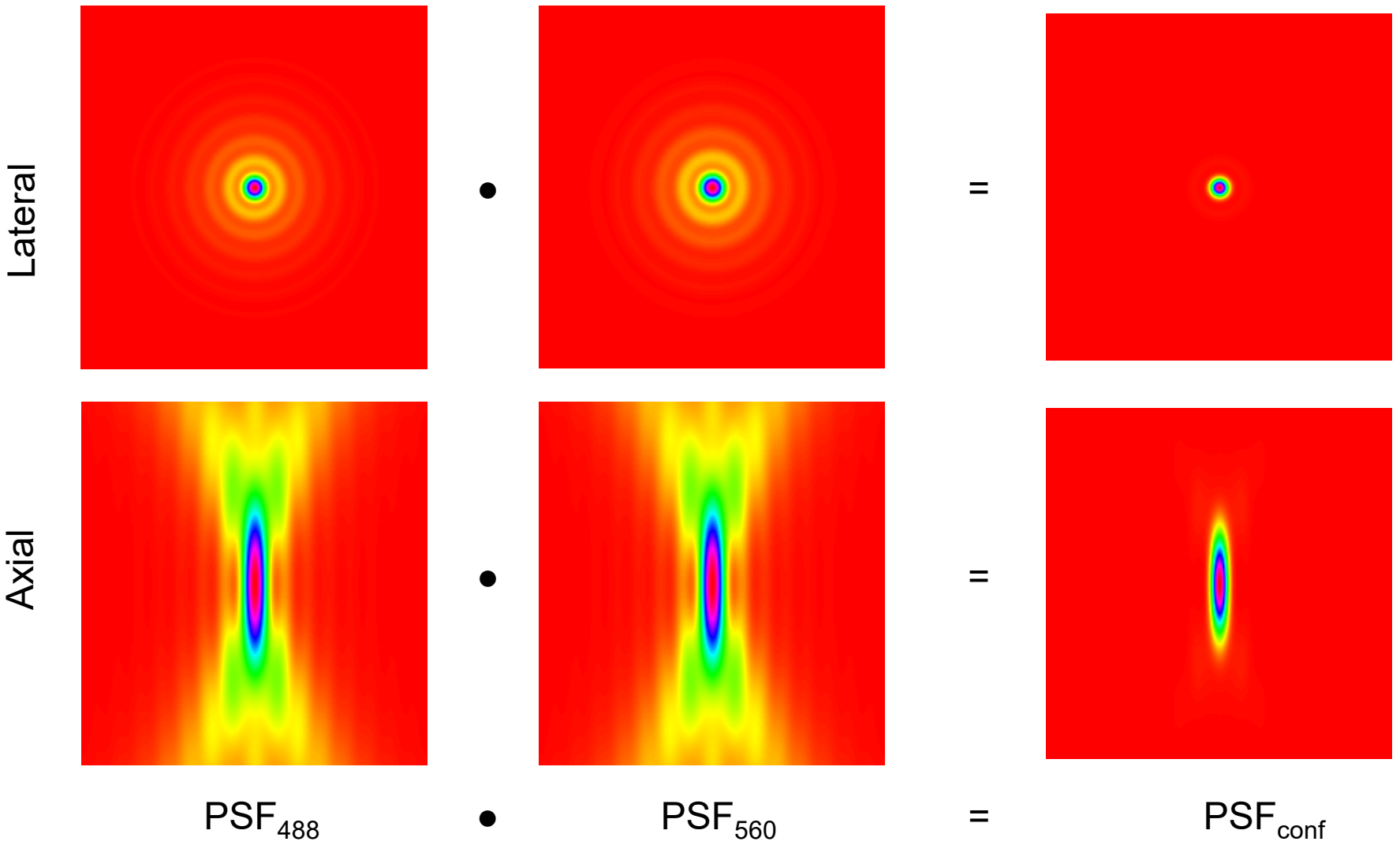

Two Approaches for Superresolution

Point-Spread-Function Engineering

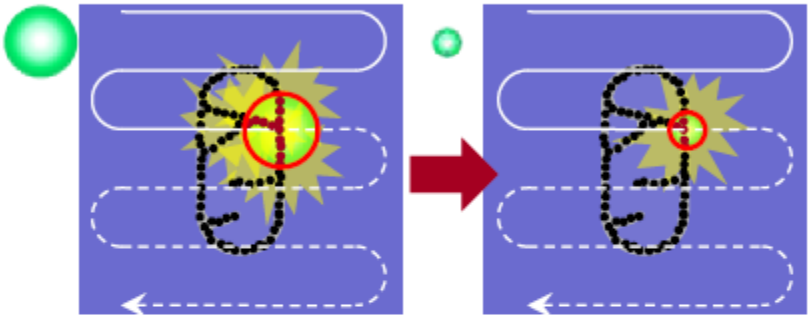

4Pi, I^{5}M, struct. illumination, …

Breaking the diffraction limit:

Targeted optical switching /non-linearity

STED, GSD, saturation, …

Single Molecule Localization

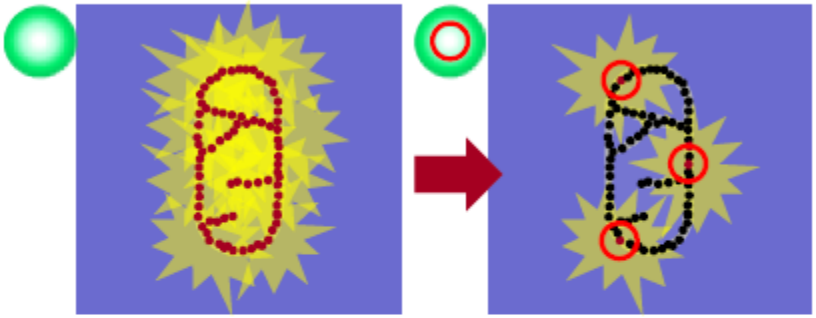

Related to particle tracking

Breaking the diffraction limit:

Stochastic optical switching

PALM, FPALM, STORM, …

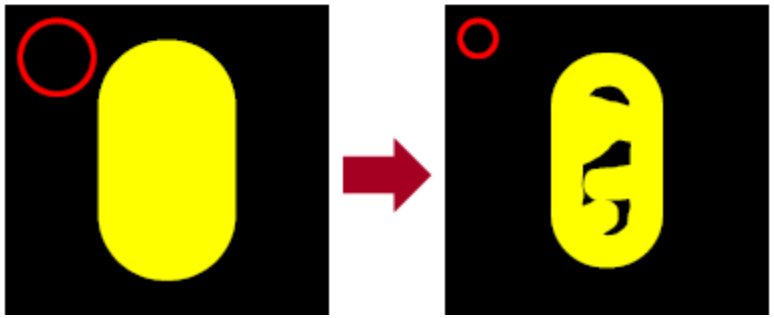

4Pi Microscopy

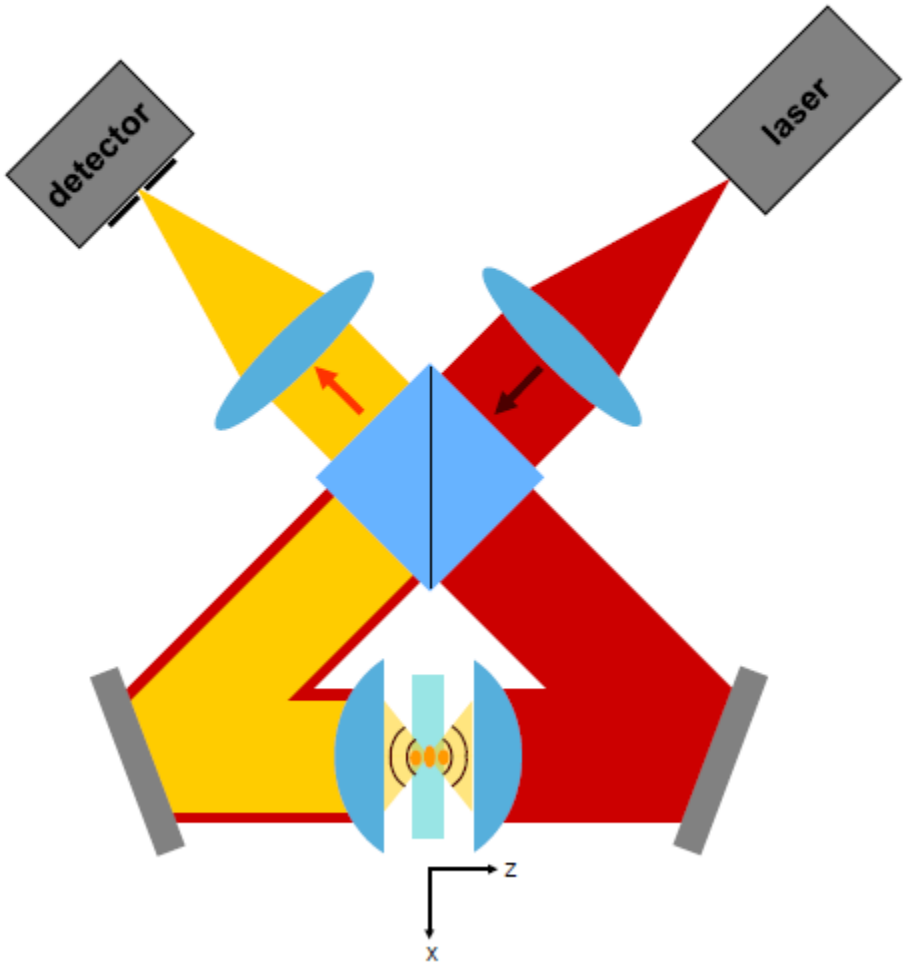

Stefan Hell 1990, 1992

Coherent excitation with two opposing objectives

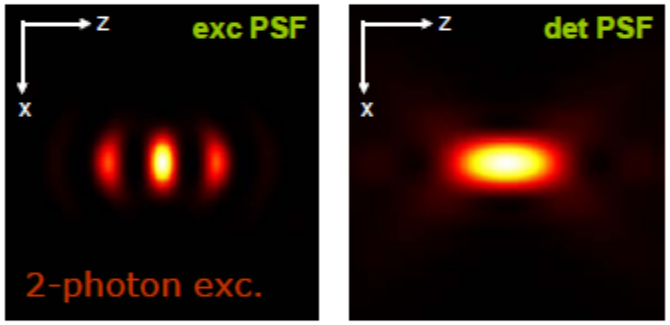

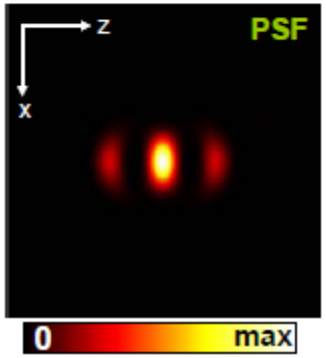

Type C 4Pi Microscopy

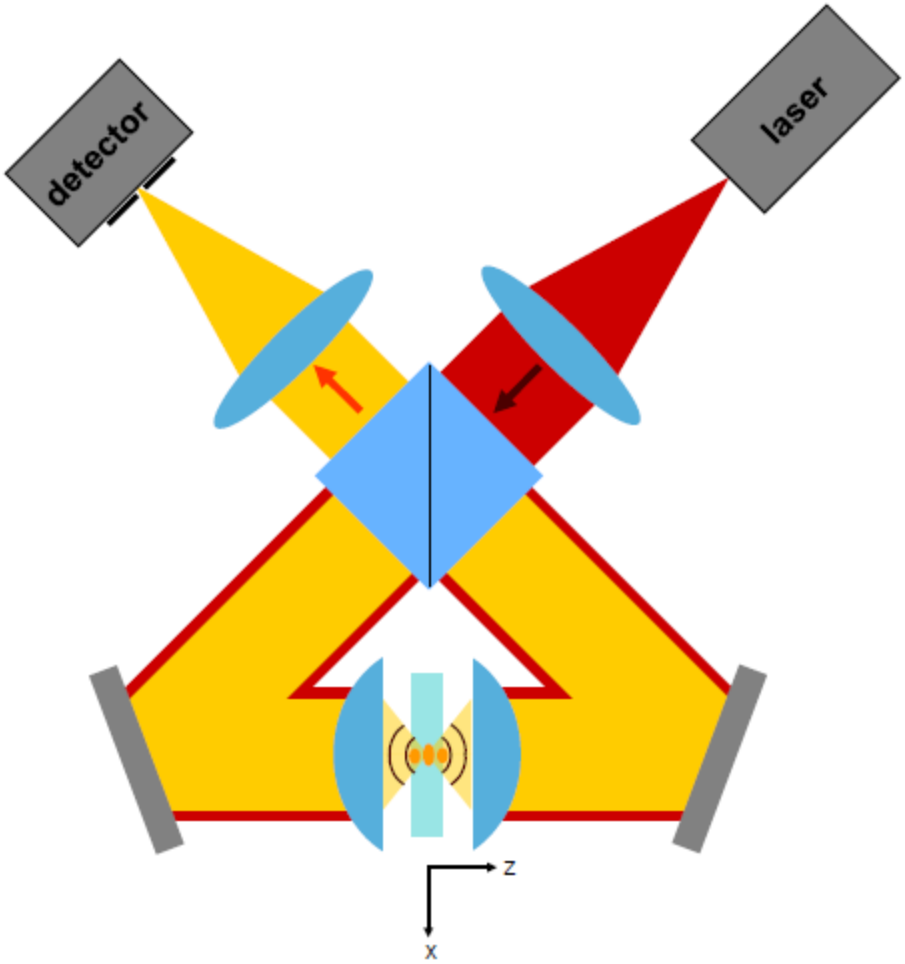

Type A 4Pi

coherent excitation & regular conf. detection

Type C 4Pi

coherent excitation & coherent detection

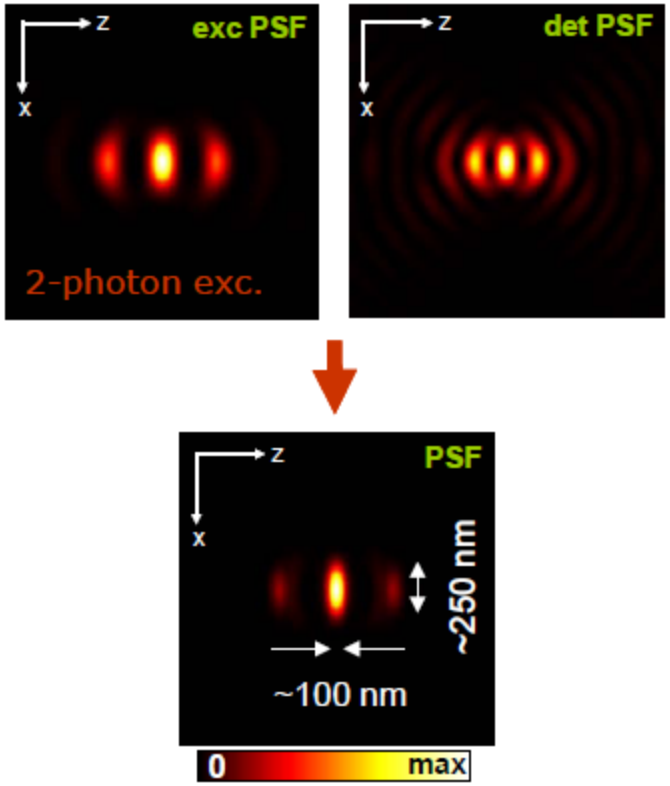

4Pi Microscopy

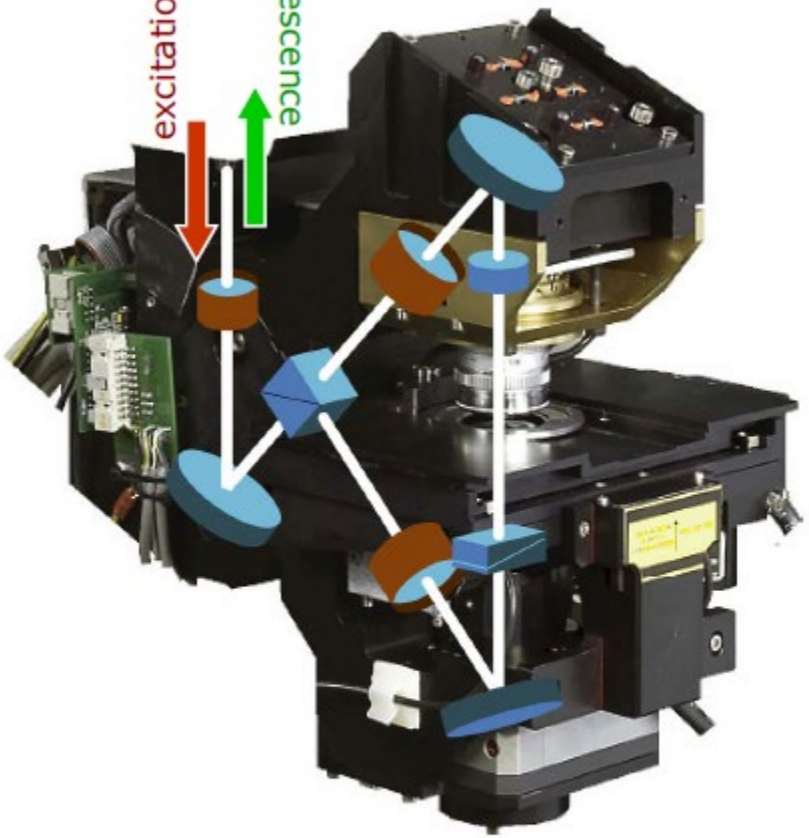

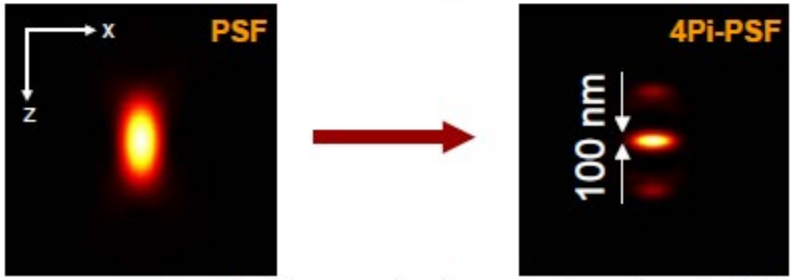

Gugel, Bewersdorf et al., *Biophys. J.* 2004

4Pi Microscopy Enhances the Depth Resolution

(confocal) Laser Scanning Microscope

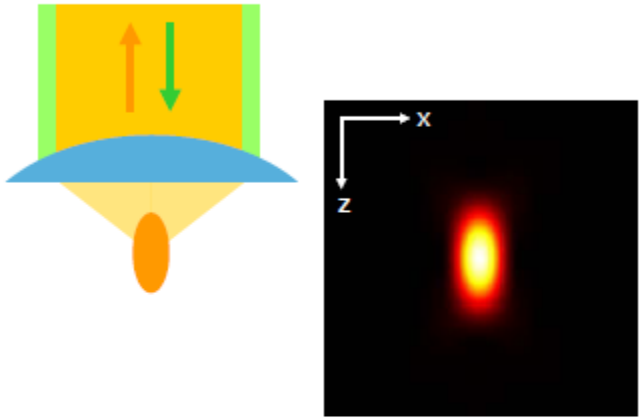

4Pi Microscope

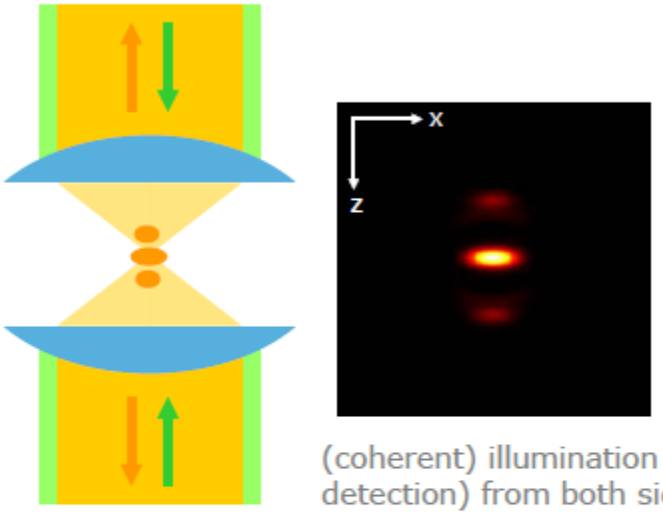

(coherent) illumination (and detection) from both sides

Depth resolution ca. 600 nm
Lateral resolution ca. 250 nm

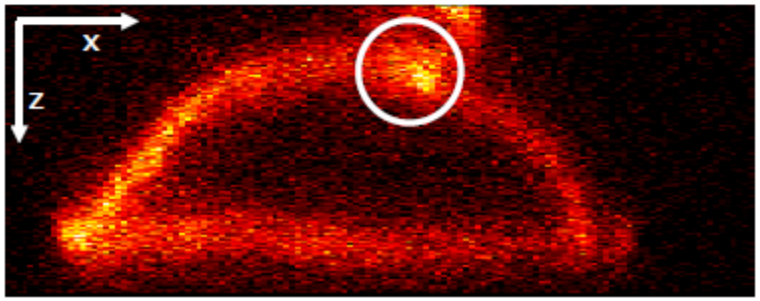

Depth resolution ca. 100 nm - 6x better
Lateral resolution ca. 250 nm - equal

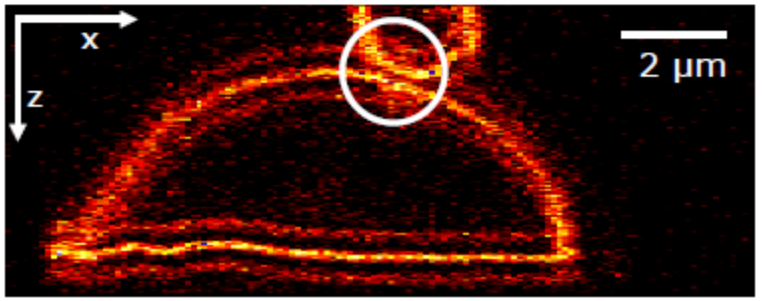

Nano Lett. 2014, 14, 211−216

NANO LETTERS

pubs.acs.org/NanoLett

Localizing and Tracking Single Nanoscale Emitters in Three Dimensions with High Spatiotemporal Resolution Using a Double-Helix Point Spread Function

Michael A. Thompson,[†,§] Matthew D. Lew,[†,⊥,§] Majid Badieirostami,[†] and W. E. Moerner*[,†]

[†]Departments of Chemistry and [⊥]Electrical Engineering, Stanford University, Stanford, California 94305

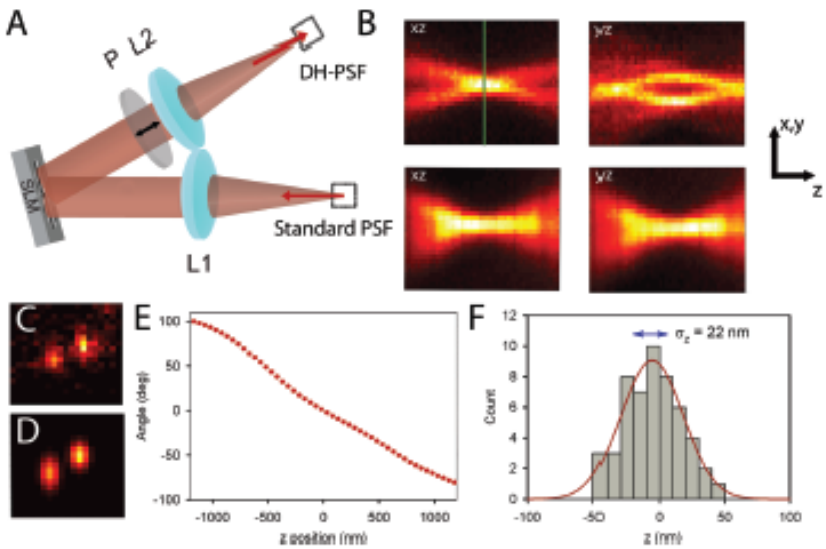

FIGURE 1. Schematic and experimental characterization of the DH-PSF imaging system. (A) Schematic of the 4*f* setup that is attached to the detection path of a standard inverted microscope. See text for details. (B) Top panels are the *xz* and *yz* cross sections of the experimentally observed DH-PSF using a 200 nm fluorescent bead. For comparison, the same cross sections taken of the standard PSF of a conventional microscope are also shown in the lower panels. The green line indicates the focal plane, denoted as $z = 0$ in this paper. Note the gradual change of the standard PSF with *z* compared with the more dramatic change of the DH-PSF throughout the depth of field. The arrows correspond to scale bars that are 2 μm long in $x-y$ and 700 nm long in *z*. The *z* axis has been lengthened for clarity. (C) Image of a single DCDHF-2V molecule in PMMA taken using the DH-PSF system. This molecule emitted on average 3100 photons per acquisition on top of a background noise of 16 photons/pixel per acquisition. (D) Output of the fitting algorithm for the data shown in (C). The fitting algorithm used in this paper fits the DH-PSF as the sum of two Gaussian functions. (E) A plot of the angle between the two lobes as a function of *z* position of the emitter that is used as a calibration curve. This curve was taken using a bright 200 nm fluorescent bead. (F) Histogram of 50 localizations in *z* of the molecule shown in (C) with a Gaussian fit shown in red. The localization precision, which is the standard deviation of the distribution, is explicitly shown on the plot.

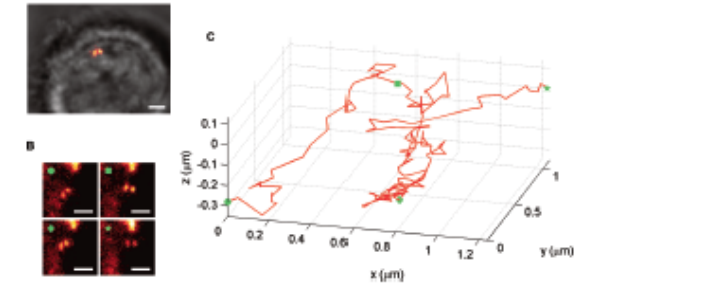

FIGURE 5. Tracking a quantum dot-labeled structure in a live cell in 3D. (A) Fluorescence image of the emitter overlaid on a white light image of the COLO205 cell (scale bar is 2 μm). (B) Images taken of the structure at different points along the trajectory showing different *z* positions, the bright aggregate at the top edge should be ignored. An average of 2400 photons/frame with a background noise of 8 photons/pixel/frame was measured for this trajectory. (C) Three-dimensional plot of the labeled structure's trajectory, showing a variety of diffusive and linear transport characteristics. Points on the curve that correspond to the images in (B) are shown by green shapes.

Breaking Diffraction Limit Using Evanescent Waves

- **Total Internal Reflection**

Evanescent wave propagating parallel to the surface

$I(z) = I(0)\, e^{-z/d}$,

$d = \lambda / [4\pi (n_3^2 \sin^2\theta - n_1^2)^{1/2}]$

TIR occurs when $\theta >=$ Critical angle, $\theta_c = \sin^{-1}(n_1/n_3)$

- **Small Aperture**
- **Metal Tip**

Total Internal Reflection Fluorescence Microscopy

Evanescent field produced adjacent to the interface between two media with a high (glass) and low (specimen) refractive index.

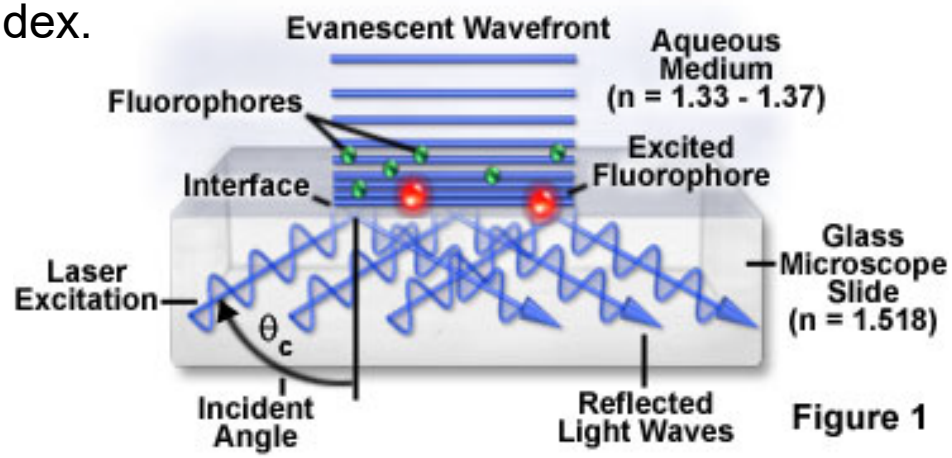

Figure 1

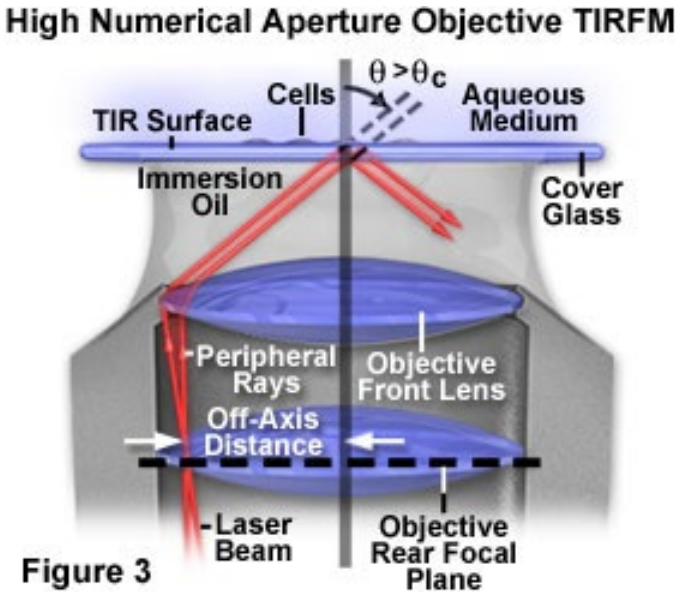

Figure 3

- Maximum depth ~ 200-300nm
- Eliminates background and out of focus fluorescence
- Optical section is only at interface

Stimulated Emission Depletion (STED) Microscopy

Prof. Stefan W. Hell (Max Planck Institute for Biophysical Chemistry)

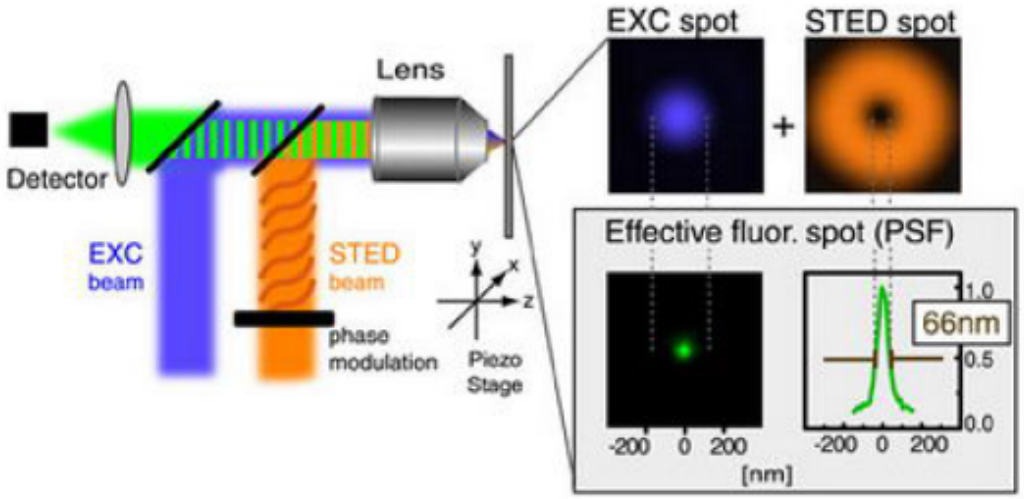

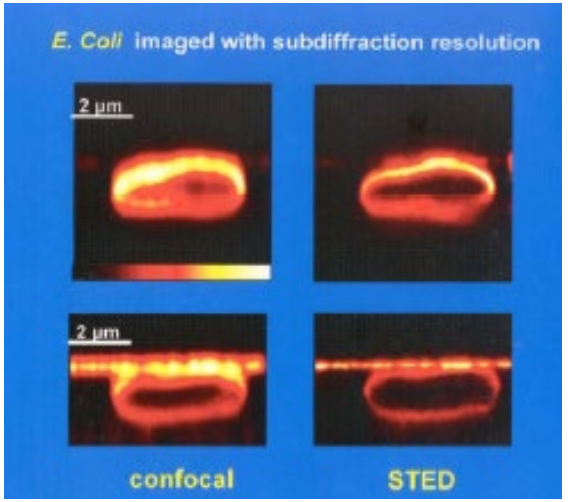

- The excitation spot is ~200 nm by focusing with a lens
- A STED beam (doughnut-shaped and centered over the excitation spot) is used to quench the fluorescent markers before they fluoresce
- Very smaller effective fluorescence spot (~60 nm)

Resolution Enhancement using STED

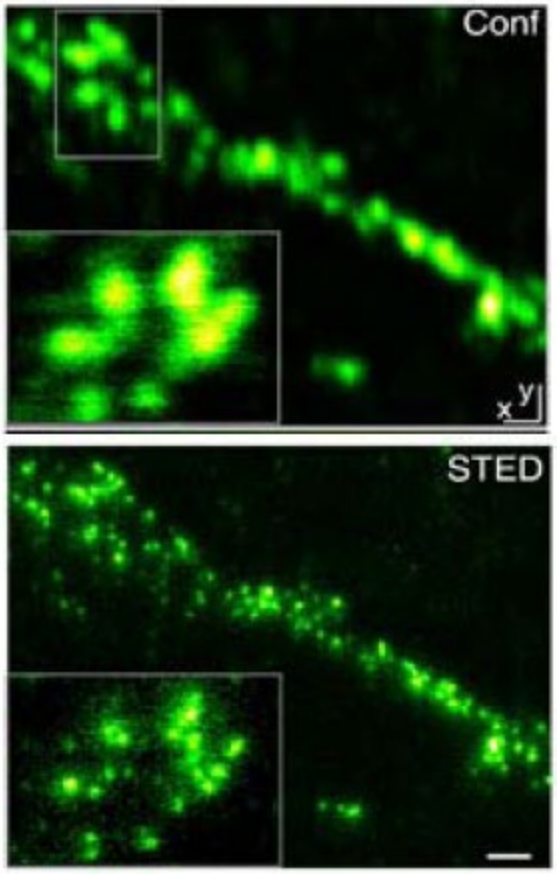

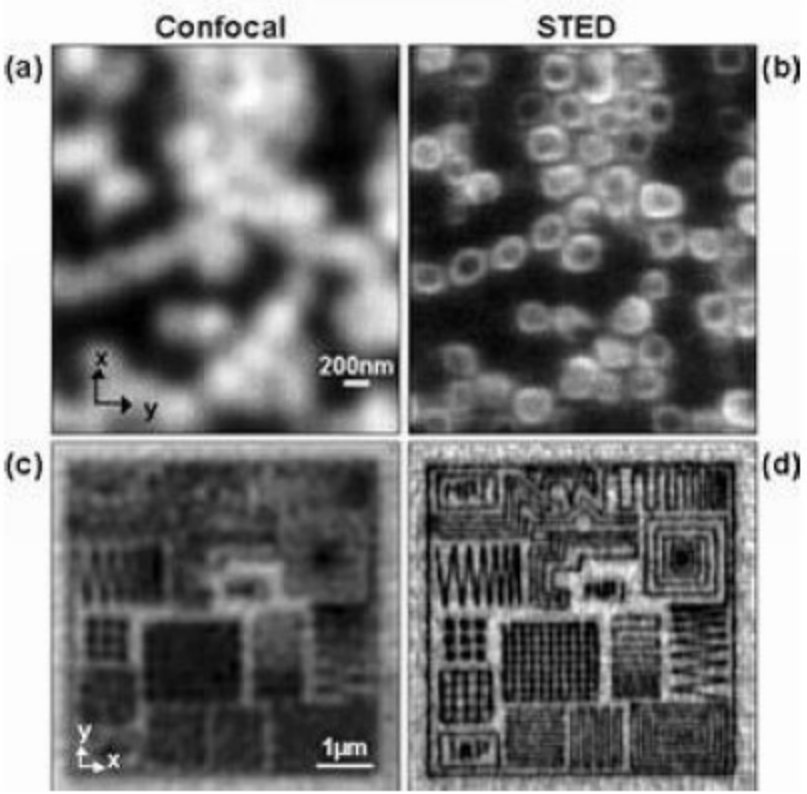

www.physorg.com

8206–8210 | PNAS | July 18, 2000 | vol. 97 | no. 15

Fluorescence microscopy with diffraction resolution barrier broken by stimulated emission

Thomas A. Klar, Stefan Jakobs, Marcus Dyba, Alexander Egner, and Stefan W. Hell†

Max-Planck-Institute for Biophysical Chemistry, High Resolution Optical Microscopy Group, 37070 Göttingen, Germany

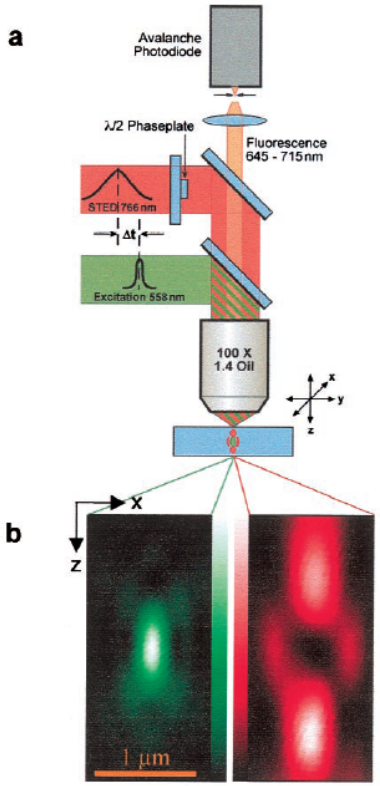

Fig. 1. Microscope. (*a*) Excitation pulses are followed by stimulated emission depletion pulses for fluorescence inhibition. After passing dichroic mirrors and emission filters, fluorescence is detected through a confocal pinhole by a counting photodiode. (*b*) Measured excitation PSF. (*c*) Measured STED-beam-PSF featuring local minimum at the center and intense maxima above and below the focal plane. Z denotes optic axis. The measurements of *b* and *c* are carried out with the pinhole removed.

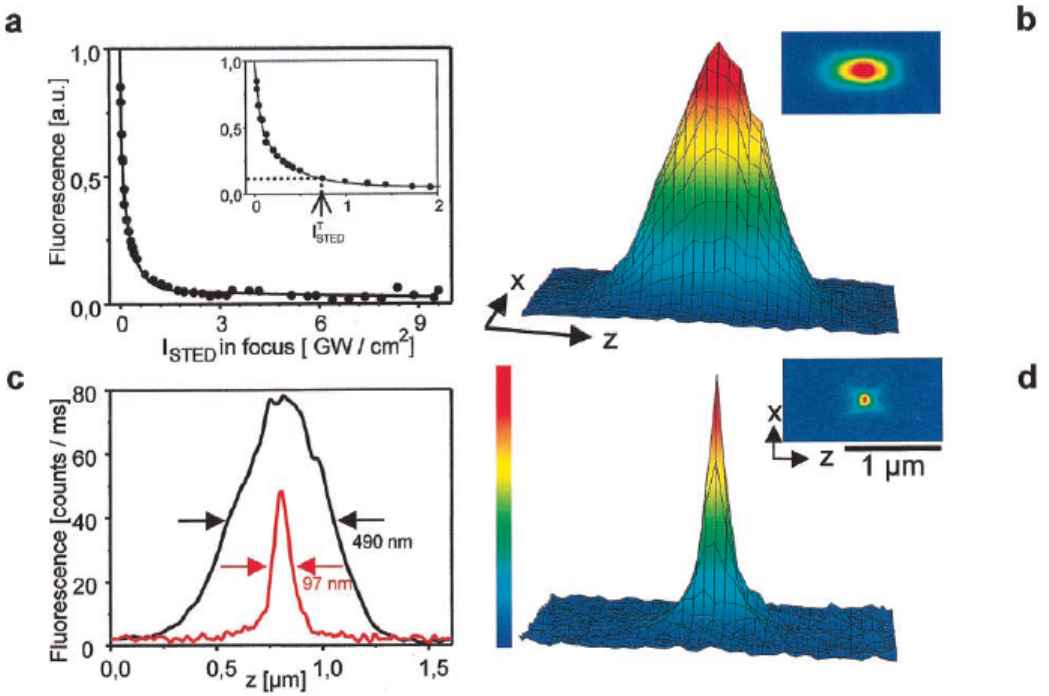

Fig. 2. (*a*) Fluorescence is a nonlinear function of stimulating intensity; 10% remaining fluorescence is obtained for I^{T}_{STED} corresponding to P_{STED} of 2.2 mW in the focus. (*b*) Surface plot of XZ-section (*Inset*) of confocal fluorescence spot for 1.4 oil immersion lens. (*d*) Same as *b* but with STED-beam PSF switched on. (*c*) Corresponding axial intensity profiles demonstrate 5.1-fold reduction of the axial width (FWHM) from 490 nm down to 97 nm.

Focal Spots of Size $\lambda/23$ Open Up Far-Field Florescence Microscopy at 33 nm Axial Resolution

Marcus Dyba and Stefan W. Hell*

High Resolution Optical Microscopy Group, Max-Planck-Institute for Biophysical Chemistry, 37070 Göttingen, Germany

(Received 19 September 2001; published 4 April 2002)

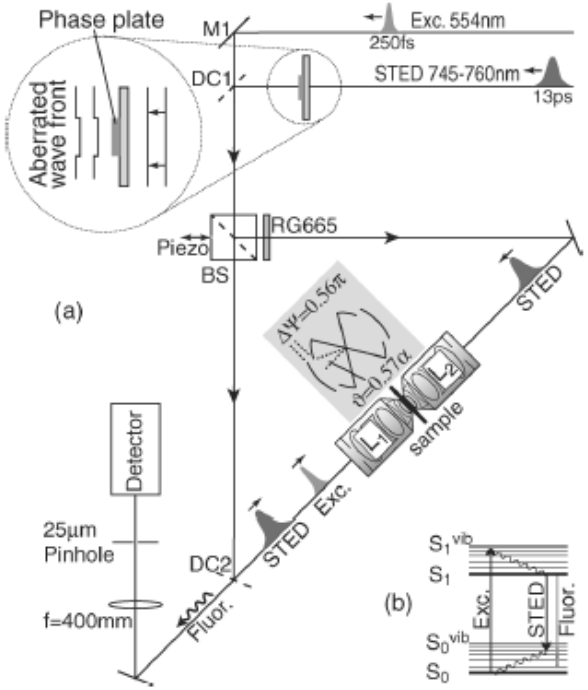

FIG. 1. STED-4Pi microscope. (a) Fluorescence excitation and detection occur via lens L_1, whereas stimulated emission is generated by the light field of counterpropagating, aberrated wave fronts of L_1 and L_2. Imaging is accomplished by scanning the sample through the sub-diffraction-sized spot of the two lenses. The inserted sketches depict the aberration induced by the phase plate on the counterpropagating STED-beam wave fronts. (b) Fluorophore energy levels.

water

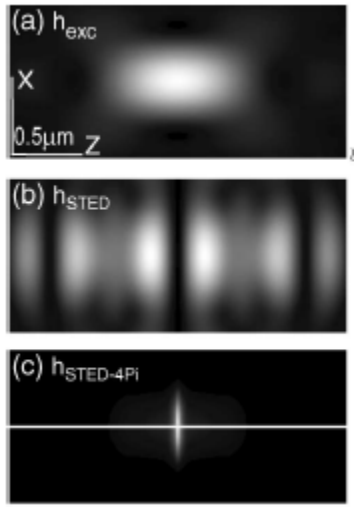

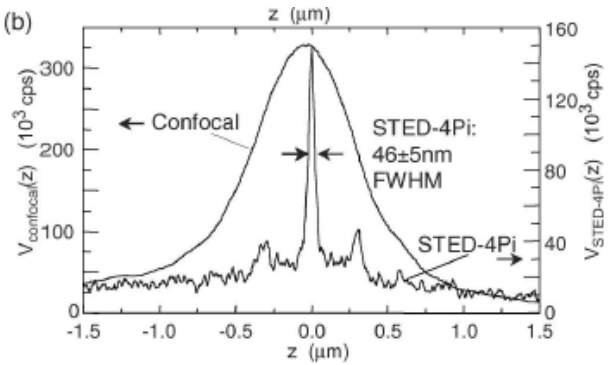

oil

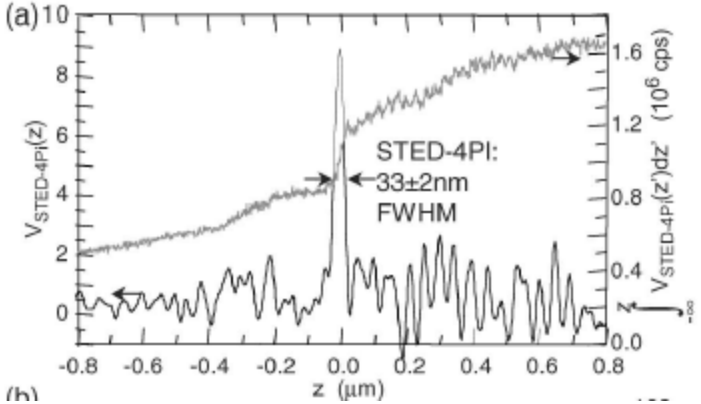

Stimulated emission depletion (STED) microscopy

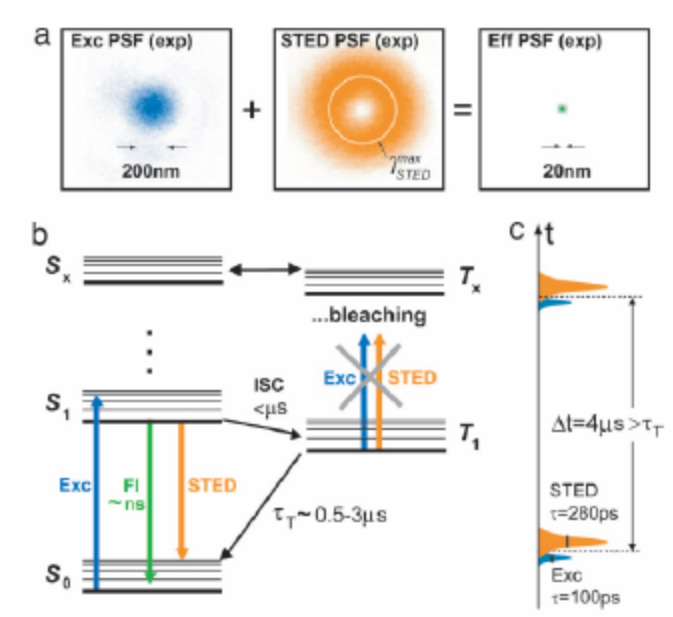

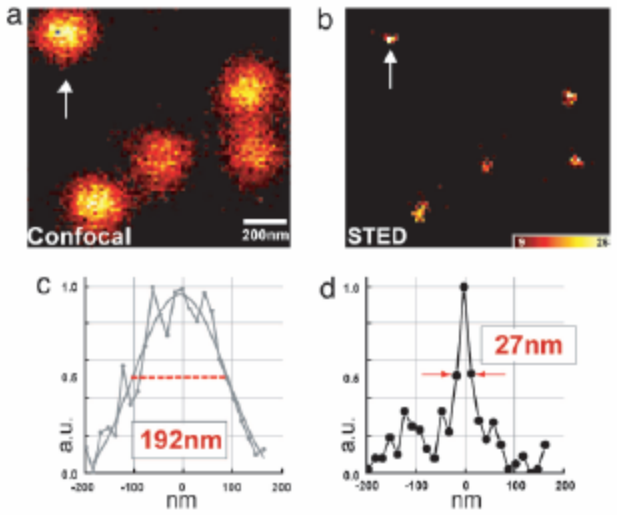

Fig. 3. Synaptotagmin I molecules form distinct spots on endosomes. (*a* and *b*) Whereas confocal microscopy exhibits a 190- to 200-nm diffraction-limited spot per endosome (*a*), STED microscopy recognizes sharp dots of 25–40 nm (*b*), both indicating its resolution as well as the punctated spatial arrangement of synaptotagmin I on the endosome. (*c* and *d*) Corresponding intensity profiles.

Ref: G. Donnert et al., *Proc. Natl. Acad. Sci. USA* **103,** 11440 (2006).

Far-Field Optical Nanoscopy

Stefan W. Hell

In 1873, Ernst Abbe discovered what was to become a well-known paradigm: the inability of a lens-based optical microscope to discern details that are closer together than half of the wavelength of light. However, for its most popular imaging mode, fluorescence microscopy, the diffraction barrier is crumbling. Here, I discuss the physical concepts that have pushed fluorescence microscopy to the nanoscale, once the prerogative of electron and scanning probe microscopes. Initial applications indicate that emergent far-field optical nanoscopy will have a strong impact in the life sciences and in other areas benefiting from nanoscale visualization.

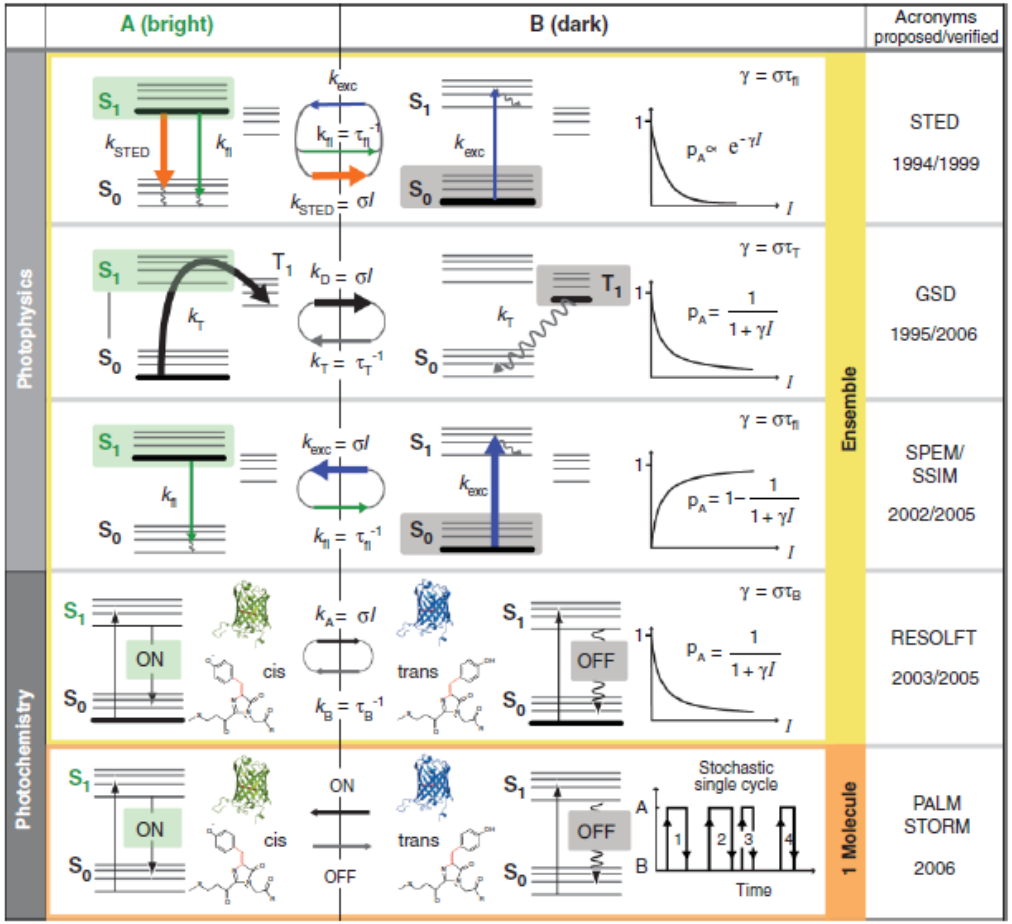

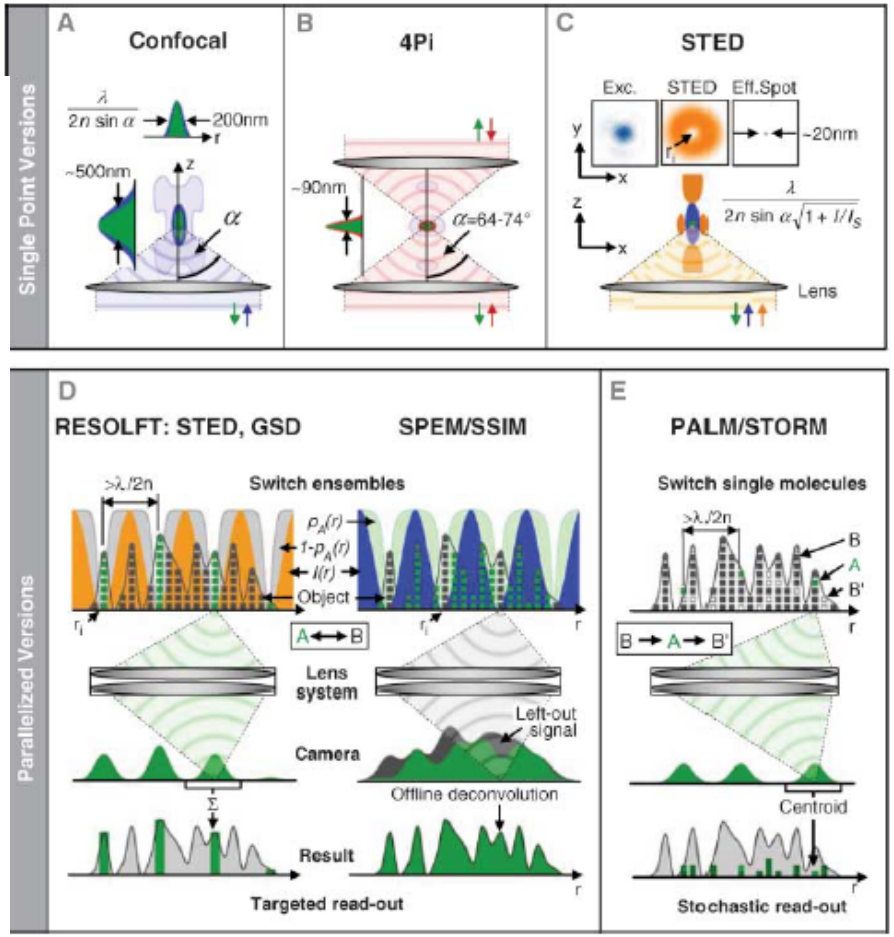

Quest for super-resolution: SM localization

history

- first single-molecule detection 05/1989
- first single-molecule fluorescence detection 1990
- first book 1996
- feature articles: *Science* 03/1999,
  Chem. Phys. 09/1999
- reviews by R.A. Keller and M. Orrit 12/1999

VOLUME 62, NUMBER 21 PHYSICAL REVIEW LETTERS 22 MAY 1989

Optical Detection and Spectroscopy of Single Molecules in a Solid

W. E. Moerner and L. Kador [a]
IBM Research Division, Almaden Research Center, San Jose, California 95120
(Received 17 March 1989)

Using two different double-modulation techniques, we have observed the optical-absorption spectrum of single dopant molecules of pentacene in a *p*-terphenyl host crystal at liquid-helium temperatures. To achieve this, frequency-modulation spectroscopy was combined either with Stark or ultrasonic modulation to remove interfering background signals from residual amplitude modulation, and the number of molecules in resonance was reduced to one by operating in the wings of the inhomogeneous line. Triplet bottleneck saturation appears to be suppressed in the single-molecule regime.

Single-Molecule Optical Detection, Imaging and Spectroscopy

Edited by
T. Basché, W. E. Moerner,
M. Orrit, U. P. Wild

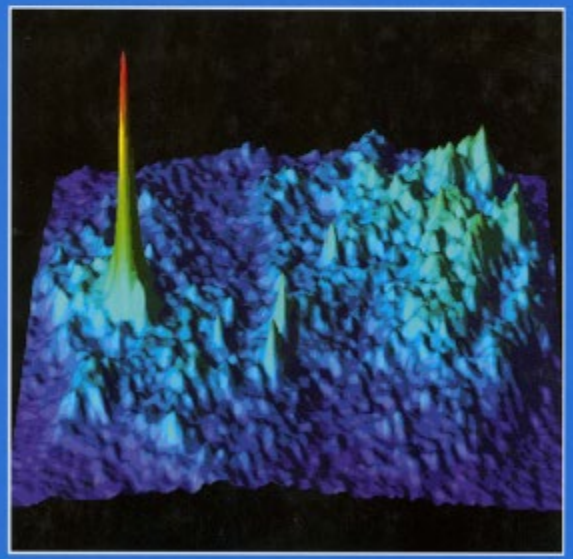

VCH

Ch. Zander, J. Enderlein, R. A. Keller (eds.)

Single-Molecule Detection in Solution

Methods and Applications

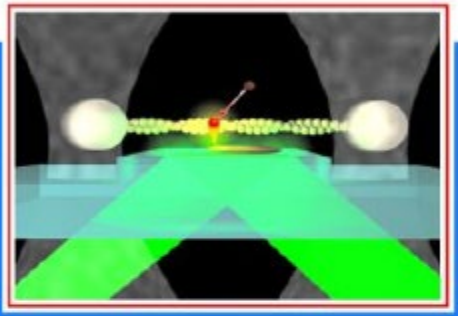

WILEY-VCH

R. Rigler
M. Orrit
T. Basché
(Eds.)

Single Molecule Spectroscopy

Nobel Conference Lectures

Springer

Single Molecules

Typical fluorescence properties used for single molecule probing and imaging

- Fluorescence depends on local polarity --- for both wavelength and quantum yield (intensity). This is normally used for single fluorophore labeling. Fluorescence intensity fluctuation reflects conformational changes of the host system (like a protein or membrane). *Draw scheme (sigmoidal plot for intensity and spectral shift). Also see a slide next.*
- Fluorescence polarization --- revealing rotation and diffusion of molecules (see last lecture), which in turn reflecting the conformation changes of the host systems.
- Fluorescence resonance energy transfer (FRET) --- revealing dynamic conformational changes involving two domains, where the fluorophores are labeled. This is unique for probing the coincident structural change within proteins or other large biological systems. a typical example is the signal transducing membrane proteins functional in neuron cells, where upon a ligand binding the membrane protein experience great structure change; some domains may transform across the membrane. Such a large change can be revealed by labeling two dyes at the active domains. Draw a scheme for a later slide.

Measurement principle: Fluorescence microscopy

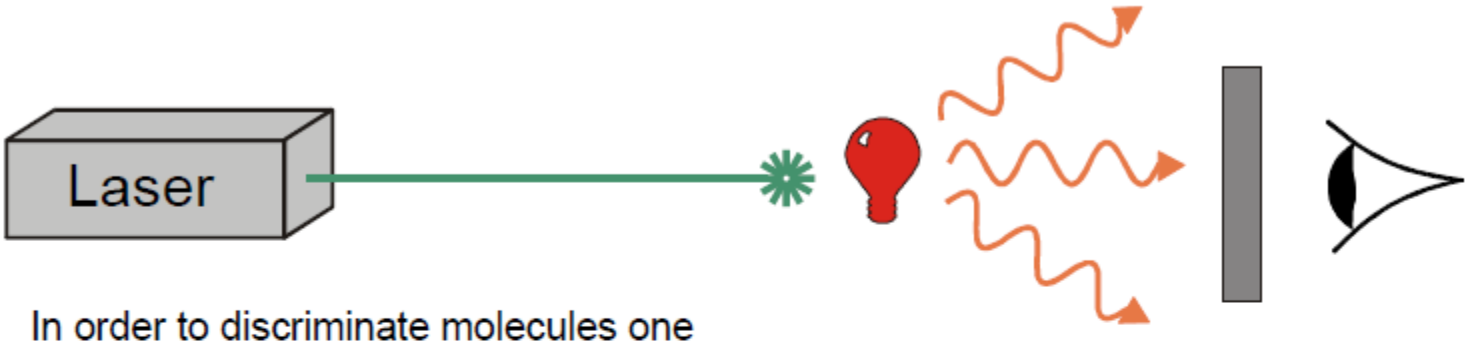

In order to discriminate molecules one from each others, it is necessary to dilute the concentration of fluorophores to such an extent that the average distance between two fluorophores is larger than the resolution of the microscope (confocal or wide-field). Depending on the experiment, the dilution will occur:

- in a cell membrane
- in an artificial membrane
- on a biomodified surface
- in a thin polymer sheet spin coated on a glass surface

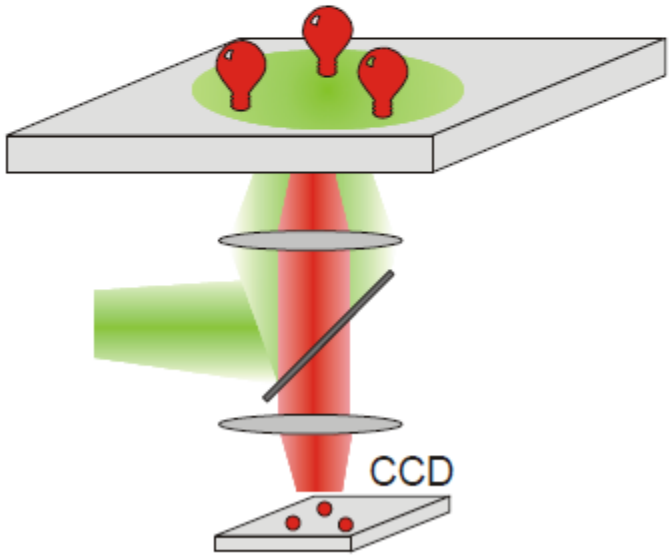

Confocal microscopy

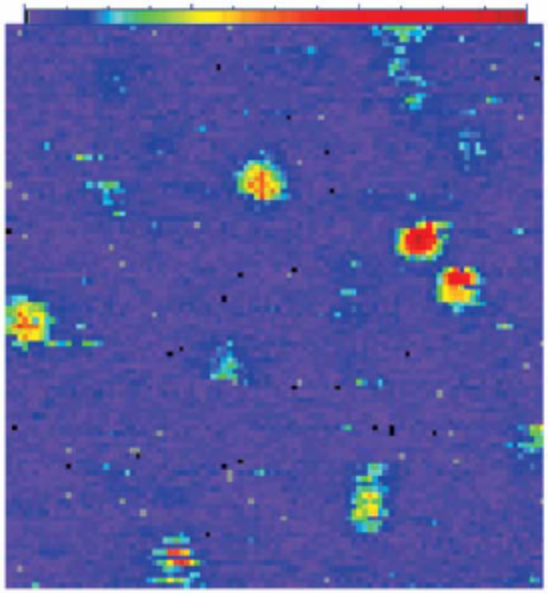

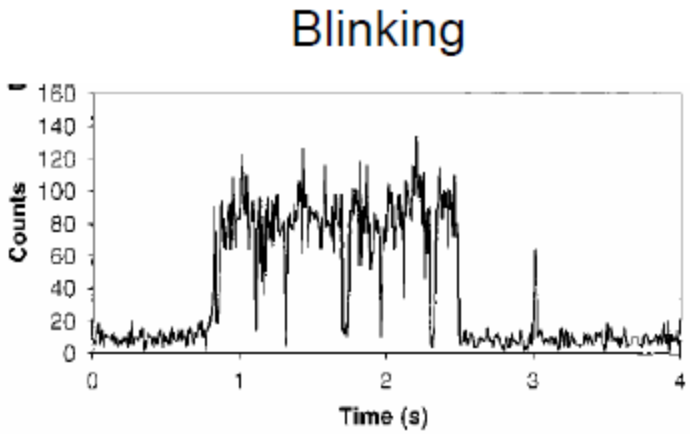

Ref: W. E. Moerner and M. Orrit, *Science* **283,** 1670 (1999).

Signal emitted by a single molecule

$$R(I_{ex}) = R_{max}\frac{I_{ex}/I_{sat}}{1+I_{ex}/I_{sat}}$$

$$R_{max} = \frac{k_f q_f}{(1+k_{ISC}/k_T)}$$

$$I_{sat} = \frac{(k_f)}{\sigma\cdot(1+k_{ISC}/k_T)}$$

$$\sigma = 3\sigma_{av}\cos^2\theta$$

R = fluorescence emission rate,
I_{ex} = laser excitation intensity,
I_{sat} = saturation intensity,
k_T = triplet decay rate,
k_{ISC} = inter-system crossing rate,
σ = absorption cross-section

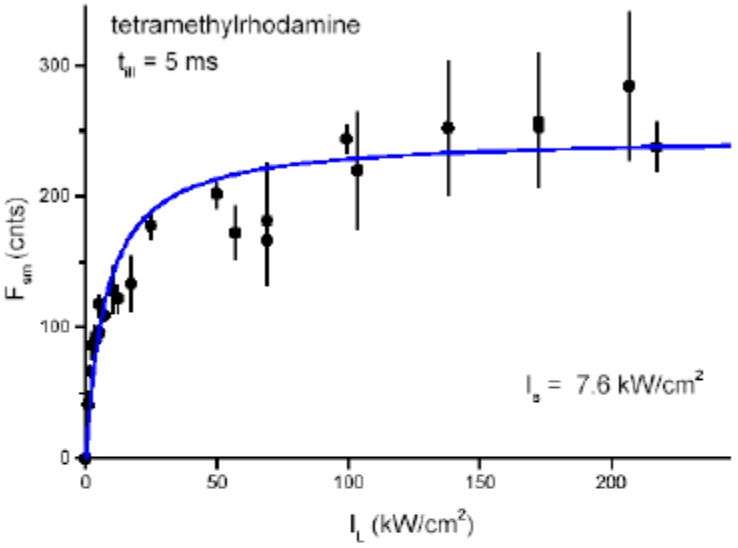

For TMR oriented // to the laser beam:

σ_{av} = 1.9*10^{-16} cm^2

q_f = 0.28

τ_f = 2.1 ns

$\tau_T = 1/k_T$ = 2 μs

$k_{ISC} = 0.03/\tau_f$

I_{sat} = 11 kW/cm^2; R_{max} = 4500 photons/ms

Signal/noise ratio

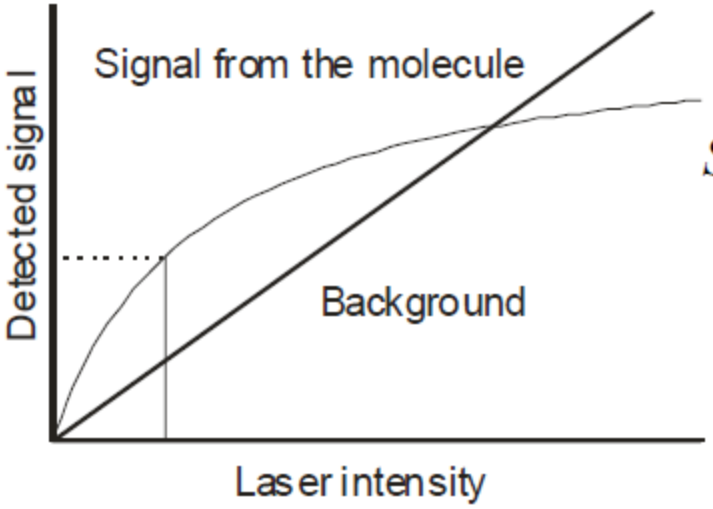

$$SNR = \frac{\eta_{det} R T_{int}}{\sqrt{\eta_{det} R T_{int} + C_b P T_{int} + N_d T_{int}}}$$

T_{int}=integration time

$C_b P$=background

N_d=noise from the detector

- The noise consists of the statistical noise of the signal, of the noise induced by the background and of the noise from the detector.
- The background has multiple origins: stray photons; autofluorescence from the filters and optics; impurities in the sample (cell autofluorescence).
- The minimal background is due to the Raman signal from the solvent.
- Practically: It is best to work slightly below I_{sat}. Reduce as much as possible the autofluorescence. Often100-200 detected counts from the molecule are sufficient to get an SNR of 8-10. This typically represents 5-10 ms measurement time. The effective number of images that can be recorded depends on the photo-bleaching.

Photobleaching

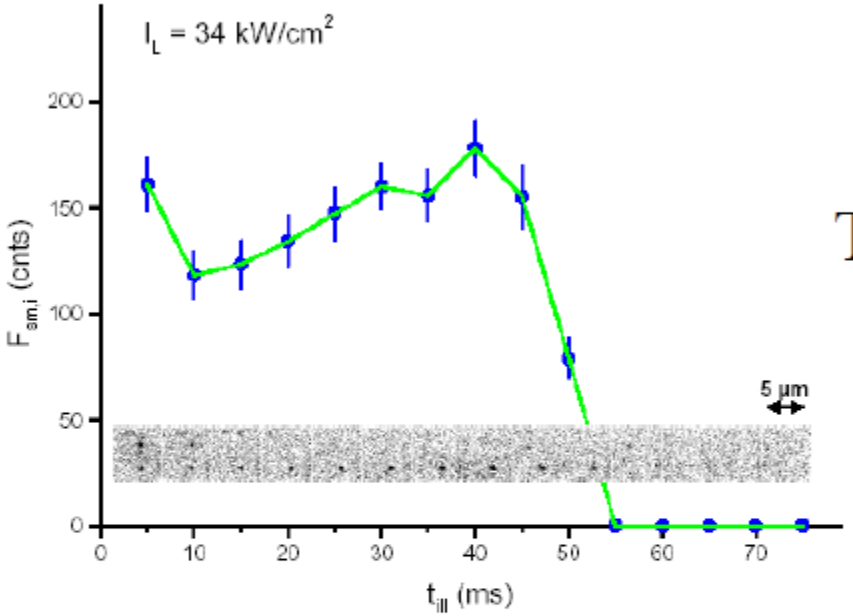

$$T_1 + {}^3O_2 \rightarrow S_1 + {}^1O_2$$

- A considerable amount of energy is flowing through single molecules. After a limited amount of time, they will undergo photodestruction.
- Most common mechanism: The molecule goes into the triplet state (S1->T1) and then decays producing higly reactive singlet oxygen that will oxidize the fluorophore.
- Photobleaching quantum yields are typically in the order of 10^{-5}-10^{-6}.
- Photobleaching drastically reduces the measurement time.

Typical fluorophores

fluorophore	λ_{exc} (nm)	λ_{em}^{max} (nm)	QE (in H_2O)	τ_S (ns)	I_S (kW/cm²)	k_∞ (kcnts/ms)	τ_{bl}^{∞} (ms)	N_{max} (10^6 photons)	Extinction coefficient, $M^{-1}\,cm^{-1}$
fluoresceine	488	520	0.71	-	-	-	-	<0.1	-
tetramethyl-rhodamine	514	580	0.28	2.1	5.6±1.6	4.0±1.5	11.5±2.5	0.6±0.2	-
Cy3	532	568	0.14	~ 1	-	-	-	-	-
Cy5	630	670	0.18	~ 1	2.2±1.0	2.3±0.3	14.8±0.3	0.67±0.11	-
TDI	630	677	~ 0	4.4±0.1	0.6±0.2*	0.9±0.08	25±2*	4.0±0.3*	-
Cy7	695	800	0.02	~ 0.8	0.7±0.2	0.5±0.06	15±6	1.5±0.5	-
eCFP	458	472	-	-	-	6±3	<1	<0.05	-
eGFP	488	512	0.6	3.2	13±3	2.9±0.2	2.8±0.2	0.14±0.05	-
eYFP	514	527	0.6	3.7	9±2	3.1±0.3	2.6±0.1	0.14±0.05	-
DsRed	532	582	0.29	2.8	50±10	18±2	0.4±0.1	0.06±0.01	-
eqFP611	559	611	0.45	-	-	-	-	0,29	78,000
drFP583	558	583	0.7	-	-	-	-	0.1-1.25	75,000
Alexa 633	632	650	-	3.2	6.7±1.6	3.9±0.6	-	9.7±0.3	-

Novel Fluorophores for Single-Molecule Imaging

Katherine A. Willets, Oksana Ostroverkhova, Meng He,[†,‡] Robert J. Twieg,[†] and W. E. Moerner*

Department of Chemistry, Stanford University, Stanford, California 94305

Experimental and Theoretical Investigations of Environmentally Sensitive Single-Molecule Fluorophores[†]

Katherine A. Willets,[‡] Patrik R. Callis,[§] and W. E. Moerner*,[‡]

Department of Chemistry, Stanford University, Stanford, California 94305, and Department of Chemistry and Biochemistry, Montana State University, Bozeman, Montana 59717

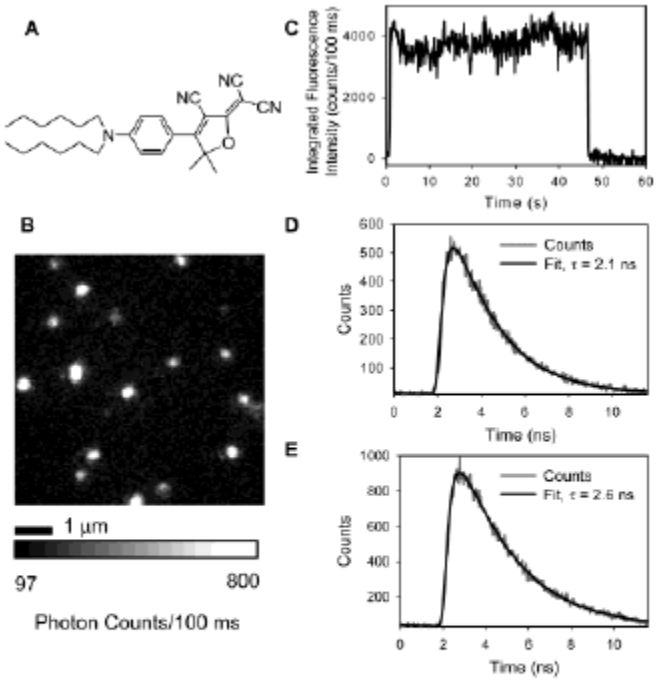

Figure 1. (A) Structure of DCDHF-6. (B) Single molecules of DCDHF-6 imaged in a PMMA film. The integrated fluorescence intensity of a single molecule as a function of time (C) and two examples of single-molecule TCSPC histograms (D) and (E) are shown for DCDHF-6 in PMMA. The lifetime data are fit to single exponentials using a maximum likelihood estimator and have decay times of 2.1 ns ($2I_t^* = 1.01$) and 2.6 ns ($2I_t^* = 1.09$), respectively.

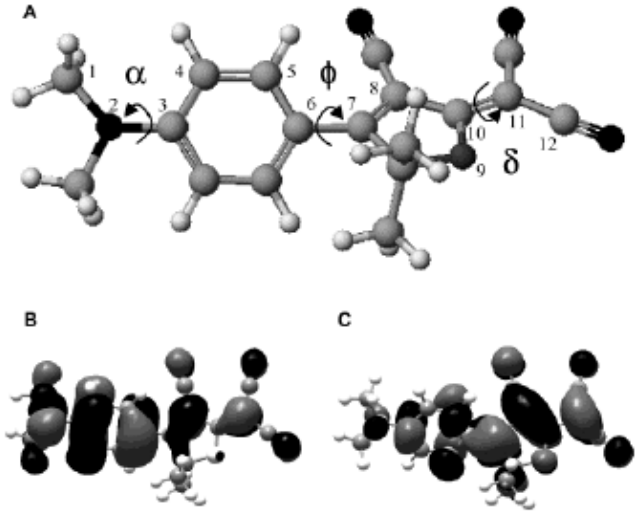

Figure 6. (A) Structure of DCDHF-1 with relevant dihedral angles for calculations shown. Twists around the amine−phenyl, phenyl−furan, and dicyano−furan bonds are denoted with angles α, ϕ, and δ respectively. The molecule is shown in the Γ_0 configuration where $\alpha = 1°$, $\phi = -39°$, and $\delta = 0°$. (B) HOMO and (C) LUMO of the DCDHF-1 molecule in the Γ_0 configuration calculated with RHF/3-21g.

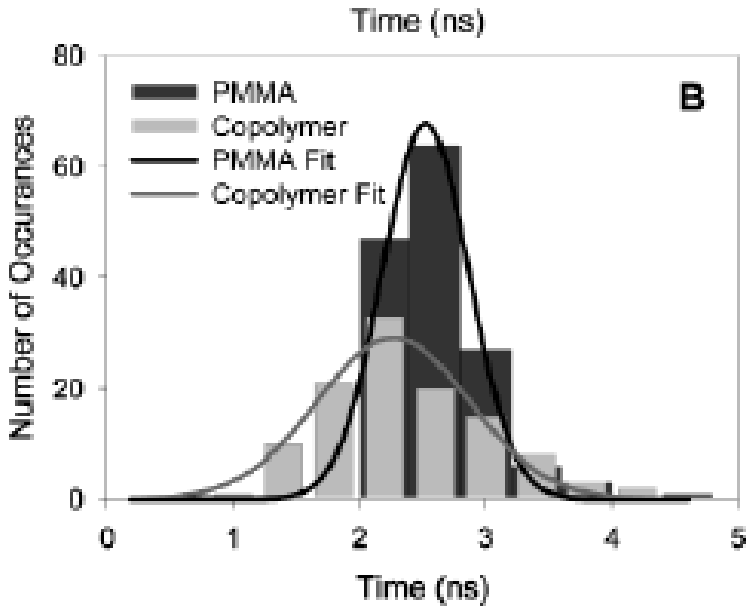

Single-molecule imaging of organic semiconductors: Toward nanoscale insights into photophysics and molecular packing

W.E.B. Shepherd [a], R. Grollman [a], A. Robertson [a], K. Paudel [a], R. Hallani [b], M.A. Loth [b], J.E. Anthony [b], O. Ostroverkhova [a,*]

Single-Molecule Level Insight into Nanoscale Environment-Dependent Photophysics in Blends

Rebecca Grollman,[†] Nicole Quist,[†] Alexander Robertson,[†] Jeremy Rath,[†] Balaji Purushothaman,[‡] Michael M. Haley,[§] John E. Anthony,[‡] and Oksana Ostroverkhova*[,†]

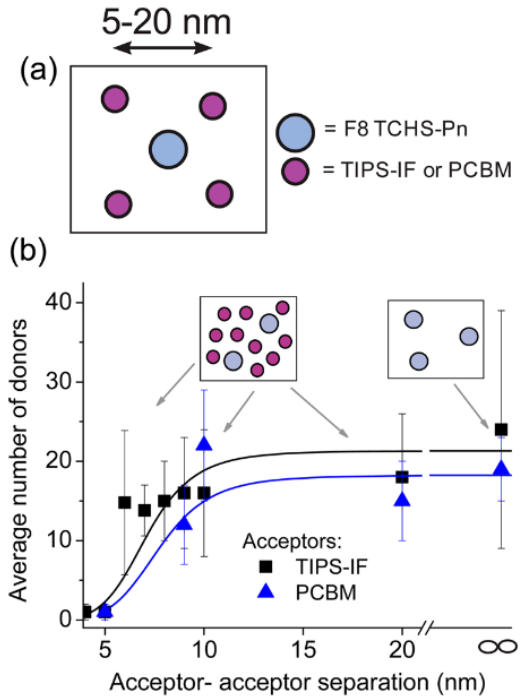

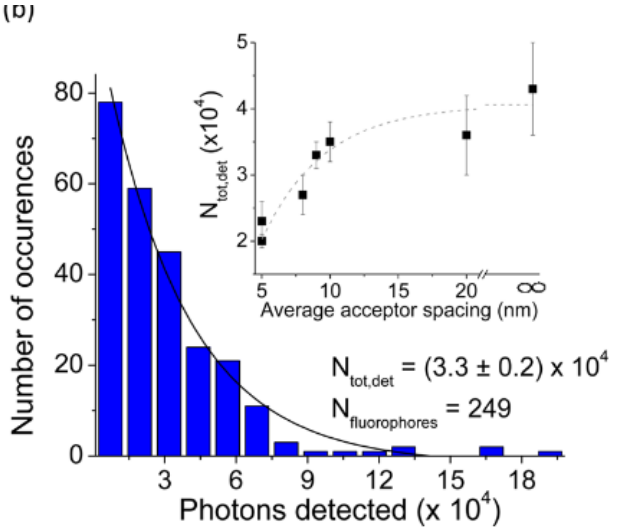

Molecular alignment

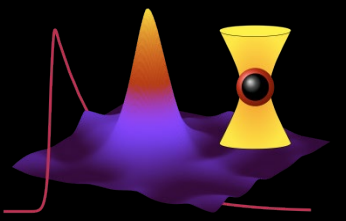

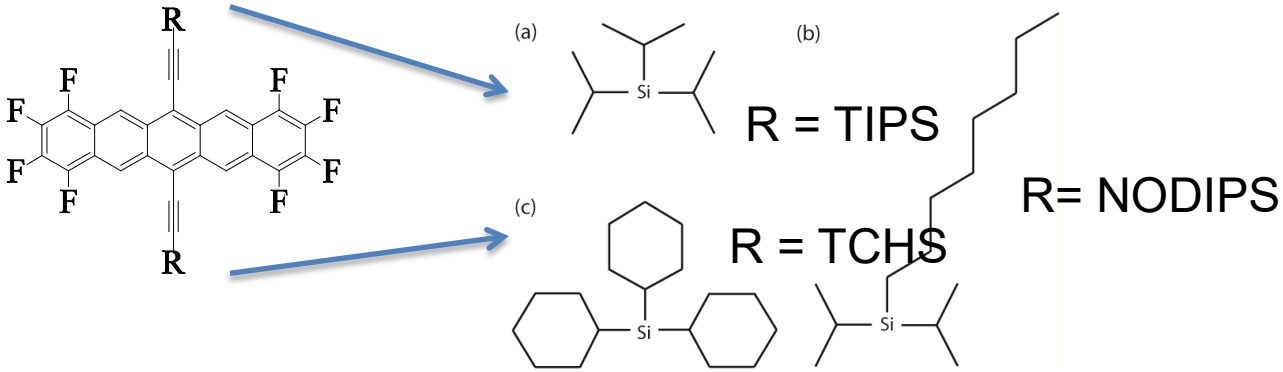

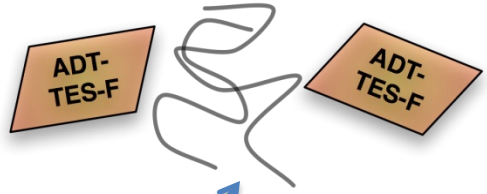

PMMA
BTBTB

BTBTB

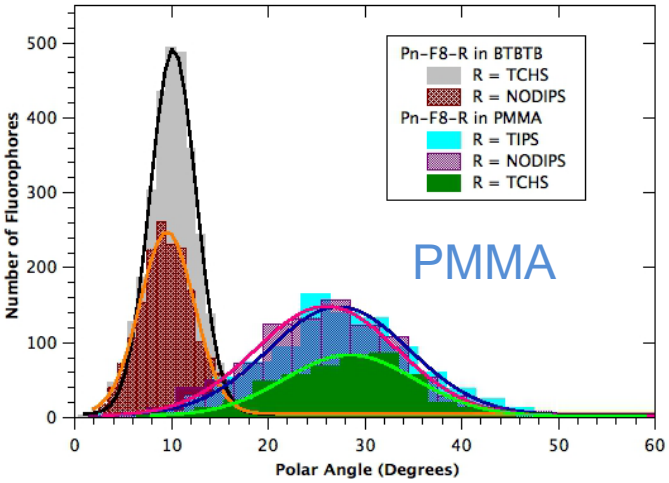

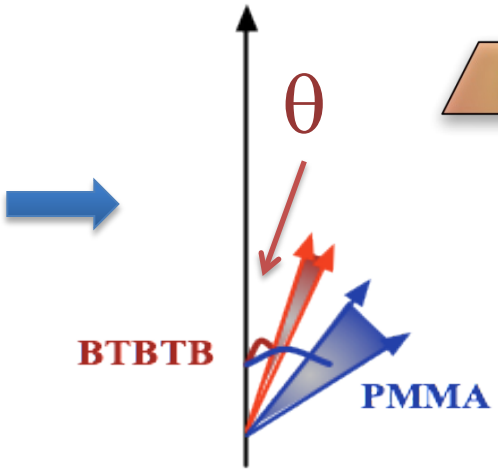

- Host-dependent molecular orientation – much stricter constraints in polycrystalline host
- guest-host interactions depending on the host and on R

REVIEW ARTICLES

Charge Transfer on the Nanoscale: Current Status

David M. Adams,[†] Louis Brus,[†] Christopher E. D. Chidsey,[‡] Stephen Creager,[§] Carol Creutz,[*,∥] Cherie R. Kagan,[⊥] Prashant V. Kamat,[⊗] Marya Lieberman,[○] Stuart Lindsay,[#] Rudolph A. Marcus,[▽] Robert M. Metzger,[◆] M. E. Michel-Beyerle,[Δ] John R. Miller,[∥] Marshall D. Newton,[∥] Debra R. Rolison,[×] Otto Sankey,[#] Kirk S. Schanze,[◇] James Yardley,[+] and Xiaoyang Zhu[∞]

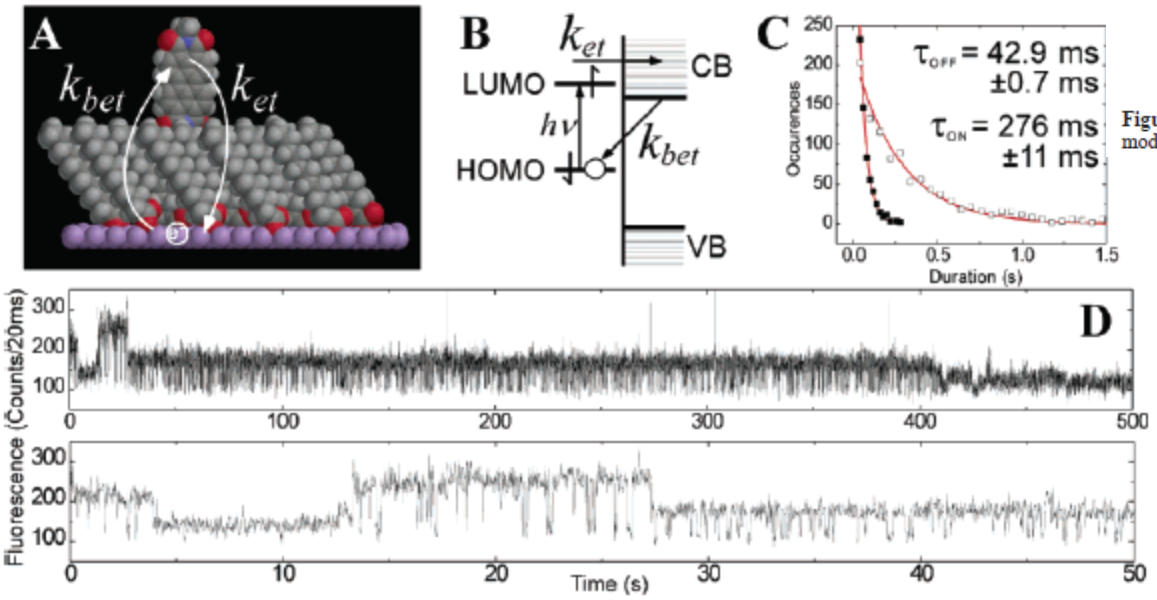

Figure 3.4. Electron transport at pyrene compounds adsorbed onto conducting substrates. (A) Schematic diagram. (B) Energy level diagram. (C) Decay kinetics. (D) Blinking phenomena.

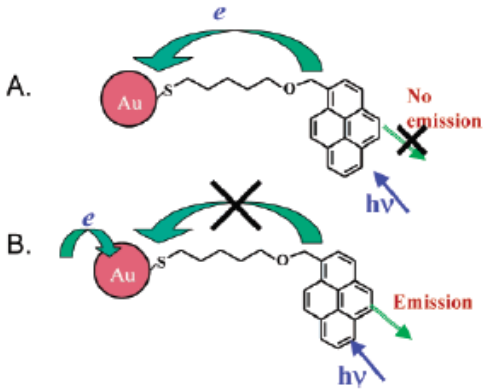

Figure 5.8. Control of charging of gold nanoparticle will enable modulation of fluorophore properties.

Acc. Chem. Res. 2005, 38, 574−582

Fluorescence Imaging with One Nanometer Accuracy: Application to Molecular Motors

AHMET YILDIZ† AND PAUL R. SELVIN*,†,‡

Center for Biophysics and Computational Biology and Department of Physics, University of Illinois, Urbana-Champaign, Illinois 61801

Received August 17, 2004

ABSTRACT

We introduce the technique of FIONA, fluorescence imaging with one nanometer accuracy. This is a fluorescence technique that is able to localize the position of a single dye within ~1 nm in the $x-y$ plane. It is done simply by taking the point spread function of a single fluorophore excited with wide field illumination and locating the center of the fluorescent spot by a two-dimensional Gaussian fit. We motivate the development of FIONA by unraveling the walking mechanism of the molecular motors myosin V, myosin VI, and kinesin. We find that they all walk in a hand-over-hand fashion.

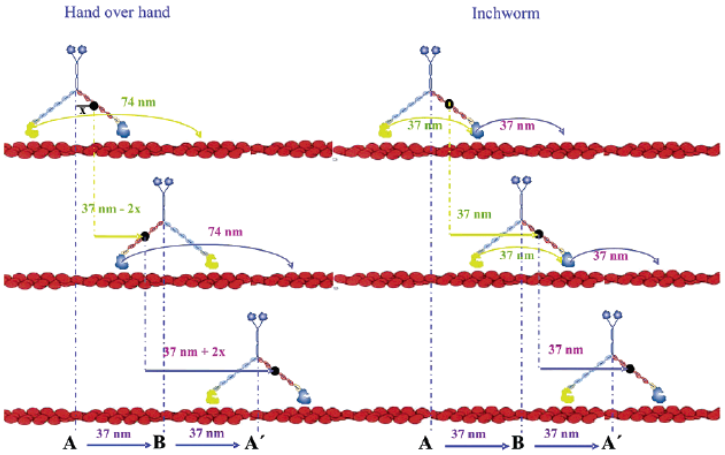

FIGURE 3. Hand-over-hand model vs Inchworm model for myosin V. In the hand-over-hand model, the rear head passes by the front head, translating a total of 74 nm, while the front head stays stationary. Therefore, heads move alternating 74 and 0 nm steps. If the dye is on the light chain, it moves $37 - 2x$, followed by $37 + 2x$ nm, where x is the distance between the dye and the center. In the inchworm model, the dye moves 37 nm regardless to where it is labeled.

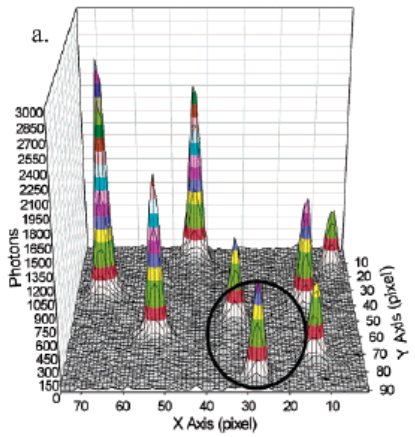

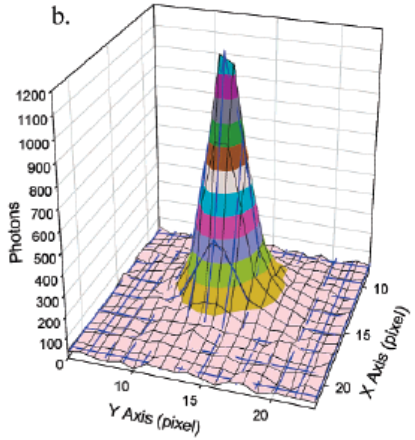

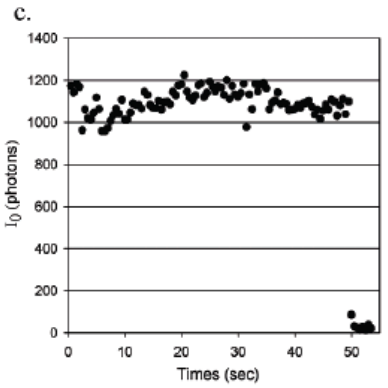

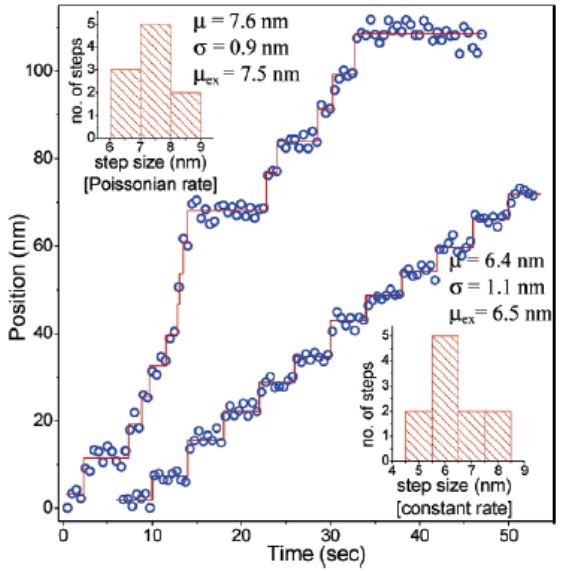

1. FIONA. (A) Pixelated image of several individual Cy3-dyes immobilized onto glass coverslip. Dyes were imaged by using objective- with 0.5-s integration time. (B) The PSF circled in (A) has a width of 287 nm, and the SNR of 32. A Gaussian curve-fit (solid blue line) 1.3 nm precision in the center localization. (C) The dye lasted for 50 s and photobleached in a single step that indicates the image s a single dye. (D) The PSF center versus time graph. The sample was moved with a nanometric stage with 6.5 nm increments either nstant rate or a Poisson-distributed rate. Red lines show the average position between each step. Steps are visually separable and ermined with 1 nm precision (σ), and the accuracy [difference between the measured step size via PSF fitting (μ) and the expected e (μ_{ex}) based on the calibrated stage] is better than 1 nm.

Example: The motion of the molecular motor myosin V

The precision is in the order of 1 nm!

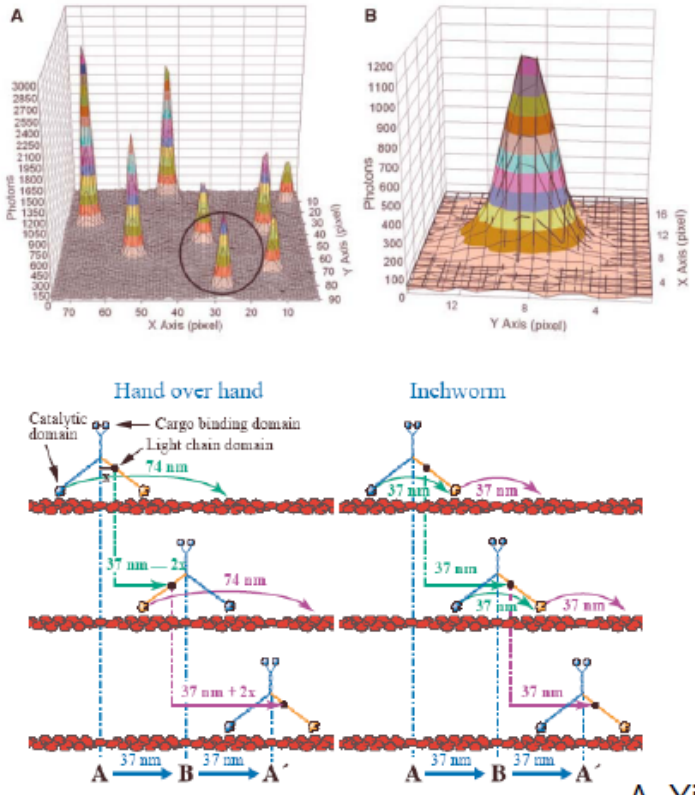

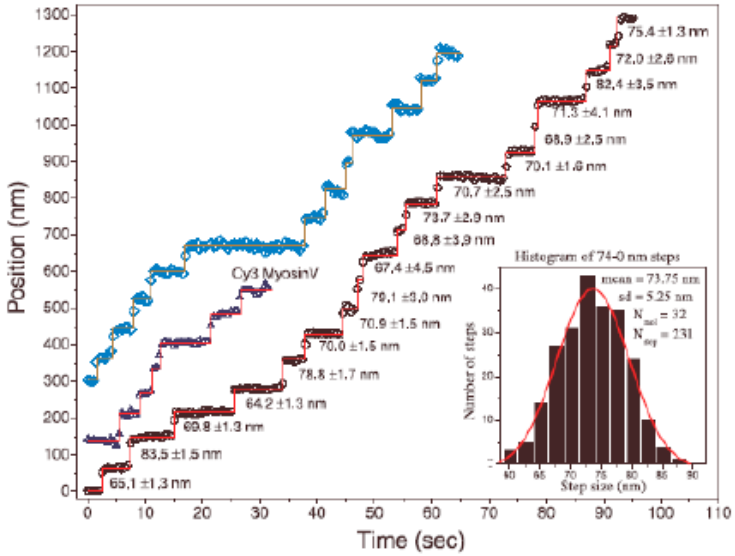

A. Yildiz, J.N. Forkey, S.A. McKinney, T. Ha,

Y.E. Goldman, P.R. Selvin, *Science* **300**, 2061 (2003)

Myosin V. Myosin V is a dimer which has the longest light-chain binding domain (24 nm), containing six calmodulin-binding sites (IQ domains) (Figure 2).[17,18] This domain likely acts as a lever arm that amplifies small nucleotide-dependent conformational changes in the motor domain to a large displacement.[19,20] Myosin V walks toward the plus end of actin by taking ~37 nm steps per ATP hydrolyzed.[21,22] Myosin V transports a wide variety of cargo including pigment granules, membranous organelles and secretory vesicles in vertebrates, and mRNA in yeast. Functional defects in this protein cause neurological diseases and pigmentation in mice and humans.[23–25]

Imaging Intracellular Fluorescent Proteins at Nanometer Resolution

Eric Betzig,[1,2*]† George H. Patterson,[3] Rachid Sougrat,[3] O. Wolf Lindwasser,[3] Scott Olenych,[4] Juan S. Bonifacino,[3] Michael W. Davidson,[4] Jennifer Lippincott-Schwartz,[3] Harald F. Hess[5*]

We introduce a method for optically imaging intracellular proteins at nanometer spatial resolution. Numerous sparse subsets of photoactivatable fluorescent protein molecules were activated, localized (to ~2 to 25 nanometers), and then bleached. The aggregate position information from all subsets was then assembled into a superresolution image. We used this method—termed photoactivated localization microscopy—to image specific target proteins in thin sections of lysosomes and mitochondria; in fixed whole cells, we imaged vinculin at focal adhesions, actin within a lamellipodium, and the distribution of the retroviral protein Gag at the plasma membrane.

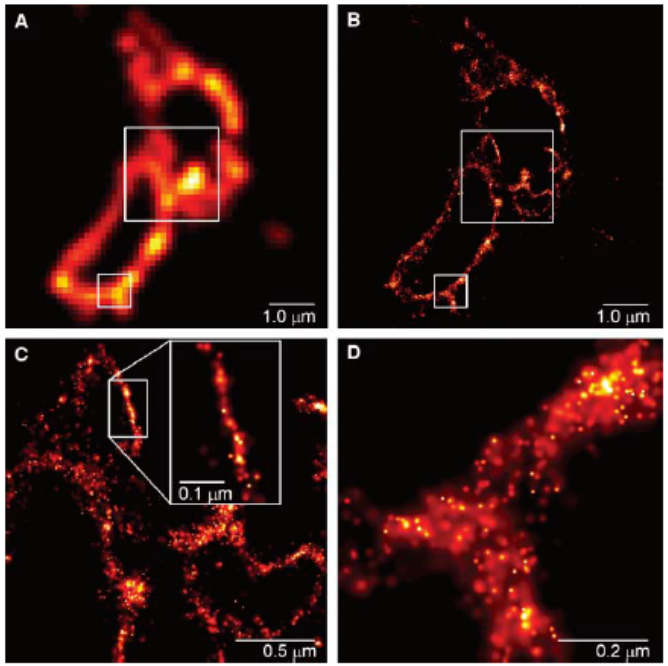

Fig. 2. Comparative summed-molecule TIRF (**A**) and PALM (**B**) images of the same region within a cryo-prepared thin section from a COS-7 cell expressing the lysosomal transmembrane protein CD63 tagged with the PA-FP Kaede. The larger boxed region in (B), when viewed at higher magnification (**C**) reveals smaller associated membranes that may represent interacting lysosomes or late endosomes that are not resolvable by TIRF. In a region where the section is nearly orthogonal to the lysosomal membrane, the most highly localized molecules fall on a line of width ~10 nm (inset). In an obliquely cut region [(**D**), from the smaller boxed region in (B)], the distribution of CD63 within the membrane plane can be discerned.

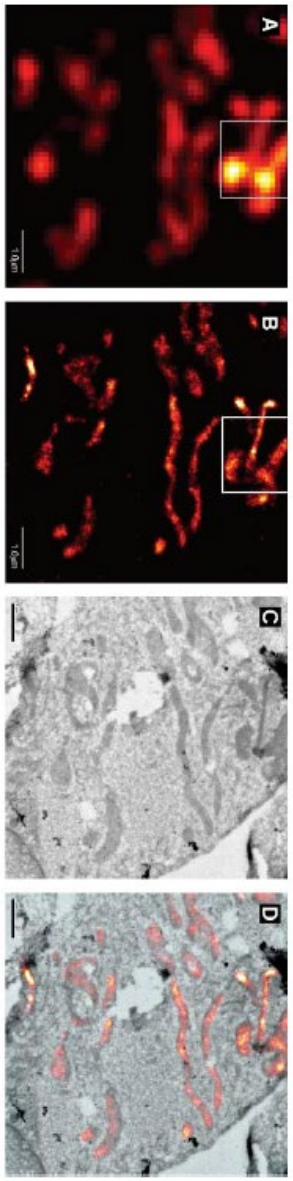

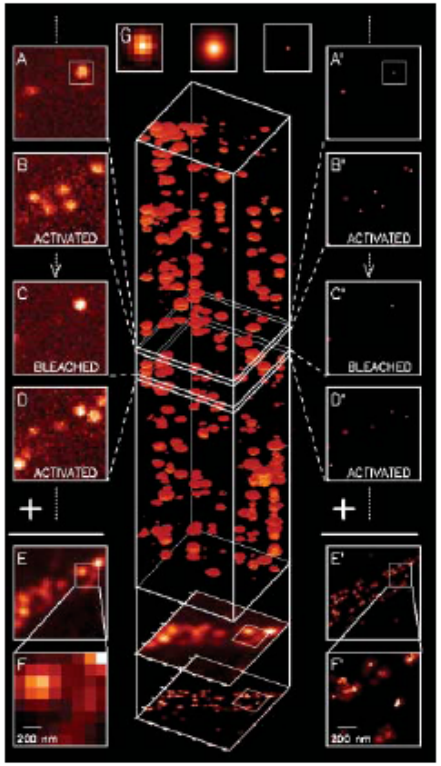

Fig. 1. The principle behind PALM. A sparse subset of PA-FP molecules that are attached to proteins of interest and then fixed within a cell are activated (**A** and **B**) with a brief laser pulse at λ_{act} = 405 mm and then imaged at λ_{exc} = 561 mm until most are bleached (**C**). This process is repeated many times (**C** and **D**) until the population of inactivated, unbleached molecules is depleted. Summing the molecular images across all frames results in a diffraction-limited image (**E** and **F**). However, if the location of each molecule is first determined by fitting the expected molecular image given by the PSF of the microscope [(**G**), center] to the actual molecular image [(G), left], the molecule can be plotted [(G), right] as a Gaussian that has a standard deviation equal to the uncertainty $\sigma_{x,y}$ in the fitted position. Repeating with all molecules across all frames (**A**′ through **D**′) and summing the results yields a superresolution image (**E**′ and **F**′) in which resolution is dictated by the uncertainties $\sigma_{x,y}$ as well as by the density of localized molecules. Scale: 1 × 1 μm in (F) and (F′), 4 × 4 μm elsewhere.

NATURE METHODS

Sub-diffraction-limit imaging by stochastic optical reconstruction microscopy (STORM)

Michael J Rust[1,5], Mark Bates[2,5] & Xiaowei Zhuang[1,3,4]

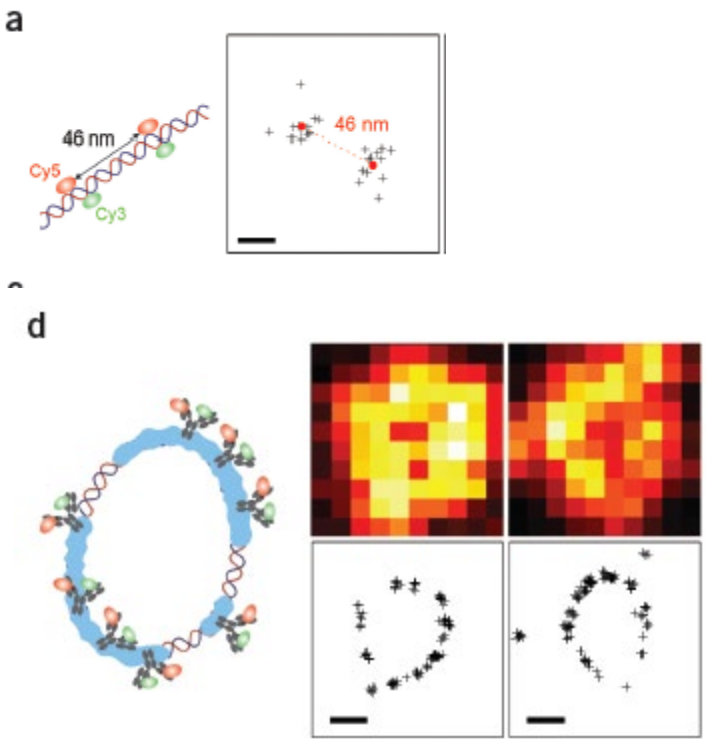

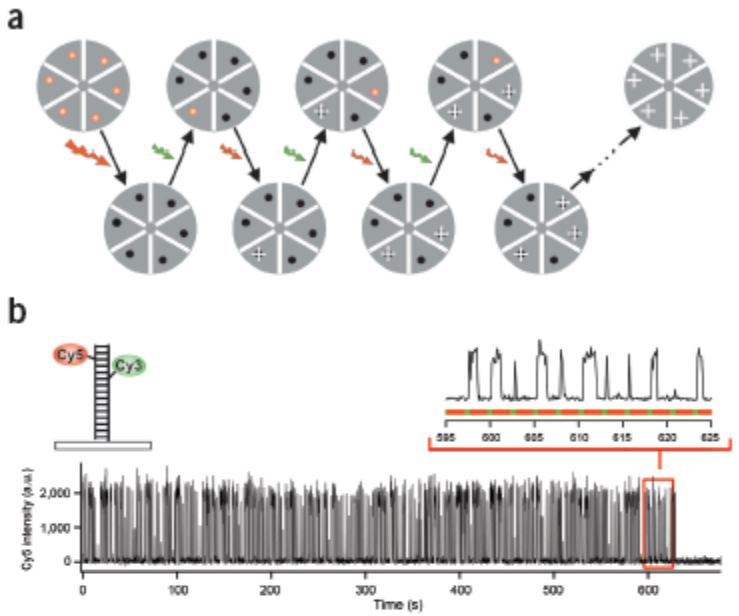

Figure 1 | STORM with photo-switchable fluorophores. (**a**) A STORM imaging sequence using a hypothetical hexameric object labeled with red fluorophores that can be switched between a fluorescent and a dark state by a red and green laser, respectively. All fluorophores are first switched to the dark state by a strong red laser pulse. In each imaging cycle, a green laser pulse is used to switch on only a fraction of the fluorophores to give an optically resolvable set of active fluorophores. Next, under red illumination, these molecules emit fluorescence until they are switched off, allowing their positions (white crosses) to be determined with high accuracy. The overall image is then reconstructed from the fluorophore positions obtained from multiple imaging cycles. (**b**) A single Cy5 switch on DNA can be turned on and off for hundreds of cycles before being permanently photobleached. A red laser (633 nm, 30 W/cm^2) is used to excite fluorescence (black line) from Cy5 and to switch Cy5 to the dark state. A green laser (532 nm, 1 W/cm^2) is used to return Cy5 to the fluorescent state. The alternating red and green line indicates the laser excitation pattern.

Nature Methods 3, 793 (2006)

Vol 466|29 July 2010|doi:10.1038/nature09163 nature

LETTERS

Subnanometre single-molecule localization, registration and distance measurements

Alexandros Pertsinidis[1,2], Yunxiang Zhang[1,2] & Steven Chu[1,2,3,4]†

Here we report a distance resolution of s_{reg} = 0.50 nm and an absolute accuracy of $s_{distance}$ = 0.77 nm in a measurement of the separation between differently colored fluorescent molecules using conventional far-field fluorescence imaging in physiological buffer conditions. The statistical uncertainty in the mean for an ensemble of identical single-molecule samples is limited only by the total number of collected photons, to s_{loc}<0.3 nm, which is 3x10^{-3} times the size of the optical PSF. Our method may also be used to improve the resolution of many subwavelength, far-field imaging methods such as those based on co-localization of molecules that are stochastically switched on in space. The improved resolution will allow the structure of large, multi-subunit biological complexes in biologically
relevant environments to be deciphered at the single-molecule level.

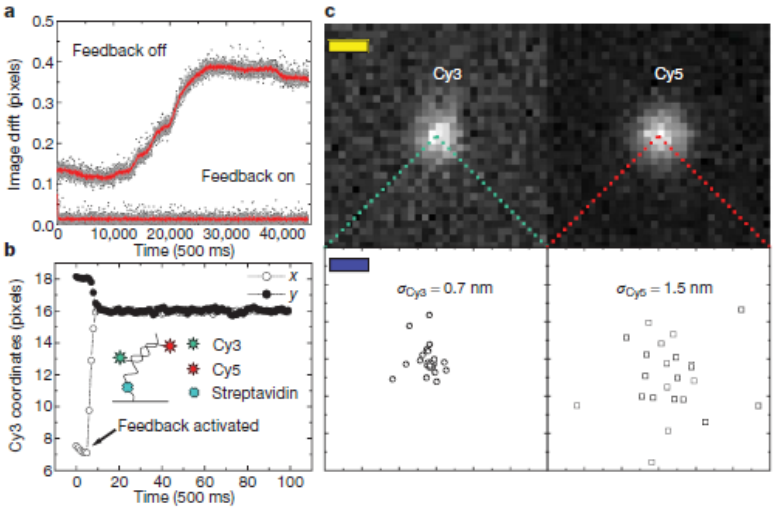

Figure 1 | Active feedback control. **a**, Performance of the actively stabilized imaging system. Black symbols: 2D registration of the green and red images at a rate of 500 ms^{-1} over 6.5 h; red lines: 64-point-average (1/10 points plotted). With feedback turned off, relative drift is ~0.3 pixels, or 19 nm, whereas with feedback on, the long-term registry is maintained to <0.01 pixels, or 0.64 nm. **b**, Feedback control on the position of single Cy3 molecules. The position noise is limited only by the number of collected photons in each frame (~3,500): $s_{loc} \approx$ 2–3 nm. **c**, Molecule-to-molecule reproducibility for the Cy3–Cy5 20-base-pair (bp) dsDNA. Top panels: images of single Cy3 and Cy5 molecules; scale bar, 320 nm. Bottom panels: each symbol represents the average position of a separate molecule (N = 25), averaged over all the frames during which the Cy3 was locked and before the Cy5 photobleached (typically 10–100 frames or 5–50 s). σ_{Cy3} and σ_{Cy5} are the standard deviations of the positions over the set of Cy3 and Cy5 molecules, respectively. Scale bar, 3.2 nm.

Nobel Prize in Physics 1997

The Nobel Prize in Physics 1997 was awarded jointly to Steven Chu (Stanford U), Claude Cohen-Tannoudji (École Normale Supérieure, Paris, France) and William D. Phillips (NIST) *"for development of methods to cool and trap atoms with laser light"*.

NSOM

Near Field Optics

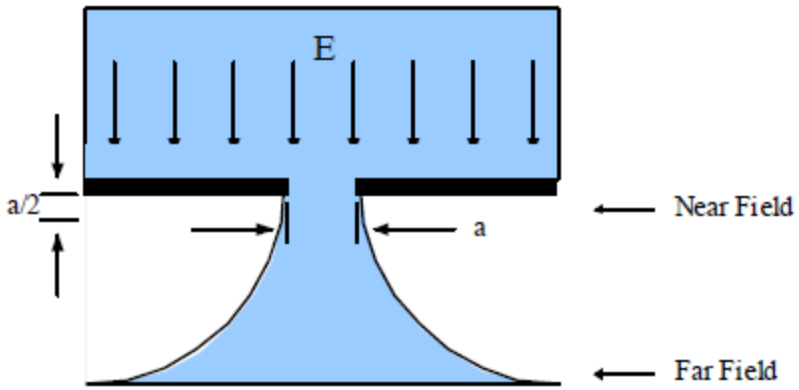

Resolution is only a function of aperture size!

1928: Proposal of concept (E. Synge, Phil. Mag. 6, 356, 1928)

1944: Calculation of sub wavelength aperture coupling (H. Bethe, Phys. Rev. 66, 163, 1944)
Correct by Bouwkamp

1972: demonstration using microwaves (Ash et al., Nature 237, 510, 1972)

1980's Work by Pohl and Lewis

Brief History of NSOM

- Ideas started in mid-1980's;

  D.W. Pohl, W. Denk, and M. Lanz, *Appl. Phys. Lett.* 44, 651-3 (1984).

  A. Lewis, M. Isaacson, A. Harootunian, and A. Murray, *Ultramicroscopy* 13, 227 (1984);

- Technology developed in 1990's;

  Eric Betzig, et al. *Science*, 262, 1422-1425 (1993).

  Eric Betzig, et al. *Nature*, 2369, 40-42 (1994).

- Prototype commercial available since 2000's;

What is Near-Field?

- requires a nanometer sized aperture (much smaller than the light wavelength).
- A specimen is scanned very close to the aperture.
- As long as the specimen remains within a distance less than the aperture diameter, an image with sub-wavelength resolution (aperture size) can be generated.
- There is a tradeoff between resolution and sensitivity (light intensity) --- aperture size cannot be too small.

Why NSOM?

- Light diffraction limit of conventional optical microscopy: $\lambda/2$, ~ 250 nm. Actually, in real cases, the optical resolution ~ λ, 500 nm; in contrast, NSOM offers higher resolution around 50 nm (or even < 30 nm), depending on tip aperture size.
- NSOM provides simultaneous measurements of the topography and optical properties (fluorescence) --- *direct correlation* between surface nanofeatures and optical/electronic properties.
- This is especially useful for the studying the inhomogeneous materials or surfaces, like nanoparticles, polymer blends, porous silicon, biological systems.

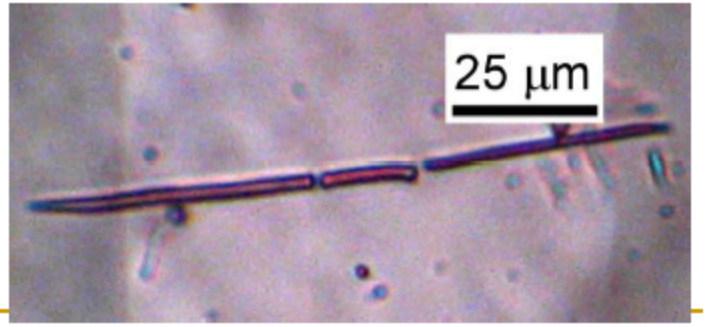

A 500 nm wide nanobelt appears wider than real size under an optical microscope.

Scanning near-field optical microscopy (SNOM)

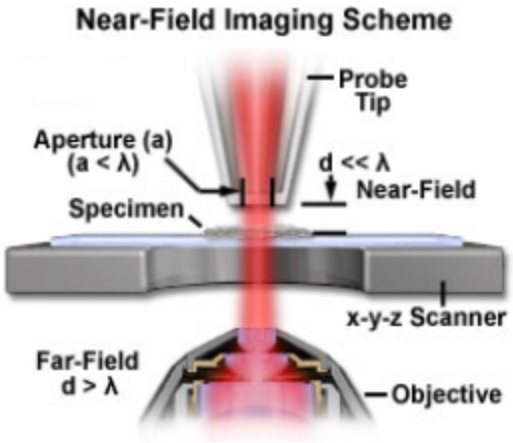

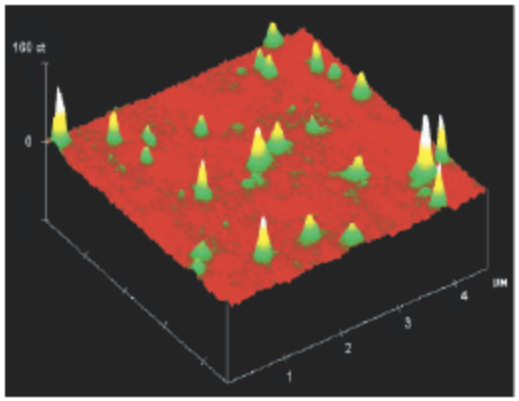

Fig. 3. Near-field fluorescence image (4.5 μm by 4.5 μm) of single oxazine 720 molecules dispersed on the surface of a poly(methylmethacrylate) film. Each subdiffraction peak (full width at half maximum, 100 nm) comes from a single molecule. Reproduced with permission from (47).

Ref: W. E. Moerner and M. Orrit, *Science* **283**, 1670 (1999).

http://micro.magnet.fsu.edu/

NSOM Operation System

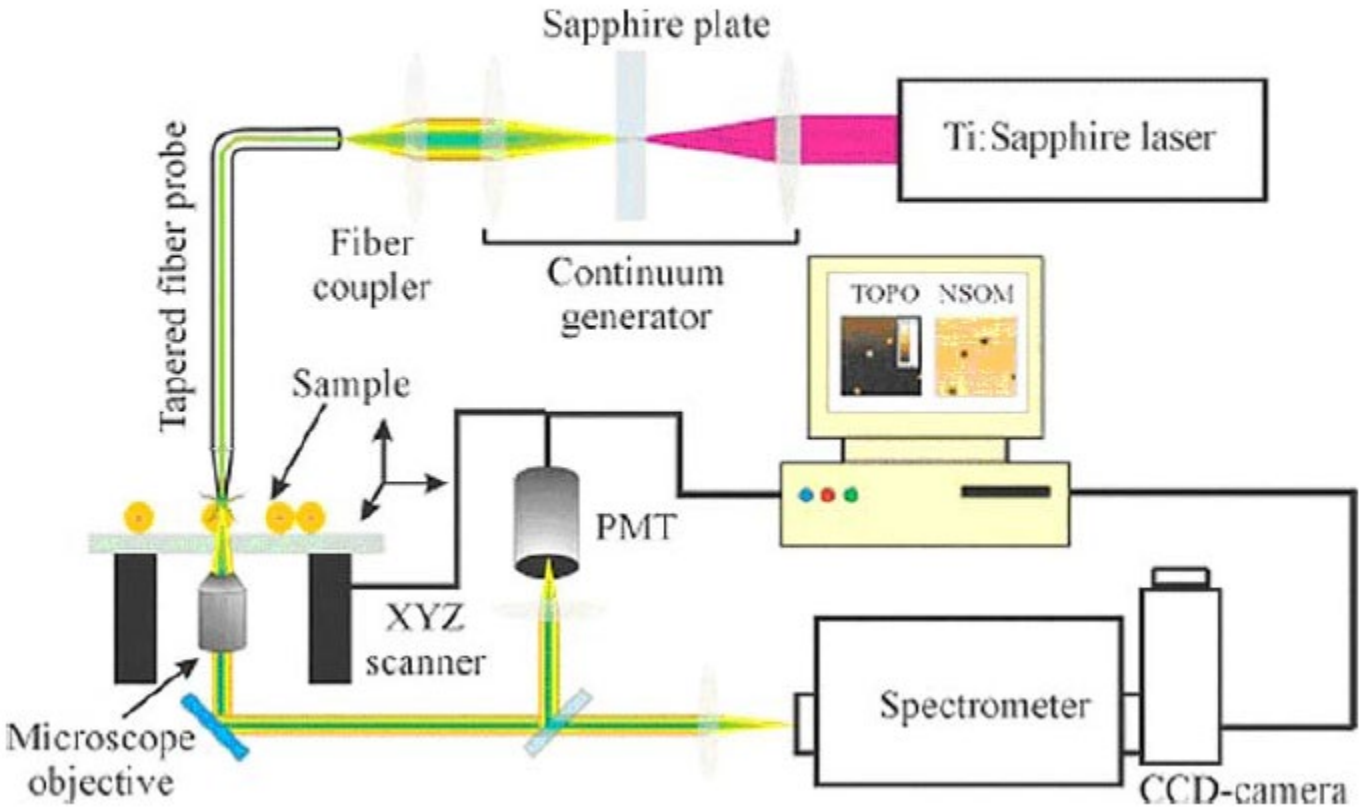

Near-field Scanning Optical Microscope (NSOM)

Principle of NSOM: Can be simply modeled by the electromagnetic interaction of two very closely positioned nano-objects, which represent a probe and sample

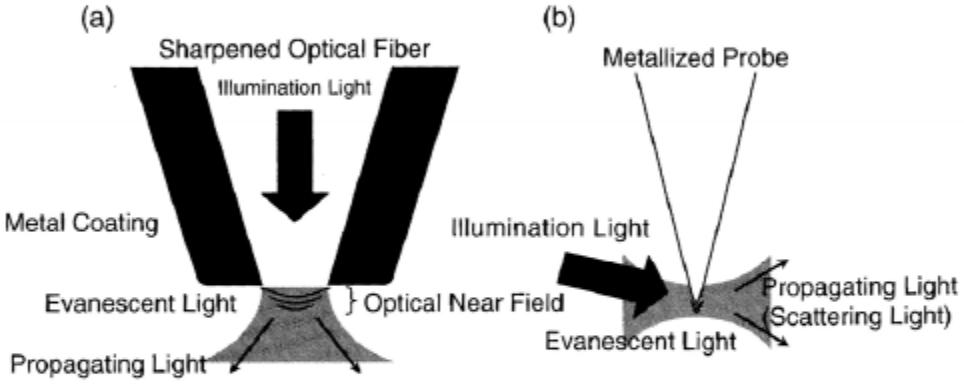

Aperture-type

- Nanoscale light spot same as aperture size
- Aperture-sample distance is regulated at < 10 nm

Scattering-type

- Sharpened homogeneous metal tip, with enhanced electric field
- Spatial resolution defined by apex diameter

Review paper: Lewis A., *Nature Biotech.* **21**, 1378 (2003)

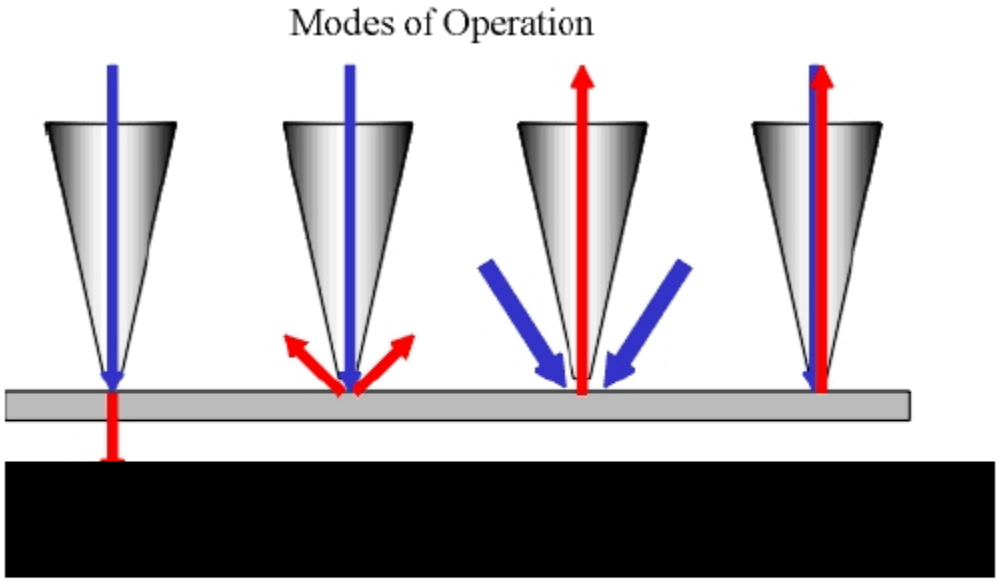

NSOM modes of operation

From L to R : Tranmission mode, Reflection Mode, Collection Mode and Illumination/Collection mode.

http://www.nanonics.co.il/main/twolevels_item1.php?ln=en&item_id=34&main_id=14

Different Operation Modes

- Illumination by the tip is probably the easiest to operate and interpret, and gives the most signal. It requires a transparent sample, so is limited for application in many samples like silicons and bio-species.
- Reflection modes give less light, and are more dependent on the details of the probe tip, but allow one to study opaque samples.
- The illumination/collection mode provides a complement to the reflection modes, but the signal contains a large background.

Structure of a NSOM Tip?

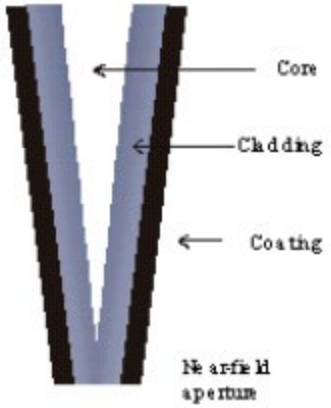

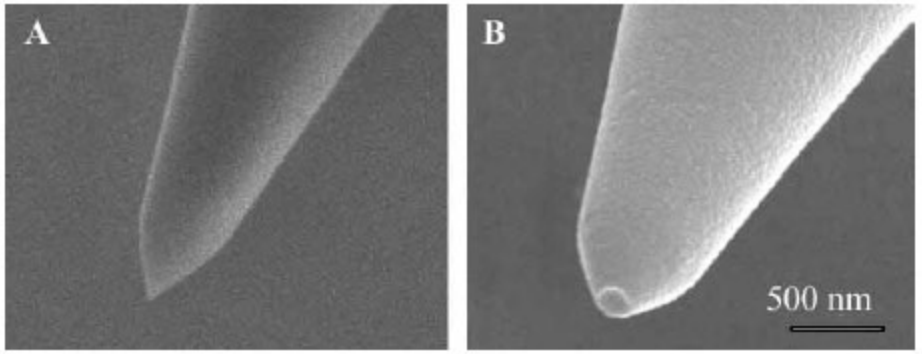

- PL spot diameter as a function of the aperture size

- *The spatial resolution is monotonously enhanced with a decrease of the aperture diameter except for the 0 nm aperture (entirely metal coated probe).*
- *The spatial resolution is almost equal to the aperture diameter.*

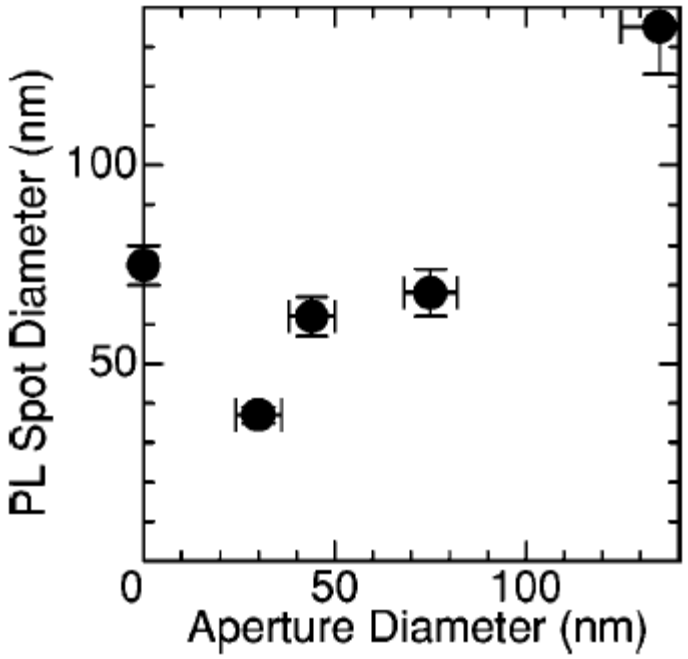

Matsuda *et al.*,APL, **81**, 2291 (2002)

Near-Field vs. Far-Field Imaging

C12 Polyfluorene Annealed

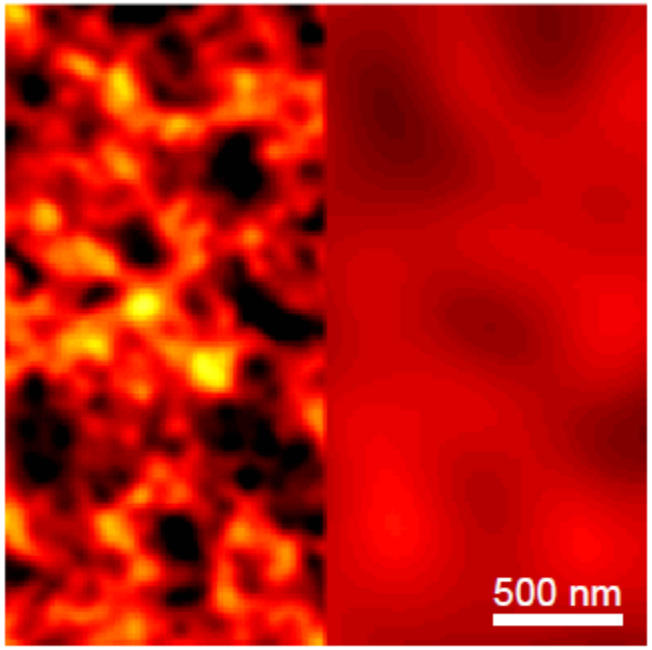

NSOM

Conventional
Far Field

NSOM imaging:

Direct correlation between nanostructure features and optical/electronic properties

NSOM topgraphy

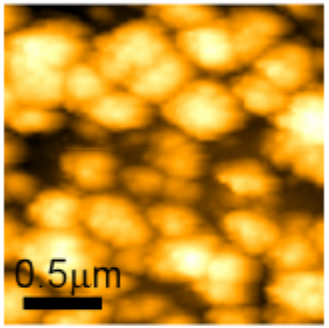

TiO_2 particles wrapped in PPV film

NSOM fluorescence

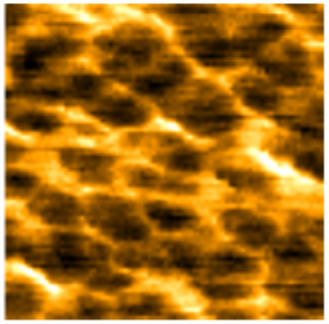

Fluorescence quenching by TiO_2 particles

Breaking the Diffraction Barrier: Optical Microscopy on a Nanometric Scale

Science_251_1468 (1991)

E. BETZIG*, J. K. TRAUTMAN, T. D. HARRIS, J. S. WEINER, R. L. KOSTELAK

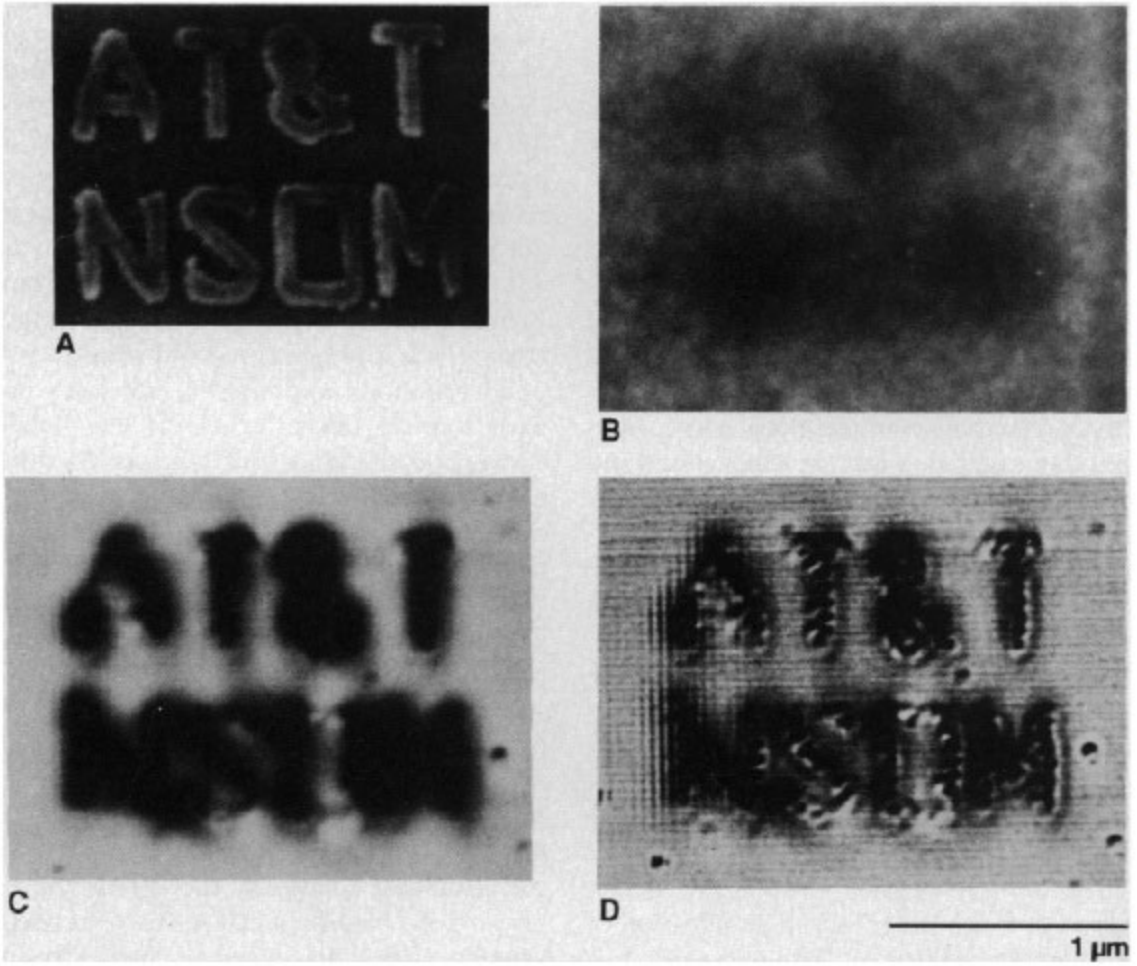

A. SEM

B. Optical microscopy (NA = 0.9)

C. NSOM

D. NSOM after deconvolution

10/25/12:
1,059 citations

Single Molecules Observed by Near-Field Scanning Optical Microscopy

Science_262_1422 (1993)

Eric Betzig and Robert J. Chichester

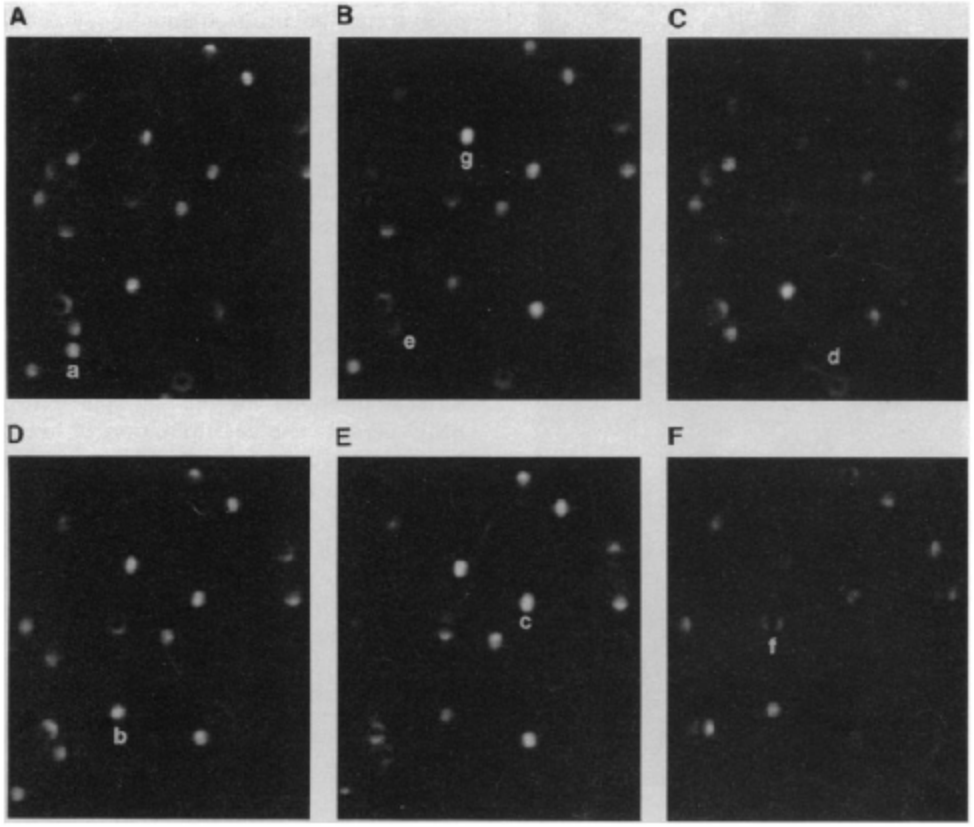

Fig. 1. Six sequential images of the exact same field of individual carbocyanine dye molecules as detected by near-field optical fluorescence microscopy. The excitation polarization is random in (**A**) through (**D**) and linear along *y* and *x*, respectively, in (**E**) and (**F**). The emission polarization is measured along *y* and *x* in (**B**) and (**C**), respectively, and not measured otherwise. Certain molecules have been labeled for discussion in the text.

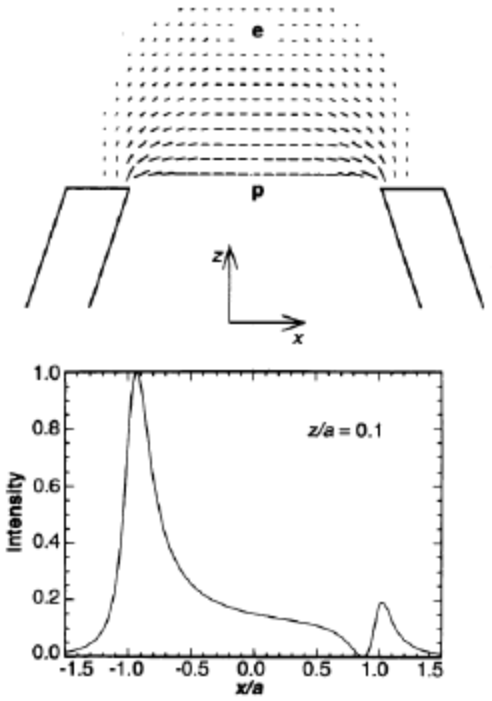

Fig. 2. (**Top**) Schematic view of a molecular dipole **p** (arrow) at a particular orientation within the electric field pattern **E** of a subwavelength aperture. (**Bottom**) Resulting intensity *I* versus *x* for this particular orientation, proportional to the square of the component of **E** along **p** ($I \propto |\mathbf{p}\cdot\mathbf{E}|^2$).

10/25/12: 824 citations

Confocal

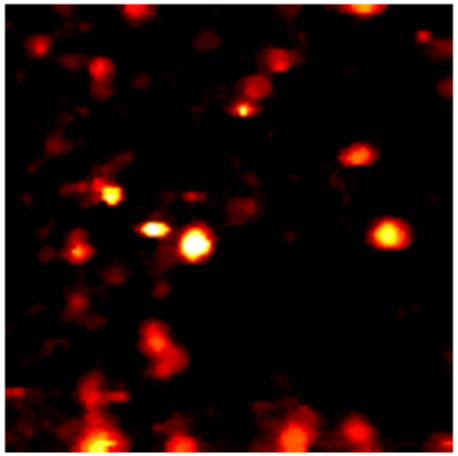

10x10 microns

NSOM

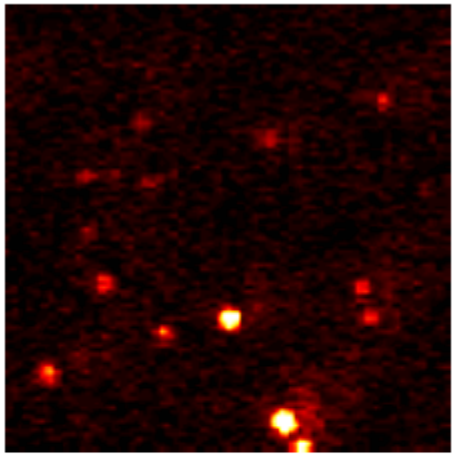

5x5 microns

By delimiting the excitation and dispersing fluorescence dye molecules the fluorescence from individual molecules can be detected.

Because of fluorescence and raman from the NSOM probe the background is actually lower in the confocal experiment despite the larger excitation volume

Apertureless NSOM

Total Internal Reflection Excitation
Scattering Collection

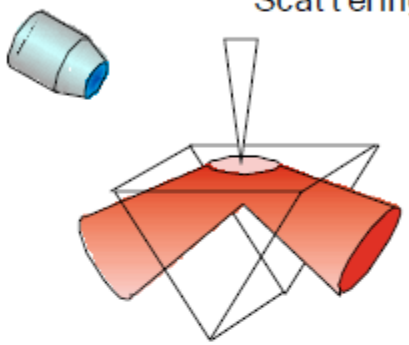

- Less excitation light collected
- Scattering measurement possible
- Sample on TIR cell
- Lower collection efficiency

Conventional Excitation
Transmission Collection

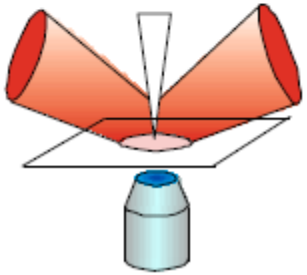

- More background from excitation
- Higher collection efficiency
- Or excitation through objective

Apertureless SNOM

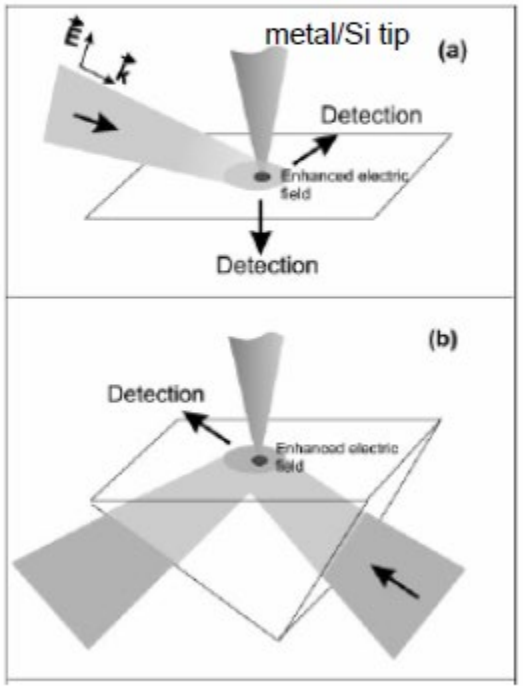

Single-molecule image of AlexaFluor 488

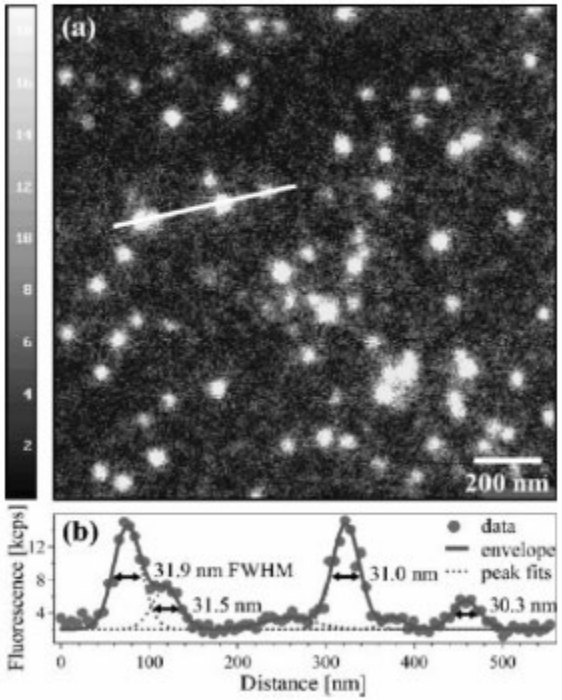

Ref: A. Bouhelier, *Microsc. Res. Tech.* **69,** 563 (2006).

VOLUME 82, NUMBER 20 PHYSICAL REVIEW LETTERS 17 MAY 1999

Near-Field Fluorescence Microscopy Based on Two-Photon Excitation with Metal Tips

Erik J. Sánchez,[1,2,*] Lukas Novotny,[1,†] and X. Sunney Xie[1,2,*]

[1] *William R. Wiley Environmental Molecular Sciences Laboratory, Pacific Northwest National Laboratory, P.O. Box 999, Richland, Washington 99352*

[2] *Department of Physics/Environmental Science and Resources Program, Portland State University, P.O. Box 751, Portland, Oregon 97207-0751*

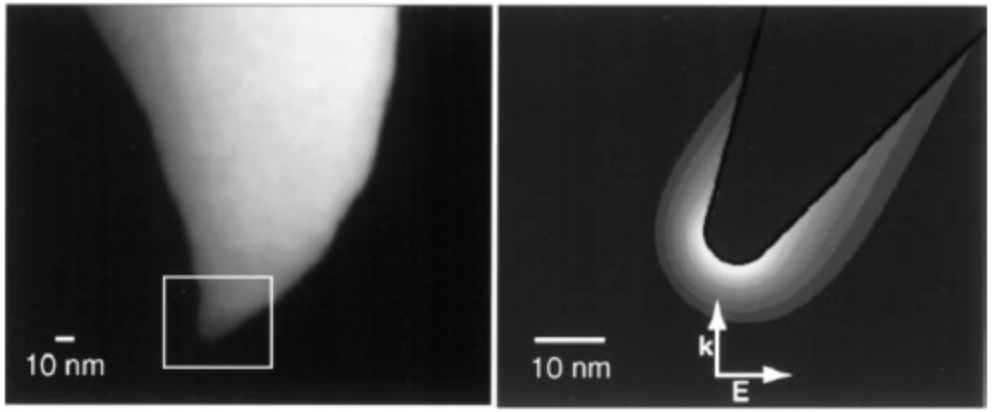

Ion beam milled tip designed to enhance in-plane electric field

Calculated field enhancement at tip is 1000:1

Metal tip near an aperture

DNA labeled with Cy-3

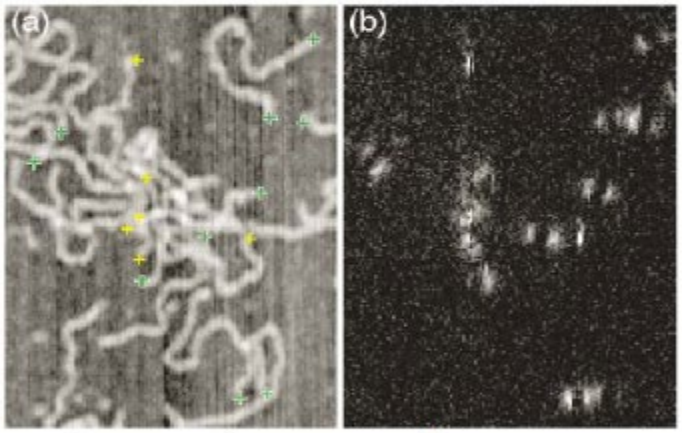

topography fluorescence

Ref: H. G. Frey, S. Witt, K. Felderer, and R. Guckenberger, *Phys. Rev. Lett.* **93,** 200801 (2004).

VOLUME 90, NUMBER 9 PHYSICAL REVIEW LETTERS week ending 7 MARCH 2003

High-Resolution Near-Field Raman Microscopy of Single-Walled Carbon Nanotubes

Achim Hartschuh,[1] Erik J. Sánchez,[2] X. Sunney Xie,[3] and Lukas Novotny[1]
[1]*The Institute of Optics, University of Rochester, Rochester, New York 14627*
[2]*Department of Physics, Portland State University, Portland, Oregon 97207*
[3]*Department of Chemistry and Chemical Biology, Harvard University, Cambridge, Massachusetts 02138*
(Received 9 August 2002; published 4 March 2003)

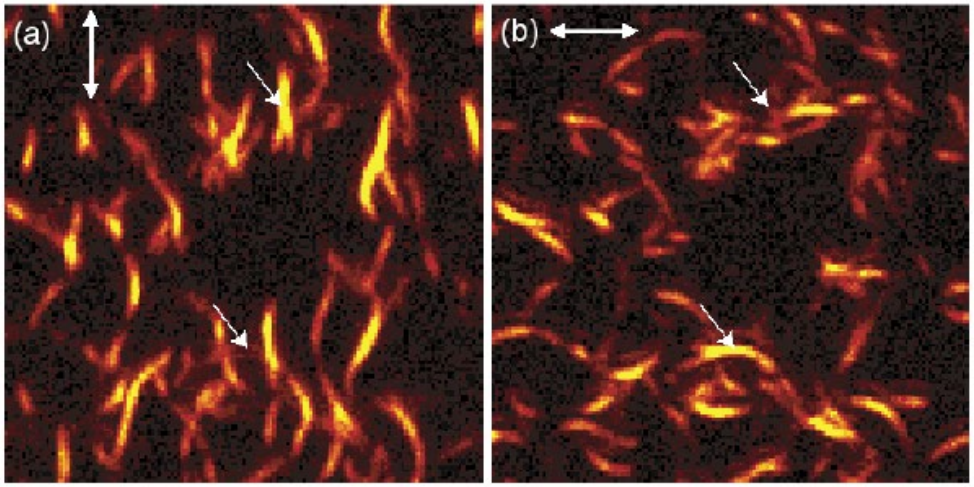

Confocal Raman Image of Carbon Nanotube

Detecting at G' band – Raman shift $\nu = 2615\ cm^{-1}$

Excitation source: 633 nm.

Raman Spectrography - Scattering

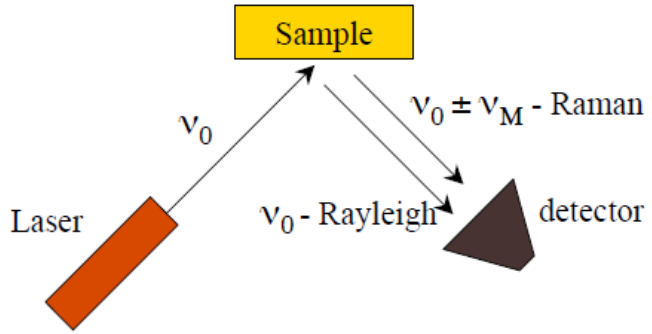

Raman Spectroscopy: Absorption, Scattering, and Fluorescence

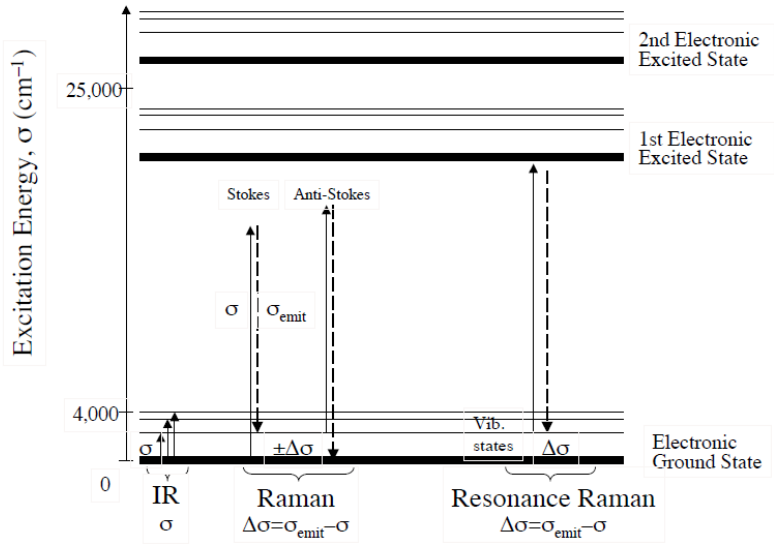

Some limitations (disadvantages) of NSOM

- Practically zero working distance (for objective) and an extremely small depth of field (for tip).
- Extremely long scan times for high resolution images or large specimen areas.
- Very low transmissivity of apertures smaller than the incident light wavelength --- low intensity of incident light for excitation, a problem for weak fluorescent molecules.
- Only surface features can be imaged and studied.
- Fiber optic probes are somewhat problematic for imaging soft materials due to their high spring constants, especially in shear-force mode

Surface enhanced Raman spectroscopy (SERS)

Chandrasekhara Venkata Raman

- 1888-1970
- Discovered the inelastic scattering phenomenon in 1928
- Was awarded the Nobel Prize for Physics in 1930

History

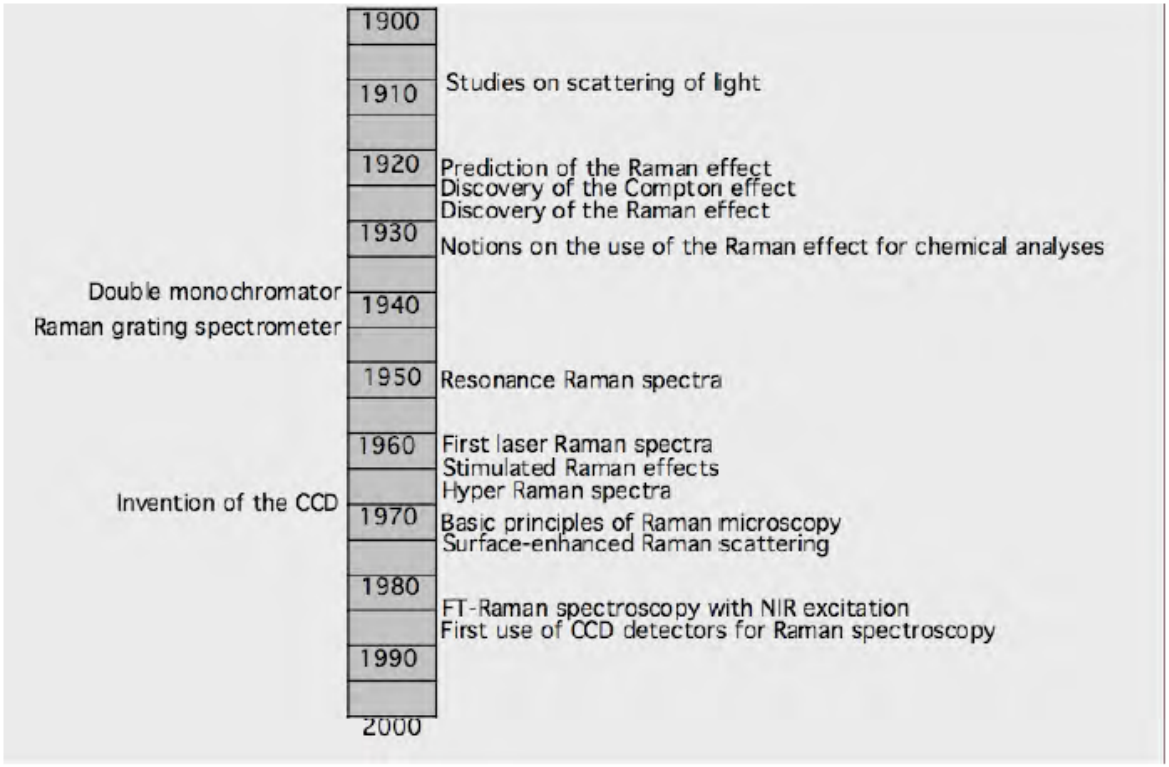

- spectra shows vibrational frequency in wavenumbers (cm^{-1})
- peaks are used to identify chemical "groups", i.e. types of bonds

- examples of characteristic stretching frequencies (group frequencies)

O-H	3600 cm^{-1}	C-C	1200 cm^{-1}
N-H	3400 cm^{-1}	aromatic C-C	1450-1600 cm^{-1}
C-H	3000 cm^{-1}	C=C	1650 cm^{-1}
C-O/C-N/C-C	1100-1200 cm^{-1}	C≡C	2200 cm^{-1}

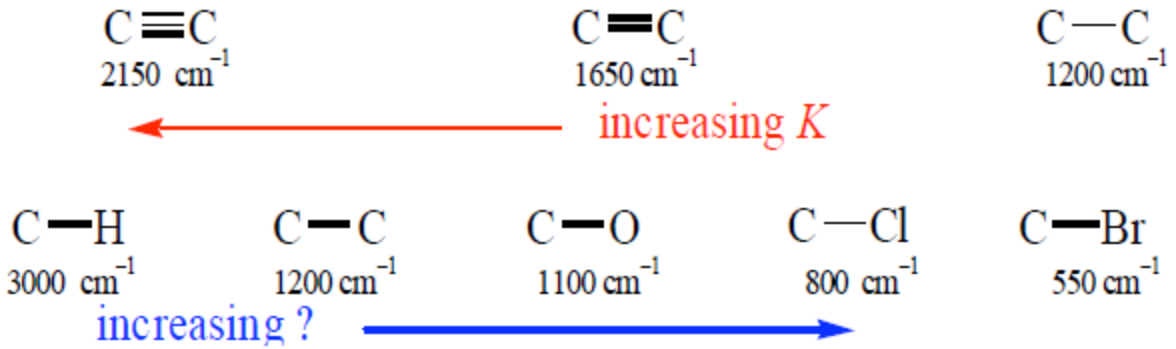

Electromagnetic Mechanism of SERS

George C. Schatz, Matthew A. Young, and Richard P. Van Duyne

Department of Chemistry, Northwestern University, Evanston, IL 60208-3113, USA
{schatz,vanduyne}@chem.northwestern.edu

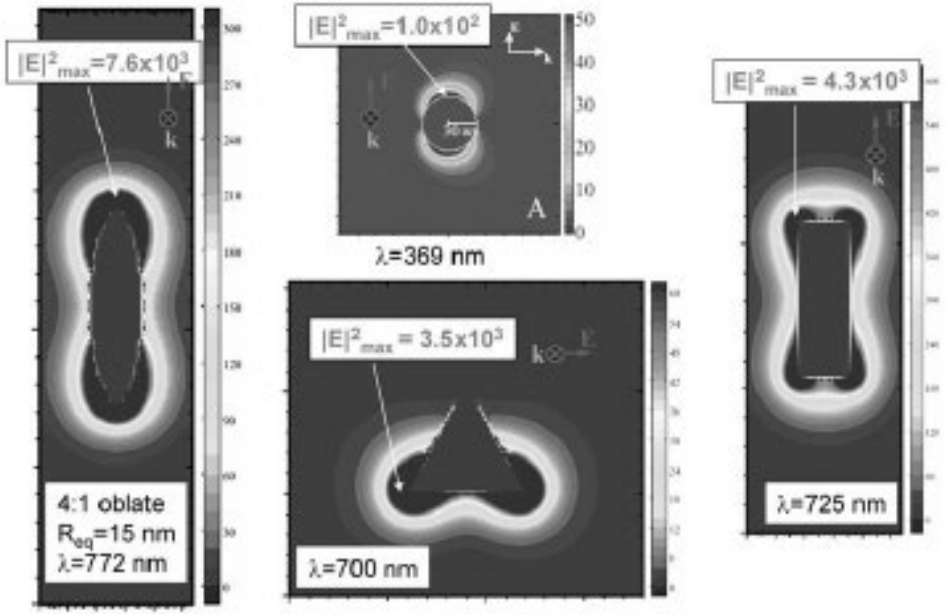

Fig. 1. Contours of the local field near silver particles at specified wavelengths, showing values of the peak field $|E|^2$

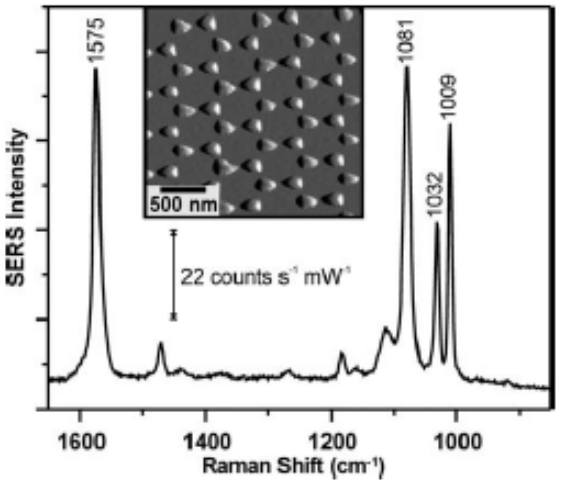

Fig. 9. Representative SERS spectrum of benzenethiol-dosed NSL substrate. λ_{ex} = 620 nm, P = 3.0 mW, acquisition time = 150 s. An atomic force micrograph of the sample is shown in the *inset*

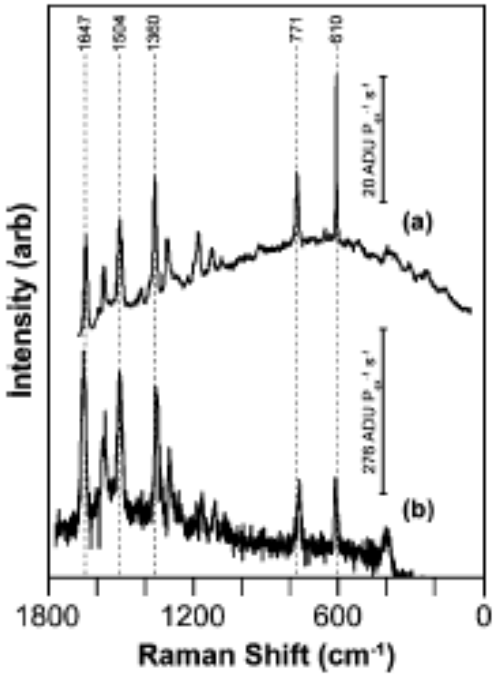

Figure 2 Surface-enhanced Raman spectra of R6G on silver obtained using 532-nm excitation. (a) Ensemble-averaged surface-enhanced resonance Raman obtained on AgIF (P_{ex} = 2.0 kW·cm^{-2}, t_{ac} = 0.1 s) and (b) single-molecule surface-enhanced resonance Raman spectrum obtained on colloidal Ag aggregate (P_{ex} = 0.050 W·cm^{-2}, t_{ac} = 30 s).

2. Theoretical explanations for SERS

A. Electromagnetic field enhancement mechanism
- excitation of surface plasmon
- tends to form spacially localized “hot areas”
- the magnitude of enhancement ~10^6- 10^7 times for single colloidal silver, and ~10^8 for the gap between two coupled particles

B. Chemical enhancement
- due to specific interactions, forming charge-transfer complexes
- the magnitude of chemical enhancement ~10-100 times

3. SERS applications

classical electrochemical studies
e.g. corrosion processes, film growth, self-assembled monolayers

trace analysis approaching single molecule detection limit
e.g. 100 pyridine molecules on Ag electrode

Efficient enhancing substrates: Ag, Au and Cu, rough surfaces or colloidal particles with the size of tens of nanometers

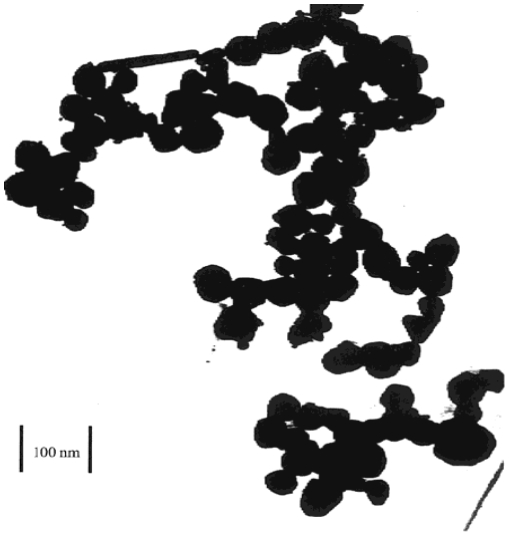

biological samples
e.g. DNA/protein detection

surface enhanced anti-stokes Raman scattering
surface enhanced resonance Raman scattering (SERRS)

Spectroscopy of Single Hemoglobin Molecules by Surface Enhanced Raman Scattering

Hongxing Xu, Erik J. Bjerneld, Mikael Käll,* and Lars Börjesson
Department of Applied Physics, Chalmers University of Technology, S-412 96 Göteborg, Sweden
(Received 22 January 1999)

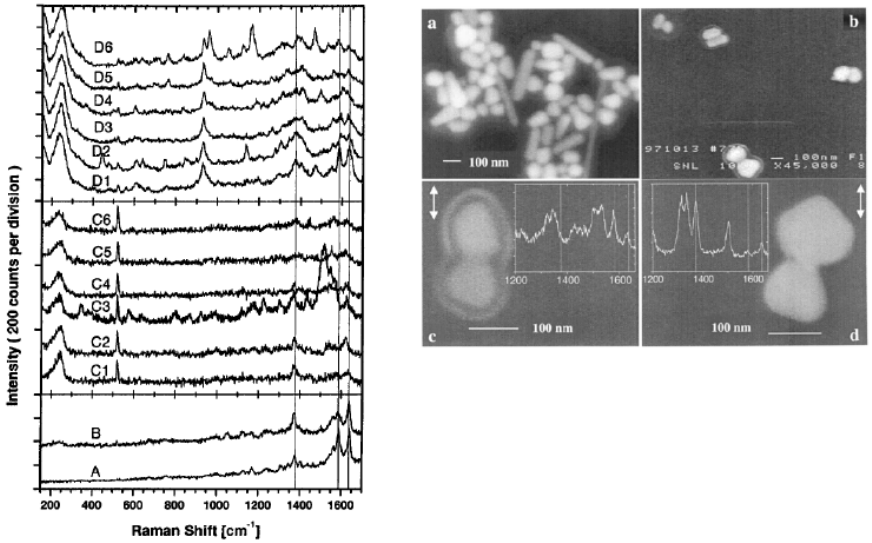

Confocal Raman spectra of crystalline met-Hb *A*, dense layer of HbAg aggregates *B*, and two time series (*C*1 *C*6 and *D*1 *D*6) of "hot sites" obtained at the single molecule detection limit. The vertical lines indicate the Hb marker modes discussed in the text. All spectra were measured with the same collection time 30 s and collection efficiency. The incident laser power was 1 mW in *A* and 1 μW in *B*-*D*.

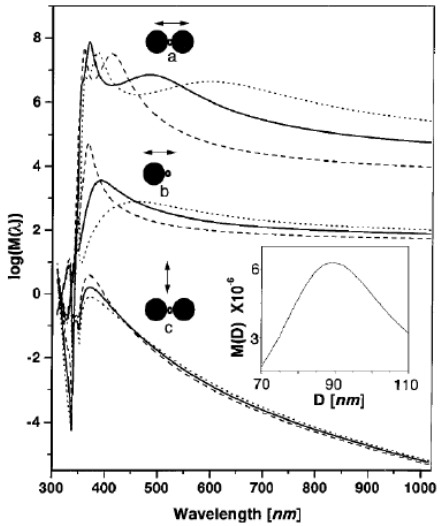

Calculated electromagnetic enhancement factor for the midpoint between two Ag spheres separated by d = 5.5 nm and for a point $d/2$ outside a single sphere. The solid and open circles indicate the position of the Ag spheres and the Hb molecule, respectively, in relation to the incident polarization vector (double arrows). The calculations have been performed for spheres of diameters D = 60 (dashed curves), 90 (solid curves) and 120 nm (dotted curves). Inset shows the enhancement versus D for λ = 514.5 nm and a Stokes shift of 1500 cm^{-1} for configuration *a*.

Commercial SERS Substrates

D3 produces the Klarite range of substrates for Surface Enhanced Raman Spectroscopy. Klarite substrates enable faster, higher accuracy detection of biological and chemical samples at lower detection limits for a wide range of applications in homeland security, forensics, medical diagnostics and pharmaceutical drug discovery. Manufactured using techniques from semiconductor processing Klarite substrates offer high levels of enhancement and reliability.

NANO LETTERS

pubs.acs.org/NanoLett

Super-resolution Optical Imaging of Single-Molecule SERS Hot Spots

Sarah M. Stranahan, and Katherine A. Willets*

Department of Chemistry and Biochemistry, The University of Texas at Austin, 1 University Station A5300, Austin, Texas 78712

ABSTRACT We present the first super-resolution optical images of single-molecule surface-enhanced Raman scattering (SM-SERS) hot spots, using super-resolution imaging as a powerful new tool for understanding the interaction between single molecules and nanoparticle hot spots. Using point spread function fitting, we map the centroid position of SM-SERS with ±10 nm resolution, revealing a spatial relationship between the SM-SERS centroid position and the highest SERS intensity. We are also able to measure the unique position of the SM-SERS centroid relative to the centroid associated with nanoparticle photoluminescence, which allows us to speculate on the presence of multiple hot spots within a single diffraction-limited spot. These measurements allow us to follow dynamic movement of the SM-SERS centroid position over time as it samples different locations in space and explores regions larger than the expected size of a SM-SERS hot spot. We have proposed that the movement of the SERS centroid is due to diffusion of a single molecule on the surface of the nanoparticle, which leads to changes in coupling between the scattering dipole and the optical near field of the nanoparticle.

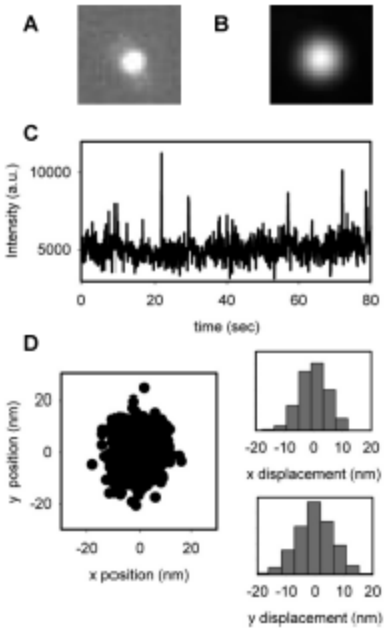

FIGURE 2. (A) Image of the PSF of the nanoparticle emission resulting from 532 nm excitation. (B) Rayleigh scattering of the same nanoparticle taken with transmission darkfield. (C) Integrated emission intensity from (A) over 80 s with 0.1 s acquisitions for 800 frames. (D) Scatter plot of the emission centroid positions located by fitting the PSF in each of the 800 image frames to eq 1 showing the nanoparticle emission originates from a single region with a standard deviation of 6 nm and an experimental precision of ±15 nm.

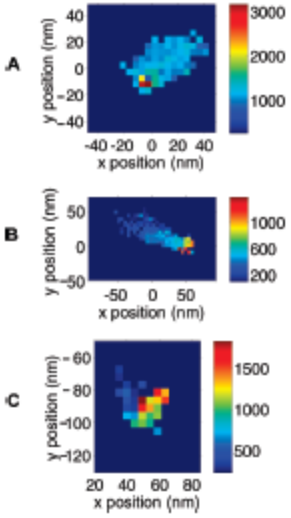

FIGURE 6. Two-dimensional SERS intensity histograms showing the average intensity measured at each centroid position (color bar = background subtracted ADC counts). Bin size is 4.6 nm. The nanoparticle emission centroid is set at (0, 0). Three different examples are shown, illustrating the correlation between the spatial position of the centroid location and the average SERS intensity at that spot.

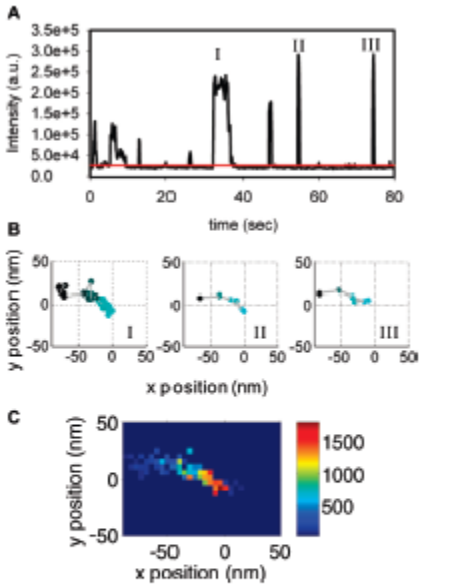

FIGURE 5. (A) Time trace showing the fluctuation of the integrated R6G SERS intensity with time, exhibiting several discrete 'on' and 'off' steps. Three 'on' events are highlighted as I, II, and III. (B) Diffusion trajectories of I, II, and III from (A) showing how the SERS centroid position and intensity change with time. In all cases, the centroid begins around (−80, 10) and moves toward (0, 0), while the SERS intensity increases (shown as a color change from dark to light blue). (C) Two-dimensional histogram showing the average SERS intensity measured at each centroid position. Bin size is 4.6 nm. The nanoparticle emission centroid is set at (0, 0).